Multi-dimensional population balance models of crystallization processes

Meisler, Kresten Troelstrup

Publication date:
2014

Document Version
Publisher's PDF, also known as Version of record

Multi-dimensional population balance models of crystallization processes

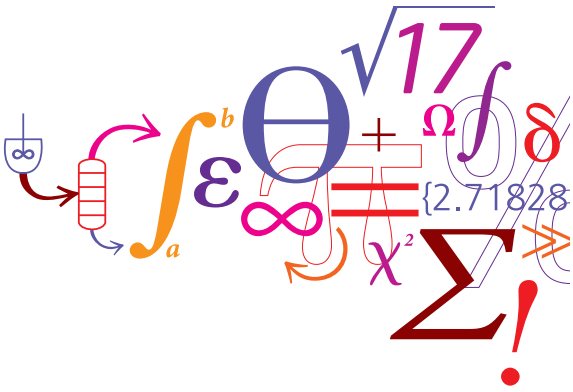

Kresten Troelstrup Meisler

Ph.D. Thesis

September 2014

DTU Chemical Engineering
Department of Chemical and Biochemical Engineering

Multi-dimensional population balance models of crystallization processes

PhD Thesis

Kresten Troelstrup Meisler

kretm@kt.dtu.dk

Supervisors:

Professor Rafiqul Gani

DTU Kemiteknik

Professor Krist Gernaey

DTU Kemiteknik

Associate Professor Nicolas von Solms

DTU Kemiteknik

September 2014

Technical University of Denmark

Preface

This thesis is submitted as partial fulfillment of the requirements for the Ph.D. degree in Chemical Engineering. The work has been carried out in the CAPEC-PROCESS group at DTU Chemical Engineering under supervision of Professor Rafiqul Gani, Professor Krist V. Gernaey and Associate Professor Nicolas von Solms in the period 2011-2014. The work has been financed by DTU Chemical Engineering. I am thankful for the guidance from my supervisors and the possibility to work in the interesting field of this project. The time spent in the past years have been interesting and I would like to thank the people at CAPEC-PROCESS for making every day interesting.

Abstract

A generic and model-based framework for batch cooling crystallization operations has been extended in terms of model library, model analysis as well as simulation of continuous and fed-batch operations. New modules for the framework have been developed, including a module for reactions, allowing the study of reactive crystallization within the framework. A crystallization kinetic model library together with an ontology for knowledge representation has been developed, in which kinetic models and relations from the literature are stored along with the references and data. The model library connects to the generic modelling framework as well, so that models can be retrieved, analyzed, used for simulation and revised versions stored again. The model library facilitates comparison of expressions for crystallization kinetic phenomena and is integrated with the model analysis tools of the framework. Through the framework, a model for a crystallization operation may be systematically generated and parameters for the model for simulation can be found in the database. A procedure for parameter estimation has been illustrated based on experimental work. The identifiability of the models has been discussed in relation to parameter estimation using sensitivity analysis. Some important identifiability issues have been investigated using the model structure to simulate perfect data and data with white noise added to it. It is found that the kinetic models may not be reliably estimated from the concentration profile using the parameter estimation procedure for both perfect and noisy data. The framework has been applied to case studies involving inorganic and organic compounds, including an active pharmaceutical ingredient (paracetamol) crystallized from different solvents. The case studies have been used to demonstrate the versatility of the framework.

Resumé (abstract in Danish)

Et generisk, modelbaseret framework til batch kølekrystallisation er blevet udvidet til at omfatte kontinuert of fed-batch processer. Moduler til frameworket er konstrueret, inklusive moduler, som tillader studier af reaktive krystallisationsprocesser. Et bibliotek indeholdende de nødvendige kinetiske modeller til krystallisationsstudier er udviklet som en ontologi. Heri er kinetiske modeller og relationer lagret med de referencer og data, hvorpå de kinetiske modeller baseret. Modelbiblioteket fungerer endvidere modulært ved at det er forbundet til frameworket, hvorved modeller kan hentes, analyseres, anvendes i simulationer af processer og lagres igen. Modelbiblioteket muliggør sammenligning af modeller og udtryk for kinetiske fænomener (modeller for vækst, kimdannelse, agglomeration og brydning) . Modelbiblioteket er tæt forbundet med statistiske værktøjer. Ved anvendelse af frameworket kan en model for en krystallisationsproces genereres systematisk og parametre kan findes i databasen. En procedure til estimation af parametre er illustreret på baggrund af eksperimentelt arbejde med paracetamol i propan-2-ol. Identificerbarheden af modellerne diskuteres på baggrund af metoder fra sensitivitetsanlyser. Den praktiske identificerbarhed er undersøgt ved anvendelse af modelstrukturen til at simulere perfekte data og datasæt med hvid støj. At anvende koncentrationsbalancen til at estimere parametrene er fundet problematisk, idet parametrene ikke kan estimerers pålideligt. Frameworket er anvendt i studier af organiske og uorganiske forbindelser, herunder farmaceutiske komponenter, i forskellige opløsningsmidler med henblik på at demonstrere alsidigheden af frameworket

Contents

Part I

Introduction and aim

CHAPTER 1

Introduction

Crystallization as a chemical unit operation has been utilized for millennia to separate chemical systems, for example, in the production of sodium chloride salt in solar evaporation ponds. With the advances in the pharmaceutical industry and specialty chemicals industrial sectors producing active (pharmaceutical) ingredients (API) with melting points above 100°C interest in crystallization as a separation and purification method for these compounds has grown. In recent years crystallization has been considered one of the major separation and purification methods for food, pharmaceuticals and fine chemicals (Markande et al., 2009). The crystallization operation can be carried out in different modes. One mode is the batch cooling operation illustrated in figure 1.1. The cooling jacket allows control of the operation at a specified temperature, which in itself is not difficult but linking it to a certain product quality dependent on the crystal size distribution (CSD), for example, can be very challenging.

According to Randolph and Larson (1971) the CSD is an important property of a product obtained through crystallization yet difficult to predict and not well understood (Randolph and Larson, 1971). Indeed, the CSD is an important characteristic of a crystallized product as it affects the flow properties, specific area and dissolution rate (Markande et al., 2009). Furthermore, the CSD is important in downstream operations for recovery of the crystals by filtration, as well as in washing and drying of the product (Markande et al., 2009). Depending on the CSD of the crystallized product, milling of the final product may be necessary.

Randolph and Larson (1971) point out that important properties of a crystallization operation are

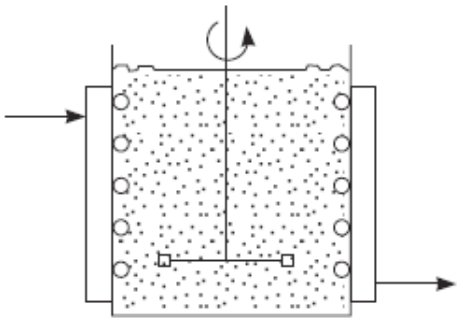

Figure 1.1: *A cooling batch crystallizer with a cooling jacket and coils. Illustration adopted from Jones (2002)*

the *crystal habit*, describing the appearance of the crystals due to the relative growth rate of the faces, and purity, the fouling of equipment, capacity and scale-up as well as crystallizer stability (Randolph and Larson, 1971), all of which can be related to the *kinetics* of the chemical system. Understanding the kinetics of the crystallization process is necessary to achieve a product of sufficient quality as well as running the operation.

1.1 Aim

This project concerns the modelling of kinetics for crystallization operations as part of a model-based framework for crystallization operation design and analysis in which the kinetic phenomena (growth, nucleation, agglomeration and breakage) are treated. The description of the crystallization operation relies on the description of thermodynamics and of the kinetic phenomena that are closely related to the operational policies. This work focuses on the models used to describe the kinetics and how they can be analysed as stand-alone descriptions of kinetic phenomena or modelled together to capture their interactions. The single phenomenon models allow the simple analysis with no masking effects of kinetic phenomena due to interactions, which is often necessary when a model is evaluated, whereas the multi-phenomena models provide a more realistic approach, where phenomena may be dominated by process design or operation, but are present nonetheless. The framework is utilized for crystallization operation simulation and analysis. The models for crystallization kinetics are identified and stored in a model library as part of the framework for future use.

1.2 Structure of the thesis

The thesis is divided into four main parts (I-IV) and a set of appendices (part V). Part I (chapters 1 and 2) introduces the scope and aim of the thesis, reviewing the literature in the field. Part II introduces the extended generic framework, establishing the generic framework concept (chapter

3), listing the kinetic phenomena and the kinetic constitutive equations (chapter 4), how the generic process model is constructed and its interactions with the kinetic constitutive equations (chapter 5) and the necessary data and available data types (chapter 6). Part III includes the case studies (chapter 7) and part IV contains the discussion (chapter 8) and conclusion and further work (chapter 9).

CHAPTER 2

Literature review

This chapter contains a review of relevant literature in the context of crystallization and generic approaches for modelling and analysis of crystallization. Several of the references related to the context of later chapters are cited there. A major group of references are located in the crystallization kinetic model library discussed in section 4.8.

2.1 Crystallization fundamentals

A crystallization operation can be described as one involving multiple balance equation types. Crystals forming, growing and interacting with other crystals as well as the surroundings can involve mass, energy and population balances. The mass and energy balances can be formulated overall for the system or as distributed balances describing spatial variation in the crystallizer depending on the desired level of information.

2.1.1 Mass balance

In this work crystallization from solution is treated and the mass balances relating to this condition are considered. The mass balance for a crystallizer can be formulated differently: The crystallizer can be analyzed from a thermodynamic point of view, assuming equilibrium, or as a

dynamic operation. The thermodynamic consideration is carried out initially as the feasibility of the operation is considered. The thermodynamics give the driving force for the crystallization. The difference in chemical potential between the component in solution and solid form determines the solubility of the solute in the solution and the saturation condition. In a crystallization operation from solution, the chemical potential of the solute is increased above that of the solid, making the solution supersaturated, and the mass balance can be formulated based on a phase diagram using the lever rule (Mullin, 2001).

The dynamic mass balance involves the kinetics of the system and describes the crystallization operation regarding the formation and increase of the solid phase, thus it involves the nucleation and growth phenomena and may be coupled with a population balance.

Supersaturation

The supersaturation of the system can be described in various ways. The thermodynamic description can be given as (Mohan and Myerson, 2002):

$$\frac{\Delta\mu}{RT} = \frac{\mu_{solute}}{RT} - \frac{\mu_{solute_{sat}}}{RT} = \ln\frac{a}{a^*} = \ln\frac{\gamma x}{\gamma^* x^*} \tag{2.1}$$

Here, the thermodynamical supersaturation is given as the difference in chemical potential between the solute in supersaturated solution and solute in saturated solution. In practical crystallization operations the thermodynamic potential is not always known and other descriptions of the supersaturation have been employed. Apart from the thermodynamic potential the *supersaturation*, *relative supersaturation* and *supersaturation ratio* are used. These can be defined as (Nývlt et al., 1985):

Absolute supersaturation	$X(T) = \Delta C(T) = C - C_{eq}(T)$	(2.2)
Relative supersaturation	$X(T) = \sigma(T) = \frac{C - C_{eq}(T)}{C_{eq}(T)} = \frac{\Delta C(T)}{C_{eq}(T)}$	(2.3)
Supersaturation ratio	$X(T) = S(T) = \frac{C}{C_{eq}(T)} = \sigma(T) + 1$	(2.4)

Here, (T) indicates that the saturation is a function of temperature. Depending on the chosen process, other relevant variables for the equilibrium concentration can be introduced which will shift the saturation curve as it is dependent on the specific chemical system.

The absolute supersaturation expresses the difference in concentration, ΔC as the difference between actual concentration c and equilibrium concentration c_{eq}, also known as saturated concentration c_{sat}. The relative supersaturation σ expresses the difference between actual concentration

and equilibrium concentration, Δc, relative to the equilibrium concentration c_{eq} leading to numerical values in the range [0;1] for most supersaturated systems. The supersaturation ratio is 1 for saturated systems. Undersaturated have a supersaturation ratio value in the range $(0;1)$. Supersaturated systems have supersaturation ratios larger than 1.

It should be noted that the numerical values of Eqs (2.2) - (2.4) are dependent on the concentration unit. Changing concentration unit directly affects Δc. Despite being dimensionless, the relative supersaturation and supersaturation ratio will change value if the concentration is changed from

$$\frac{\text{mass of solute}}{\text{mass of solvent}} \quad \text{to} \quad \frac{\text{mass of solute}}{\text{mass of solute-free solvent}}$$

There is no literature convention on the symbols used and S is frequently used as the symbol to describe the relative supersaturation $\frac{\Delta c}{c_{eq}}$.

It is also possible to define the supersaturation by the supercooling of the system (Nývlt et al., 1985). This is used in another context than the growth models.

The mass balance can be formulated differentially as a concentration balance

$$\frac{dC}{dt} = \frac{-\rho_c}{m_{solvent}} \frac{dV_c}{dt} \tag{2.5}$$

where C is the concentration of solute (dimensionless), ρ_c is the crystal density, $m_{solvent}$ is the mass of solvent and V_c is the volume of crystals.

2.1.2 Energy balance

The energy balance for the crystallization operation is formulated depending on the vessel type and properties of the system. The crystallization operation involves the heat of crystallization, for which a constitutive relation may be included, and the operation itself may involve heating or cooling. The energy balance can thus be connected to the mass balance and analyzed overall (from thermodynamic relations) or dynamically coupled with the dynamic mass balance.

The energy balance can be formulated as

$$m_{magma} c_{p,magma} \frac{dT}{dt} = -\Delta H_{cryst} \frac{dm_c}{dt} - UA\Delta T \tag{2.6}$$

where m_{magma} is the mass of magma in the crystallization chamber, $c_{p,magma}$ the heat capacity of the magma, T the temperature, ΔH_{cryst} the crystallization enthalpy, m_c the mass of crystals and $UA\Delta T$ the heat exchange with the surroundings. This may stem from either natural convection, forced convection, a cooling jacket or other exchange.

2.2 Kinetics

The overall mass balance describes how the process components interact and the overall energy balance describes the energy involved. For a model involving the time of the operation (a transient simulation), the kinetics are necessary. For this purpose time-dependent models can be formulated for the description of the crystallizer. The time-dependent models require kinetic models for the chemical system and process equipment which must be supplied.

The kinetic models for a crystallization operation can include several variables describing the phenomena encountered in a crystallization process. (Mullin, 2001; Myerson, 2002) *Nucleation* is the formation of nuclei or minuscule crystals that grow. When the crystals are formed the crystals *grow* while new crystals are formed and the rate of formation and growth will determine the size distribution of the crystals. *Agglomeration* and *breakage* of crystals can also contribute to the CSD. The respective kinetic phenomena and the models relating to them are covered in chapter 4.

The driving force for the crystallization operation is the supersaturation and a supersaturation relation is needed to describe this. This relation can be based on data (correlation) or model based for the specific operation to be studied. The supersaturation relation can be used in the framework with the equipment description and operational policies to formulate the time-dependent mass and energy equations.

2.3 Population balances for crystallization operations

The population balance approach combines a set of equations describing the conservation laws, rate equations and fluid mechanics of the system (Garside, 1985). This allows the CSD characterization, which is an important part of the crystal product properties to be calculated. Different variables such as rate of birth, growth and death can be included. These variables can be subdivided and related to the kinetic phenomena they represent and a constitutive equation can be formulated. As an example the birth rate variable describes the rate of generation of a new particle in the population balance. This new crystal or particle may stem from a nucleation, agglomeration or breakage related phenomenon and the number of particles formed is the sum of particles originating from the different phenomena.

$$B = B_{nucleation} + B_{agglomeration} + B_{breakage}$$

Deciding which phenomena to include in the kinetics, the population balance equation can be set up in its general form as as (2.7):

$$\frac{\partial n(L,t)}{\partial t} = -\frac{\partial [n(L,t)G(L,X,\phi)]}{\partial L} + Birth - Death \tag{2.7}$$

$n(L,t)$ is the number of particles of size L for a given time t. This is a discrete number, but is often treated as a continuous variable. $G(L,X,\phi)$ is the growth function for a particle depending on size, supersaturation (X) and selected phenomena ϕ. ϕ covers such phenomena as temperature effect, transport phenomena or apparent size dependency for a growth model including these terms. The growth function is continuous. *Birth* represents new particles formed through nucleation, agglomeration or breakage and *Death* represents destruction of particles through agglomeration or breakage. The birth and death terms are similarly discrete functions, but are often treated as continuous functions, assuming that the number of particles is large, whereby the relative error from this assumption is small. Authors have chosen different approaches for including the fluid dynamics, which is discussed in chapter 4.

The population equation can be formulated in multiple dimensions, allowing crystals to be described in different shapes. However, the necessity of including an additional dimension should be considered carefully, since each additional dimension may come along with a considerable computational burden for detailed simulations (Costa et al., 2007).

2.3.1 Solution methods

The methods for solution of a model based on a population balance are classified into moment-based methods and bin-based methods. For the moment-based methods, the population is characterized from its moments, which may be weighted. Bin-based methods discretize a dimension of the crystal and characterize the crystals according to the value on this axis. A size characteristic is often used. Other methods have been proposed as well, however, in the context of this project, the method of moments (Hulburt and Katz, 1964) and method of classes (Marchal et al., 1988) are the focus, as the major part of the work has been carried out in a framework proposed by Samad et al. (2011) with these methods.

Moment methods

Moment methods offer limited information about a distribution compared to bin-based methods as they supply overall information about a distribution. The solution method often involves fewer equations and may thus be faster. Simulation studies in this project indicate that this is the case, when the method of classes (Marchal et al., 1988) is compared to the method of moments (Hulburt and Katz, 1964).

Hulburt and Katz (1964) applied an analysis of the evolution of a particle population through its moments to a crystallizer, including one or two dimensions in the population balance for a continuous crystallizer. The discussion of the method of moments was further undertaken in Randolph and Larson (1971), where the evolution of a particle distribution was discussed for a continuous crystallizer and the equations resulting from different distributions (gamma (Γ), normal or log-normal) were discussed. The method here was applied to steady and un-steady

state crystallizers. The method of moments discussed by (Hulburt and Katz, 1964) in terms of a Laguerre series, while limitations or restrictions of the method of moments have been discussed by them and others (Hulburt and Katz, 1964; McGraw, 1997; Gimbun et al., 2009). McGraw (1997) proposed the quadrature method of moments, giving a broader application of moment-based approaches and possibly combined with bin-based methods, for example Aamir et al. (2009).

Bin-based methods

An alternative to the moment approach is to discretize the population balance equation (PBE) (eq.2.7); this allows the transformation of the PBE (a partial differential equation) into a set of ordinary differential equations (ODE). Marchal et al. (1988) discretized the population balance and formulated the method of classes, which may include nucleation, growth, agglomeration and breakage. The method discretizes the PBE according to a size regime, the characteristic length, which is connected to a characteristic dimension of the crystal. The method then tracks the number of crystals in a specified size region (a bin), where all the crystals are assumed to be of the same (characteristic) size (Marchal et al., 1988). The resolution depends on the number of discretization points (number of classes), which results in a trade-off between accuracy and speed of solution due to the increased number of ODEs (Costa et al., 2007).

Combinations of moment and other methods

Combinations of moment and other methods have been utilized in order to obtain the advantages from several methods. Aamir et al. (2009) proposed the combination of the quadrature method of moments with the method of characteristics for computational efficiency (Aamir et al., 2009).

Other methods

Several methods for solution of PBE have been discussed by Ramkrishna (2000). Methods for solution of the population balance equations have been applied, a few examples are: the method of lines has been used to model a sucrose crystallization (Quintana-Hernández et al., 2004) and high-resolution finite volume methods have been employed by authors to simulate processes as well (Ma et al., 2002; Qamar et al., 2007).

Part II

Framework and kinetics

CHAPTER 3

General Framework

Modelling and model development has been undertaken in many fields and multiple approaches to model development have been applied (Cameron and Gani, 2011). An approach with a systematic and flexible, model-based framework has been suggested (Gernaey and Gani, 2010) and a generic modelling framework for crystallization has been proposed by Samad et al. (2011). This framework has been extended further in terms of addition of a model library for crystallization kinetics that is integrated into the framework together with other options such as model identification, model-operation design and analysis. The generic modelling framework contains the specifications for a given crystallization process and can be used for simulation of this process.

3.1 Input

The input needed to use the framework is a problem description including the chemical system and an equipment description. When this description is given, the framework provides the workflow to retrieve the needed model, if available, from the model library or, to construct a new model using the model generation procedure of Samad et al. (2011). For the population balance approach a set of balance equations needs to be derived and solved for the specific crystallization operation: Mass, energy and population balance equations. The mass and energy balance equations are derived as overall balance equations for the planned (or specific) crystallization operation. With these overall balance equations the it should be possible to investigate specific

crystallization operations.

Different phenomena found in crystallization operations have been modeled with varying sets of assumptions. Figure 3.1 shows a diagram of the interactions between phenomena, constitutive equations and balance equations.

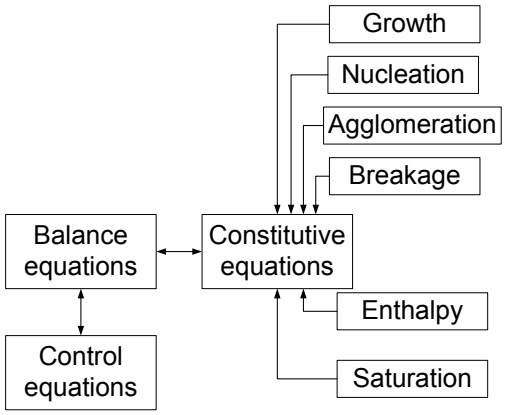

Figure 3.1: *A simple diagram of the constitutive equations relation to phenomena and other equations. The balance equations involve mass, energy and population balances, in which constitutive relations are necessary. These constitutive equations involve the kinetics (growth, nucleation, agglomeration and breakage) for time dependent solutions and the enthalpy and saturation relations. Control equations can be added to include a control aspect, and they will interact with the balance equations*

Figure 3.2 illustrates how the model equations interact with the models from the framework (in grey) and each other when the crystallization operation is modeled. The models needed to represent the kinetic phenomena may be modified for specific applications for the corresponding phenomena and the model library may also have several models developed by other researchers available.

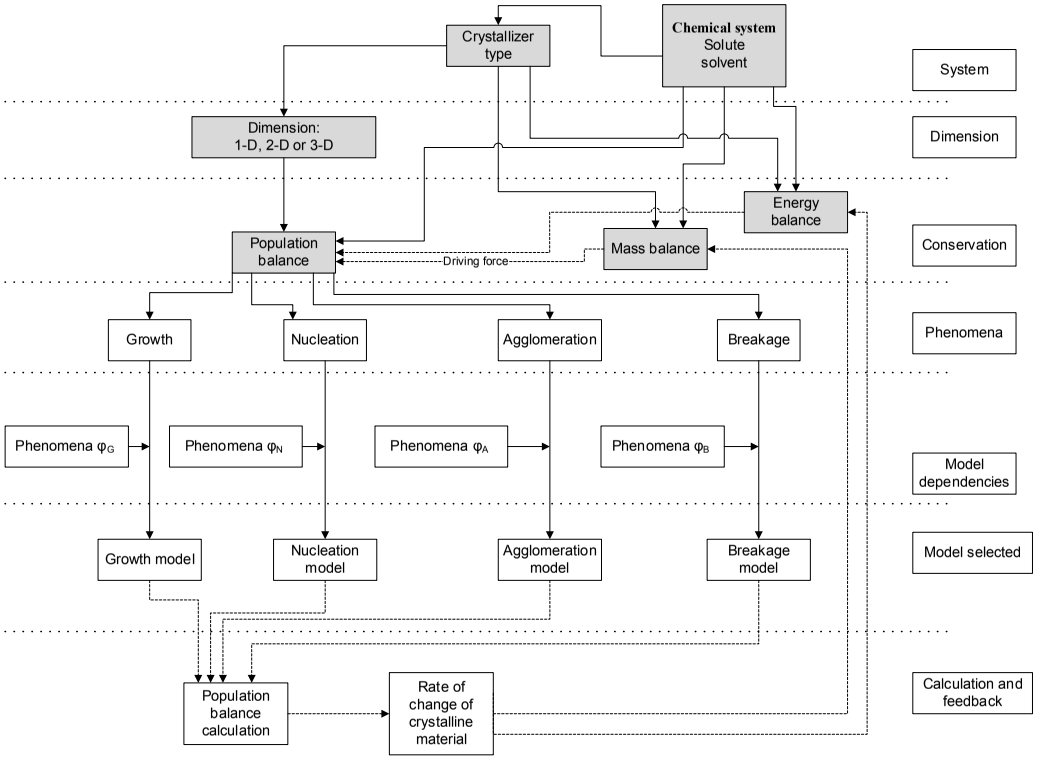

Figure 3.2: *The diagram of the framework relation. On the system level the chemical system and crystallizer type (technical system) is selected in the framework. The dimensionality of the models are chosen afterwards, and the relevant balances for the system chosen. This involves selecting the depth of the model. The model balances have interdependencies, as the driving force is described in the mass (concentration) balance. The phenomena in the population balance are selected, these in turn include phenomena, such as temperature dependence, which may be included, and a constitutive model generated and selected leading to the population balance formulation. The formulation will determine the rate of change in the population of crystals, which interacts with the balances in the framework*

The overall modelling approach is shown in Figures 3.3 - 3.5. These figures show the scenario for operations and the corresponding data flow with supporting tools within the framework. Figure 3.3 shows the overall (top) framework, which starts with the formulation of the objective. This can be to simulate a crystallization operation. Using the scenario ontology, the necessary (process) definitions are then given for the scenario to be generated and a crystallization model can be constructed. This model (Figure 3.4) involves establishing the model criteria for a model that can handle the crystallization scenario

1. Defining the scenario is the initial step
2. This model (Figure 3.4) involves establishing the model criteria for a model that can handle the crystallization scenario
3. An initial feasibility study may involve only mass balances and equilibrium relations, where later studies may involve kinetics and the population balance. Relevant considerations are also the type of equipment and type of chemicals used. Having established the model criteria, the involved balances, constitutive relations and control equations may be chosen for the model construction.
4. As the model is defined data may be required (if parameters are not already found in the database). The data requirements are evaluated, for some relations data and experimental points are necessary, for others models, possibly with predictive qualities (such as UNIFAQ (Fredenslund et al., 1975)) may be used.
5. With the data requirements established, the necessary data should be retrieved from literature, experiments or databases.
6. Then, all the necessary requirements for the model to be simulated and the simulation performed.
7. Depending on the outcome of this simulation and the desired purpose, the simulation results can be accepted or rejected. The evaluation of the model result can be based on a visual inspection (a plot) or comparison with experiments, in the latter case a new set of experimental data is necessary. This data set should be obtained, if it is possible to analyze by visual inspection, a plot of the model and the statistical analysis can be used to decide whether the model and experiment agrees. If not, a data handling procedure (Figure 3.5) may be employed after which the results should be possible to inspect visually. If the model fails in verification, it is necessary to identify the cause of this and correct it. Possible causes can be model validity (the structure of the model and included phenomena may not be sufficient to capture the behaviour in the process).

Experimental data for the crystallization operation may be available in many forms, as discussed in chapter 6. The data type may therefore be known or unknown in the framework, in which case a translation policy exists or is needed. When a new translation policy is developed, it is stored in the data type translation library. Having translated the data, a consistency check should be

carried out, if the data is consistent, it is ready for use in the crystallization model (Figure 3.4). However, if the data is found to be inconsistent an evaluation is necessary: Can the data set be refined to make it consistent? If so, the data set is refined and the procedure repeated. Otherwise a new experimental design may be needed or an experiment rerun to collect a new data set.

The overall process model is treated in chapter 5, where the forms of the balance equations and constitutive equations in generic forms are discussed, as well as the possibilities to make the models generic and handle the crystallization operation within the framework. The crystalization kinetics are a major part of the constitutive equations and are treated in chapter 4.

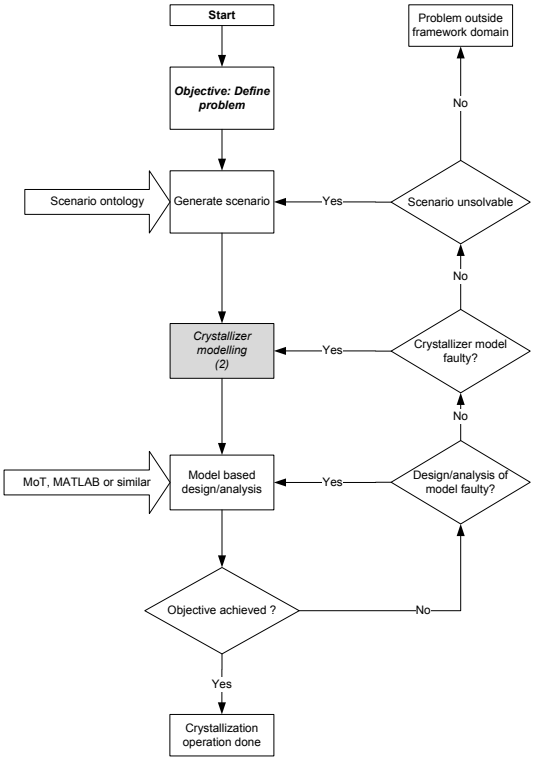

Figure 3.3: *The overall diagram of the framework relation. Initially a problem is defined. Using the scenario ontology, the necessary (process) definitions are then given and a scenario generated. A crystallizer model is formulated and used for the desired purpose, which may be design or analysis. In this step simulation tools such as MATLAB, MoT or similar may be necessary. Having the results of the simulation, it is evaluated whether the objective has been achieved. If so, the problem is solved. If not, the steps are retraced and any faults located. If no fault is found, but the scenario is unsolvable, it falls outside the domain of the framework*

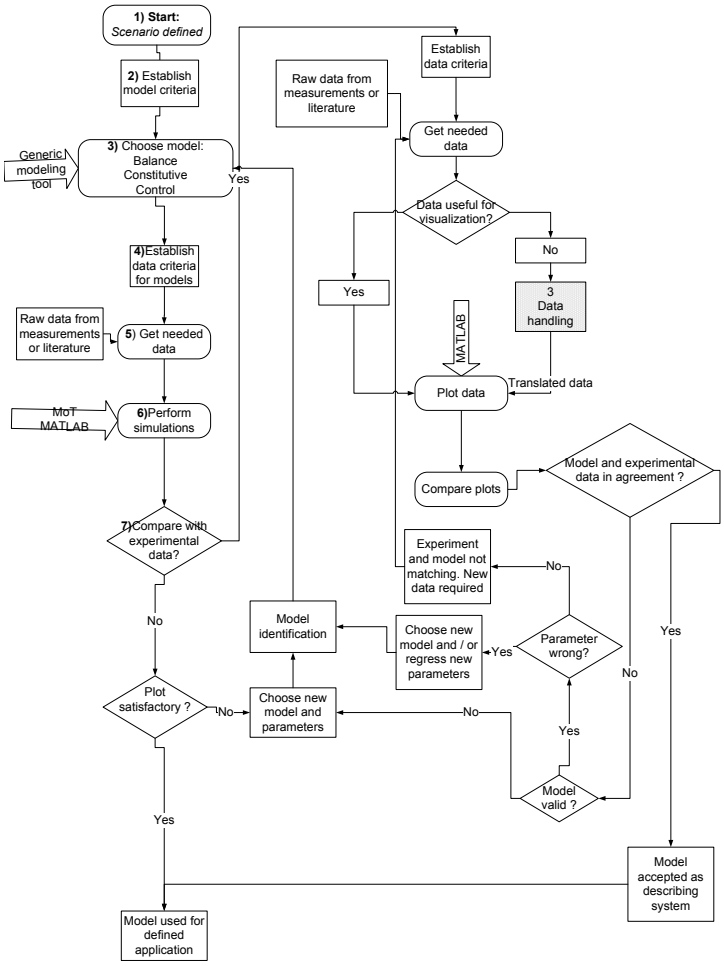

Figure 3.4: *The diagram for the crystallizer relation. With the scenario defined from Figure 3.3, the model criteria are established and the relevant balances chosen. These are stored in the generic modelling tool and require data, which must be provided from literature or experiments. With the model established, the simulation can be performed. If experimental data exist, these can be used for comparison and verification, if not a plot is made to evaluate the result, and if satisfactory the model is used for the application. If experimental data is required for model comparison, the data criteria must be established and the necessary data obtained. Graphical representation is considered useful here and a subroutine involves getting the data to a form, which may be visualized. The plots are compared (along with statistical analysis) and if in agreement, the model is accepted. Otherwise the validity of the model should be checked and possibly updated. A parameter may also have the wrong value, and have to be updated. If neither is the case, there can be a model-experimental mismatch and the experimental results should be checked with a new data set.*

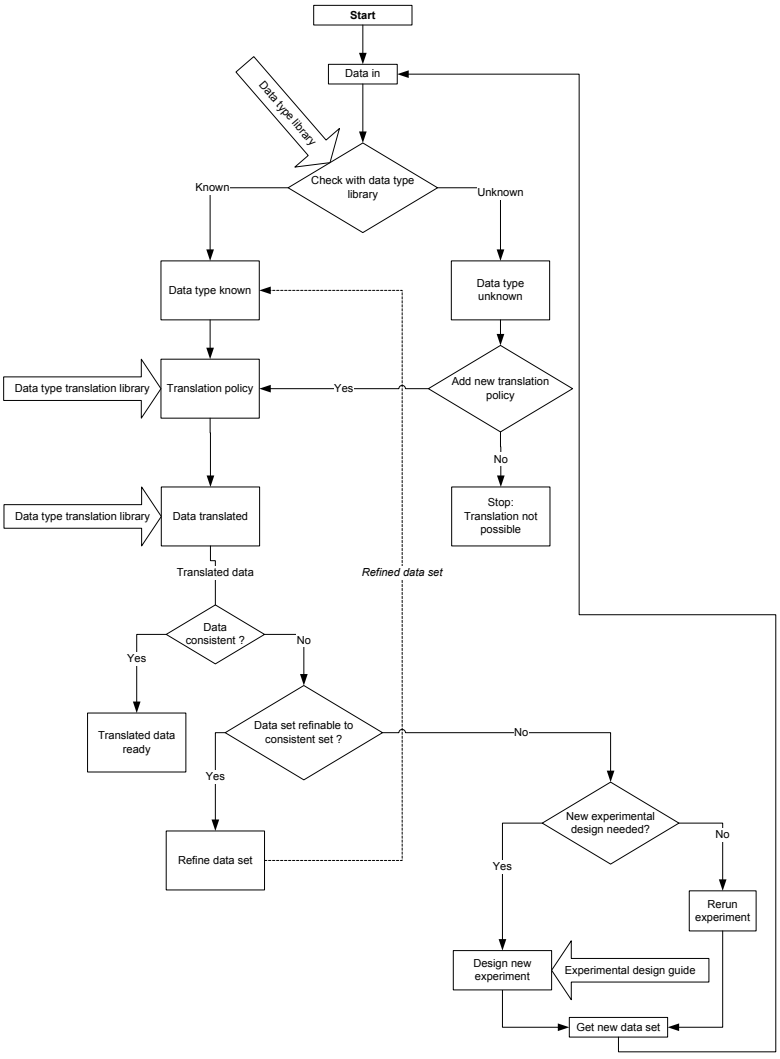

Figure 3.5: *The diagram of the data treatment. The data are entered and it is investigated whether this data type is known and therefore has a translation policy or unknown (in which case a data translation policy does not exist). A data translation policy must exist for the data to be used, and if no such policy exists, it must therefore be constructed for the data to be translated. The user may choose not to do so, in which case the data is not translated. If a new translation policy is developed, it is stored in the data type translation library. Having translated the data, a consistency check should be carried out: if the data is consistent, it is ready for use in the crystallization model (Figure 3.4), if the data is found to be inconsistent an evaluation is necessary: Can the data set be refined to be consistent? If so, the data set is refined and the procedure re-iterated, otherwise a new experimental design may be needed or an experiment rerun to obtain a new data set.*

CHAPTER 4

Constitutive Models

The constitutive models found through a literature search have been collected into a model library and are discussed in this chapter. The growth models are covered first, followed by nucleation, agglomeration and breakage.

4.1 Growth models

The population balance models are in general based on experience-based equations for the growth functions as authors have found that theoretical functions have been orders of magnitude away from describing the growth accurately and have not been able to describe observed changes in growth (Mullin, 2001). The growth functions can be divided into mass growth (volume growth), area growth or length growth. Growth of mass is a measurement of the amount of formed material per unit of time for a given crystal, whereas area growth is the increase in surface area. Both of these are less commonly used with the population balance compared to the growth of length in which the growth of a crystal is described as the change in a characteristic dimension.

The relevant phenomena have been discussed among authors from the growth mechanism and understanding of growth to the relevant phenomena for a specific mechanism (Mersmann, 2001; Mullin, 2001). Surface energy theories have been proposed; however, they have largely failed to

explain the observed results of growth in the crystals and the effect of supersaturation (Mullin, 2001).

Other theories have been suggested as well, but have not been able to describe crystal growth sufficiently (Mohan and Myerson, 2002) and hence a number of empirically adapted theories are usually used for the description of crystal growth.

Semi-empirical relations have been developed through the suggestion and development of a multi-step mechanism (Kossel, 1927; Burton et al., 1951). In this mechanism the growth rate of crystals depends on the transport of solute to the surface of the crystal followed by subsequent integration of new material into the crystal structure. Ideally the theory favours crystals to grow through the build-up of consecutive planes. The addition of new material into kinks in a plane under completion is energetically favoured compared to the addition of new material on a plane and hence the planes are completed before a new plane is added (Kossel, 1927). This theory is able to explain some observed growth phenomena but not how some crystals can grow at a rapid pace at low supersaturation, where the introduction of new nuclei at the surface is found to be minimal.

The introduction of the Burton-Cabrera-Frank (BCF)-theory (Burton et al., 1951) with the screw-dislocation has given another perspective and accounts for the continued growth of crystals at low supersaturation. The screw-dislocations have been documented through several works and although the theory is developed for crystal growth from gaseous media it has been applied to crystals grown from solutions (Mullin, 2001).

4.1.1 General Growth Model

A general model has been developed from a diffusion-reaction scheme (Chernov, 1989; Mullin, 2001). This general model has been adapted and used by multiple authors (Nagy et al., 2008) to describe the growth of the crystals in a crystallization operation. The model is often adapted to account for observed phenomena and effects through expressions describing these phenomena multiplied with the growth constant.

Diffusion and reaction The diffusion-reaction scheme for crystallization has been discussed by multiple authors (Noyes and Whitney, 1897; Nernst, 1904; Kossel, 1927; Chernov, 1989). It is treated similarly as diffusion-reaction schemes for multiple other processes (Cussler, 2009) Originally the diffusion was considered to limit the inclusion of new material solely and the growth of the crystal depended on the deposition. This theory suggests that crystal growth is a function of supersaturation, X, which itself is a function of temperature T, $X = X(T)$ and hence $G = f(X(T))$. From this theory a relationship describing the change of crystal mass as function of time

$$\frac{dm}{dt} = k \cdot A(C - C_{sat}) \tag{4.1}$$

was derived. Here k is a rate constant, A is the surface area, C is the concentration of solute in solution and C_{sat} is the saturation concentration. The equation was modified to include a diffusion mass transfer element (Nernst, 1904; Myerson, 2002):

$$\frac{dm}{dt} = \frac{D}{d} \cdot A(C - C_{sat}) \tag{4.2}$$

Here D is the diffusion rate and d is the length of the diffusion path.

Later observations indicated that the solution around the growing crystal was supersaturated suggesting that a second step where the solute molecule was integrated into the crystal structure existed. This led to a modification of the theory to a two-stage mechanism: Initial diffusion from the supersaturated solution with mean concentration C through a diffusion layer with mean concentration C_i and separate integration from the diffusion layer into the crystal (Valeton, 1923). Figure 4.1 illustrates the assumptions

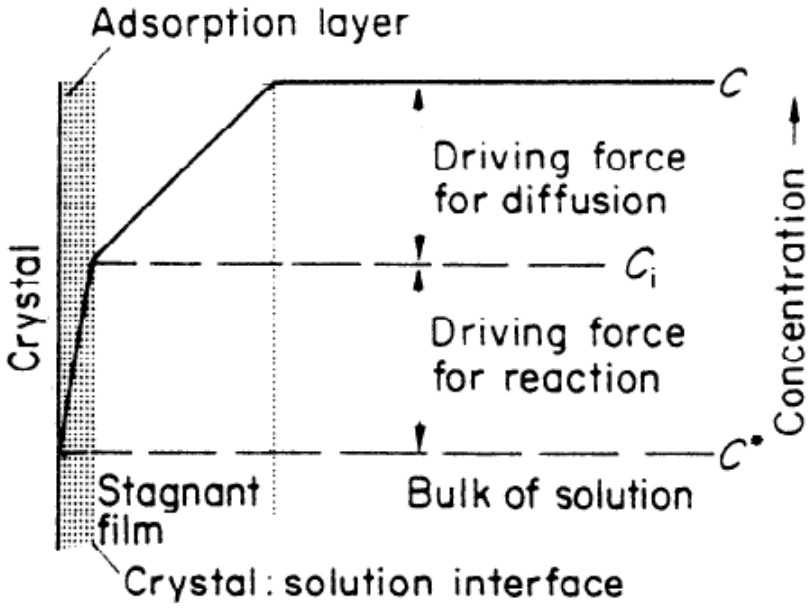

Figure 4.1: *Illustration of the boundary layer and surface of the crystal. The film theory assumes that a crystal has a surface in contact with a boundary layer saturated at the surface of the crystal and with an increasing concentration through a stagnant film forming a boundary layer around the crystals through which solute material has to diffuse to the surface of the crystal to be integrated in the crystal structure. Figure adopted from Mullin (2001)*

The corresponding model can be formulated as (Myerson, 2002)

$$\frac{dm}{dt} = k_{diffusion} \cdot A(C - C_i) \tag{4.3}$$

$$\frac{dm}{dt} = k_{integration} \cdot A(C_i - C_{sat}) \tag{4.4}$$

The two equations can be combined into a single growth expression. The diffusion-reaction scheme theory assumes a first order integration reaction, but this assumption is not necessarily true Mullin (2001). For higher order integration, the equation:

$$\frac{dm}{dt} = k_{integration} \cdot A(C_i - C_{sat})^r \tag{4.5}$$

can be used, where r is the reaction order (Garside, 1985).

In both cases the combined expression becomes:

$$\frac{dm}{dt} = k \cdot A(C - C_{sat})^g \tag{4.6}$$

This expression covers the overall growth of the crystals with k being an overall rate coefficient and g the order of the overall growth process. The expression relates the mass growth of the crystal to the supersaturation as the driving force and indirectly of the mass flow around the crystal through the boundary layer associated with the diffusion.

For a description of the dimensions of the crystal a growth model describing the length growth of the crystal can be related to the mass growth. This dimension based growth is frequently used in the population balance approach. The conversion between the expressions is possible by

$$\frac{dm}{dt} = 3A\frac{\alpha}{\beta}\rho\frac{dL}{dt} \tag{4.7}$$

Here A is the surface area, α is the volume shape factor, β the surface shape factor, ρ the crystal density and L the characteristic length. From eq. (4.6) and eq. (4.7) it is seen that

$$3A\frac{\alpha}{\beta}\rho\frac{dL}{dt} = k \cdot A(C - C_{sat})^g \tag{4.8}$$

$$\frac{dL}{dt} = k\frac{\beta}{3\alpha\rho}(C - C_{sat})^g \tag{4.9}$$

The latter equation (4.9) can be rewritten as

$$G = k_g^{'} \cdot (C - C_{sat})^g \tag{4.10}$$

where G is the length growth rate of the crystals, and k_g' is a rate constant. This growth model is frequently employed in crystallization models (Garside, 1985; Myerson, 2002; Nagy et al., 2008).

Temperature Dependence The growth rate of the crystals has in many systems been found to exhibit temperature dependence where growth rate measurements carried out at equivalent supersaturation show different growth rates at different temperatures. To compensate for this several authors (Rawlings et al., 1993; Myerson, 2002; Ouiazzane et al., 2008) have introduced temperature dependence in the kinetic model, often through an Arrhenius expression for the growth constant.

Transport Phenomena The diffusion through the boundary layer and integration of material into the crystal is dependent on the conditions in the crystallizer.

From the diffusion-reaction theory the combined reaction rate will change as the diffusion conditions change. The effects of the transport phenomena are considered among authors with a series of experiments at different hydro-dynamical conditions. The stirring is considered to be the cause of these effects, and they are often modeled as such. There is a tendency for crystal growth to approach a steady rate as the speed of stirring increased. Several authors (Angelov et al., 2008; Akrap et al., 2012; Hofmann and Raisch, 2012) employ a power expression of the stirring rate ω to account for transport phenomena in a stirred tank vessel.

Apparent Size Dependency The assumption of a growth independent of the size of the crystal in the length direction is known as McCabe's ΔL-law from McCabe and Stevens (1951). Other authors argue that particle size has an effect due to effects from smaller crystals flowing with eddies leaving them in a state with little supersaturation and slow growth (Rawlings et al., 1993; Mersmann, 2001; Mullin, 2001). The effect of smaller crystals having a high surface area to volume ratio and hence lower stability from the Gibbs-Thompson theory is also considered as well as larger crystals being more prone to damaging interactions with their environment and hence greater occurence of growth inducing crystal defects is also a possibility. The clear mechanisms have not been understood fully and rather empirical expressions have been developed to compensate for the observed behaviour.

4.1.2 Specific Terms of the Growth Model

The growth models can be categorized into few classes of models. These models represent growth under a given set of assumptions and different terms can be included to integrate relevant phenomena. An overall general model can be set up combining the phenomena-descriptions employed by different authors. This section describes the way the phenomena have been described

with specific terms for the growth model. The phenomena for the growth model are shown in Figure 4.2. These phenomena are discussed below.

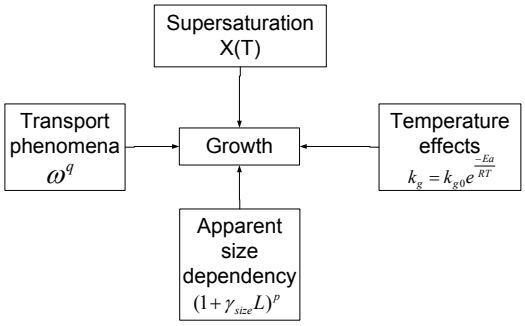

Figure 4.2: *Phenomena governing the crystal growth. The supersaturation is the driving force and temperature effects, apparent size dependency and transport phenomena may be included to account for observed growth rates when modelling.*

Specific Term: Temperature Dependence of kinetics

The employed temperature description for the models is often encountered in the form of an Arrhenius equation (Myerson, 2002):

$$k_g^{'} = k_{g0} \cdot e^{(\frac{-E_a}{RT})} \tag{4.11}$$

E_a is the activation energy, R the gas constant and T the absolute temperature.

As the saturation for the system is temperature dependent as well $(X(T))$, temperature dependence is present in all models for the growth kinetic models.

Specific Term: Transport Phenomena

The transport phenomena may be described by a power expression of the stirring rate or other measureable variable linked to the transport phenomena in the crystallization vessel (Angelov et al., 2008; Akrap et al., 2012; Hofmann and Raisch, 2012):

$$\tau = \omega^q \tag{4.12}$$

Specific Term: Apparent Size Dependency

The apparent size dependent growth has been studied by several authors. An empirical model term has been developed based on their observations (Nagy and Aamir, 2012):

$$\phi = (1 + \gamma_{size} L)^p \tag{4.13}$$

where γ_{size} and p are parameters and L is the characteristic size of the crystal. The description is used with the expression for length growth to describe the occurrence of apparent size dependent growth. Nagy and Aamir (2012) note: "It is important to note that the size dependent growth used is an apparent expression, i.e., it should be considered as a generic empirical expression which is often used to describe the experimentally observed evolution of the CSD, which may be the result of actual size dependent growth, growth rate dispersion or a combination of both as well as other mechanisms" (Nagy and Aamir, 2012).

General Growth Model with Specific Terms

Collecting the terms describing the different phenomena into the diffusion-reaction model yields a general model:

$$G = (k^{'})(X^{'})(\phi)(\tau) \tag{4.14}$$

Substituting each term on the right hand side of Equation (4.14) the following is obtained:

$$G = k_{g0} \cdot e^{(\frac{-E_a}{RT})} \cdot (X(T))^g \cdot (1 + \gamma_{size} L)^p \omega^q \tag{4.15}$$

The function $X(T)$ is given in different forms. This general model combines the phenomena related models and can be adapted to describe the growth involving each of the phenomena models for a desired application.

Model analysis

The general growth model Equation (4.15) has a set of process variables and parameters. This set is called $\underline{\theta} = (\underline{\theta_1}, \underline{\theta_2}, \underline{\theta_3}, \underline{\theta_4})$ and subsets are characterized by the variable type as

System parameters	$\underline{\theta_1}$	(4.16)
Process variables	$\underline{\theta_2}$	(4.17)
Model parameters	$\underline{\theta_3}$	(4.18)
Universal Constants	$\underline{\theta_4}$	(4.19)

Using the above variable classification the model parameters of the growth model Equation (4.15) are listed as:

Known variable	$\in \theta_i$	Description	Unit
k_{g0}	θ_1	rate constant	unit length pr. unit time
R	θ_4	Universal gas constant	$\frac{J}{mol \cdot K}$
E_a	θ_1	Activation energy	$\frac{J}{mol}$
T	θ_2	Absolute temperature	K
g	θ_1	Growth exponent	$-$
γ_{size}	θ_1	Growth length constant	pr. unit length
p	θ_1	Apparent size exponent	
ω	θ_2	Stirring rate	Revolutions pr. time
q	θ_1	Stirring rate exponent	$-$

The system parameters $\underline{\theta_1}$ and model parameters $\underline{\theta_3}$ need to be known before the growth model can be used. That is, these parameters need to be regressed with suitable experimental data before the growth model can be used.

The process variables define the condition at which the crystallizer is operated, and thus, the conditions at which the growth must be determined.

Calculation Procedure

The calculation procedure for the growth model is given as follows:

1. Specify (retrieve from library) growth model with appropriate phenomena from Equation (4.15)
2. Specify (retrieve from library) system parameters $\underline{\theta_1}$ and universal constants $\underline{\theta_4}$

3. Specify process variables $\underline{\theta_2}$
4. Specify (retrieve from library) model parameters $\underline{\theta_3}$ (such as parameters in thermodynamical models not relating to the chemical system)
5. Calculate supersaturation X at relevant temperature and composition using the appropriate Equations (2.2) - (2.4). If the saturation model is explicit X is calculated directly (equilibrium composition is initially unknown). If the model involves an implicit saturation model, such as an activity coefficient model, X is calculated through an iterative procedure where X satisfies the SLE condition (activity coefficients and equilibrium composition are initially unknown).
6. For all datapoints repeat from step 3 with new values of θ_2, then new values of θ_3 for step 4 until all datapoints are calculated.
7. Calculate growth G through the specified model from eq. (4.15)

The calculation procedure if the supersaturation is calculated from an activity model and an SLE-condition (solid-liquid equilibrium) is:

1. Give activity model
2. Give equilibrium equation
3. Specify accepted *error* in x_{eq} and stepsize α
4. Specify a temperature
5. Give initial estimate for x_{eq}
6. Calculate $\gamma_{eq,estimate}$ through activity coefficient model and activity $a_{eq,estimate}$ through equilibrium equation
7. Calculate new $x_{eq,estimate}$ from $\frac{a_{eq,estimate}}{\gamma_{eq,estimate}}$.
8. if $\left(x^{calculated}_{eq,estimate} - x^{specified}_{eq,estimate}\right) \leq error$ STOP and go to 10. Else continue
9. Give new $x_{eq,estimate} = x^{specified}_{eq,estimate} + \alpha\left(x^{calculated}_{eq,estimate} - x^{specified}_{eq,estimate}\right)$ and repeat from 6
10. Calculate x and supersaturation

4.1.3 Generation of Growth Models

The general model (Equation (4.15)) combines the different phenomena with the relevant terms. For a given application the relevant terms are selected by the modeler. The selection procedure is shown in the diagram (see Figure 3.2). For the generation of a growth model the selected path in the diagram is highlighted in Figure 4.3

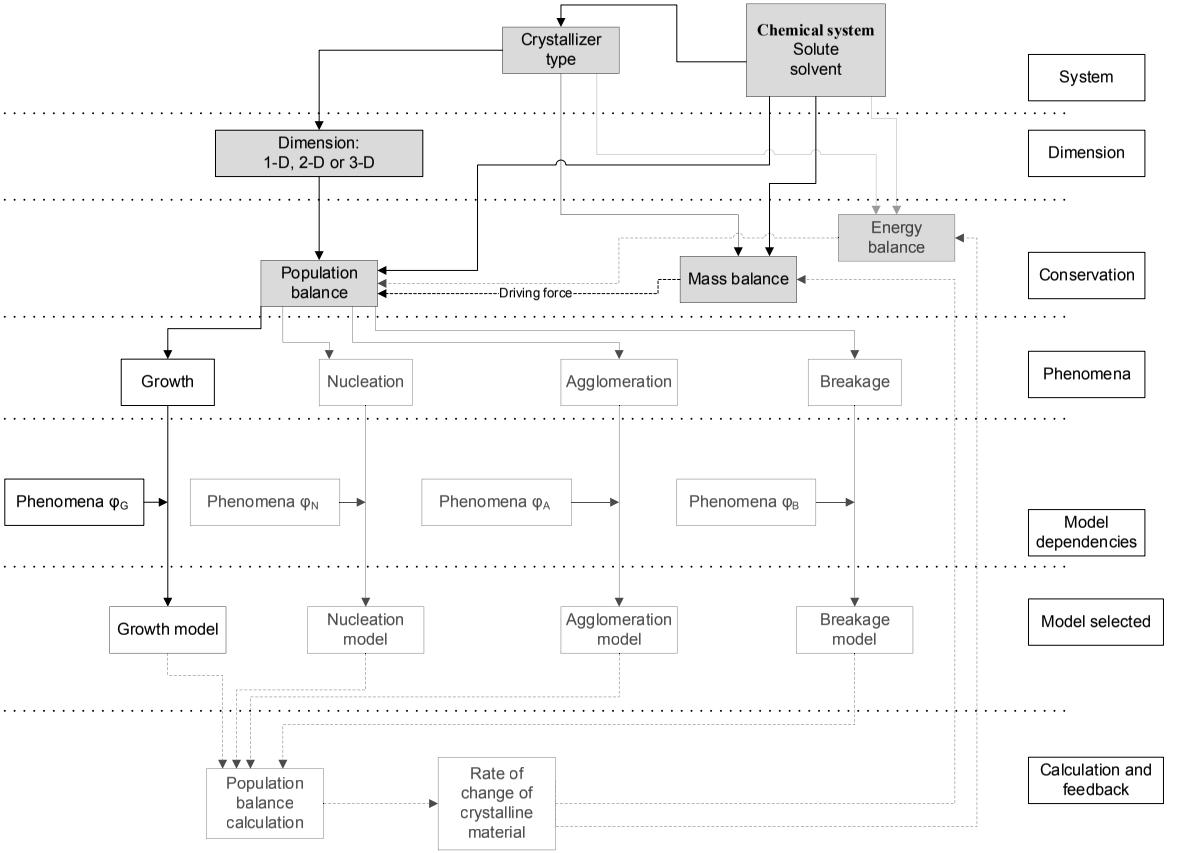

Figure 4.3: *The procedure for model generation and use highlighted from figure 3.2. Following the path, a growth model including the relevant phenomena ϕ_i (temperature effects, apparent size dependency and transport phenomena) may be generated*

Example 1: Sucrose

This example is based on Ouiazzane et al. (2008).

System The chemical system under study is the sucrose-water system. The equipment used is a stirred batch vessel with a jacket to control the temperature in the system. A saturated solution is cooled from 70 °C to 40 °C. The supersaturation is modeled as the thermodynamical supersaturation.

Model Objective The objective of the model is to describe growth in a sucrose cooling crystallization with thermodynamical driving force, accounting for temperature effects.

Assumptions Based on the model objective, a set of assumptions is made (Ouiazzane et al., 2008). These assumptions are formulated here as:

- Nucleation and growth are the dominant phenomena (change in particle size stems from growth)
- The growth is temperature dependent
- The growth is independent of size (no apparent size dependency)
- Transport phenomena are near constant and changes have negligible effect

Kinetics The growth kinetics are investigated. For this system temperature dependent growth is assumed and the crystals are assumed to grow independent of size (no apparent size dependency). The effect of transport phenomena is not considered and the variation of transport properties is neglected. From the above phenomena descriptions model terms can be included to generate the appropriate model. The phenomena model terms are:

Phenomena	Model term	Used	Not used	
Temperature dependence	$e^{(\frac{-E_a}{RT})}$	*		(4.20)
Apparent Size dependency	$(1+\gamma_{size}L)^p$		*	(4.21)
Transport phenomena	ω^q		*	(4.22)
Supersaturation	$\left(\frac{\gamma x - \gamma_{eq} x_{eq}}{\gamma_{eq} x_{eq}}\right)$	*		(4.23)

The selected path in diagram 3.2 is shown in 4.3 .

The supersaturation description relies on a thermodynamic description by Peres and Macedo (1996) and investigated by Ouiazzane et al. (2008). The system is bi-component and no subscript is used to indicate the solute compound. The description of the model and the calculation procedure is given here (Peres and Macedo, 1996):

A modified UNIQUAC model is derived for the sucrose-water system. The model can be used for the description of SLE where the UNIQUAC model is used to calculate the activity coefficients for a mixture. The model combines an expression for the combinatorial $\ln\gamma_i^C$ and residual $\ln\gamma_i^R$ contributions (Ouiazzane et al., 2008):

$$\ln\gamma_i = \ln\gamma_i^C + \ln\gamma_i^R \tag{4.24}$$

The combinatorial part is given by (Ouiazzane et al., 2008):

$$\ln\gamma_i^C = \ln\left(\frac{\phi_i}{x_i}\right) + 1 - \frac{\phi_i}{x_i} \tag{4.25}$$

where

$$\phi_i = \frac{x_i \cdot r_i^p}{\sum_j x_j \cdot r_j^p} \tag{4.26}$$

Thermodynamical model parameters for the combinatorial part are taken from Ouiazzane et al. (2008) and Peres and Macedo (1996) and shown below.

Parameter	Value	$\in \underline{\theta_i}$
p	$\frac{2}{3}$	$\underline{\theta_3}$
r_{water}	0.92	$\underline{\theta_1}$
$r_{sucrose}$	14.5496	$\underline{\theta_1}$

The residual part is given by (Ouiazzane et al., 2008):

$$\ln\gamma_i^R = q_i \cdot \left(1 - \ln\sum_j \theta_j\tau_{ji} - \sum_j \frac{\theta_j\tau_{ij}}{\sum_k \theta_k\tau_{kj}}\right) \tag{4.27}$$

where

$$\theta_i = \frac{x_i \cdot q_i}{\sum_j x_j \cdot q_j} \tag{4.28}$$

and

$$\tau_{ij} = e^{\left(\frac{-a_{ij}}{T}\right)} \tag{4.29}$$

The temperature dependence of the thermodynamical interaction parameters is given for the components as:

$$a_{ij}(T) = A1_{ij} + A2_{ij}(T - 298.15K) \tag{4.30}$$

Here $T = 298.15K$ is used as reference temperature and the relevant parameters are (Peres and Macedo, 1996)

Parameter	Value	$\in \underline{\theta_i}$
$A1_{sucrose-water}$	-89.3391	$\underline{\theta_1}$
$A2_{sucrose-water}$	0.3280	$\underline{\theta_1}$
$A1_{water-sucrose}$	118.9952	$\underline{\theta_1}$
$A2_{water-sucrose}$	-0.3410	$\underline{\theta_1}$

The parameters q_i are (Peres and Macedo, 1996):

Parameter	Value	$\in \underline{\theta_i}$
$q_{sucrose}$	13.764	$\underline{\theta_1}$
q_{water}	1.4	$\underline{\theta_1}$

With the stated parameters it is possible to calculate the activity coefficients for the sucrose-water system. At this point the equilibrium condition is introduced

Equilibrium Condition For the equilibrium condition Peres and Macedo (1996) stated that the activity for the sucrose must obey:

$$\ln \gamma_{eq} x_{eq} = \left(-\frac{\Delta H_f}{R} + \frac{\Delta A - \Delta B T_{ref}}{R} T_m + \frac{\Delta B}{2R} T_m^2 \right) \left(\frac{1}{T} - \frac{1}{T_m} \right) + \frac{\Delta A - \Delta B T_{ref}}{R} \ln \frac{T}{T_m} + \frac{\Delta B}{2R} (T - T_m) \tag{4.31}$$

Model parameters for the sucrose-water system are taken from Peres and Macedo (1996). The parameters are:

Parameter	Value	Unit	$\in \underline{\theta_i}$
ΔH_f	46187	$\frac{J}{mol \cdot K}$	$\underline{\theta_1}$
ΔA	316.1153	$\frac{J}{mol \cdot K}$	$\underline{\theta_1}$
ΔB	-1.1547	$\frac{J}{mol \cdot K^2}$	$\underline{\theta_1}$
T_{ref}	298.15	K	$\underline{\theta_1}$
T_m	459.15	K	$\underline{\theta_1}$

With the stated models the equilibrium activity can be calculated through an iterative procedure:

1. Give activity model: Equation (4.24)
2. Give equilibrium equation: Equation (4.31)
3. Specify accepted *error* in x_{eq} and stepsize α
4. Specify a temperature
5. Give initial estimate for x_{eq}
6. Calculate $\gamma_{eq,estimate}$ through activity coefficient model and activity $a_{eq,estimate}$ through equilibrium equation
7. Calculate new $x_{eq,estimate}$ from $\frac{a_{eq,estimate}}{\gamma_{eq,estimate}}$.
8. if $\left(x^{calculated}_{eq,estimate} - x^{specified}_{eq,estimate}\right) \leq error$ STOP and go to 10. Else continue
9. Give new $x_{eq,estimate} = x^{specified}_{eq,estimate} + \alpha\left(x^{calculated}_{eq,estimate} - x^{specified}_{eq,estimate}\right)$ and repeat from 6
10. Calculate x and supersaturation

As the equilibrium conditions have been calculated it is now possible to define the supersaturation as

$$X = \left(\frac{\gamma x - \gamma_{eq} x_{eq}}{\gamma_{eq} x_{eq}}\right) \tag{4.32}$$

The general growth model is (4.15) and under the stated assumptions it is reduced to:

$$G = k_{g0} \cdot e^{\left(\frac{-E_a}{RT}\right)} \cdot \left(\frac{\gamma x - \gamma_{eq} x_{eq}}{\gamma_{eq} x_{eq}}\right)^g \tag{4.33}$$

This model describes the linear growth of the crystals as a function of the thermodynamic supersaturation accounting for temperature dependence.

Calculation Procedure The calculation procedure (given in section 4.1.2 is followed.

Initially all system parameters ($\underline{\theta_1}$) and universal constants $\underline{\theta_4}$ are specified.

Variables and Parameters The growth is function of the two variables composition (X) and temperature (T). A set of parameters are needed as well. These are:

Parameter	θ	Value
k_{g0}	θ_1	2.24 m/min
R	θ_4	8.314 $J/(molK)$
E_a	θ_1	46.5 kJ/mol
g	θ_1	1

The growth is calculated for varying temperatures and initial concentrations. The process variable (temperature) and initial concentration $\underline{\theta_2}$ are set accordingly.

The supersaturation is calculated next. For this procedure the equilibrium is initially calculated using the modified UNIQUAC equation using the procedure above

1. Give activity model: eq. (4.24)
2. Give equilibrium equation: eq. (4.31)
3. Specify accepted $error = 0.01$ in x_{eq} and stepsize α
4. Specify a temperature: T=300 K
5. Initial estimate for $x_{sucrose,eq} = 0.1$
6. Calculate $\gamma_{sucrose} = 0.539$ through activity coefficient model (4.24) and $activity_{sucrose,eq} = 0.019$ through SLE-equation (4.31)
7. Calculate new $x_{sucrose,eq}$ from $\frac{a_{sucrose}}{\gamma_{sucrose}} = \frac{0.019}{0.539} = 0.035$.
8. if $\left(x^{calculated}_{sucrose,eq} - x^{specified}_{sucrose,eq}\right) \leq 0.01$ STOP and go to 10. Else continue
9. Give new $x_{eq,estimate} = x^{specified}_{eq,estimate} + \alpha\left(x^{calculated}_{eq,estimate} - x^{specified}_{eq,estimate}\right)$ and repeat from 6
10. Calculate x and supersaturation

The activity coefficients are calculated through the modified UNIQUAC model Equation (4.24). With this model implemented the growth expression becomes explicit and the growth can be calculated.

Calculation Example The growth of a crystal in a slightly supersaturated sucrose solution at $T = 300K$ is calculated. The models for activity Equation (4.24) and eq. (4.31) are used. Error is specified as $error = 0.01$ in x_{eq}. An initial estimate of the equilibrium is given as $x_{sucrose,eq} = 0.1$, from which $\gamma_{sucrose} = 0.539$ is calculated and an activity of $activity_{sucrose,eq} = 0.019$ through SLE-equation (4.31). A new estimate of $x_{sucrose,eq}$ is set by $\alpha = 0.5$: $x^{new}_{sucrose,eq} = 0.1 + 0.5(0.035 - 0.1) = 0.068$ At this point the process is automated and $x_{sucrose,eq}$ converges to $x_{sucrose,eq} = 0.0601$ With this $\gamma_{sucrose,eq} = 0.3205$ is calculated. The solution is assumed to be supersaturated at 1.5% increase in $x_{sucrose}$. $x_{sucrose} = 1.015 \cdot x_{sucrose,eq} = 0.061$. At this point the activity coefficient is calculated as $\gamma_{sucrose} = 0.3254$. The supersaturation is calculated from Equation (4.32). At $T = 300K$ and $x_{sucrose} = 0.061$

$$X = \left(\frac{\gamma x - \gamma_{eq} x_{eq}}{\gamma_{eq} x_{eq}} \right) = \left(\frac{0.3254 \cdot 0.061 - 0.3205 \cdot 0.0601}{0.3205 \cdot 0.0601} \right) = 0.0299$$

Using the parameters, the sucrose growth,$G_{sucrose}$, is calculated from eq. (4.33). At $T = 300K$ and $X = 0.0299$

$$\begin{aligned} G_{sucrose} &= k_{g0} \cdot e^{\left(\frac{-E_a}{RT}\right)} \cdot (X)^g \\ &= 2.24 m/min \cdot e^{\left(\frac{-46.5 \cdot 10^3 J/mol}{8.314 J/(mol \cdot K) 300K}\right)} \cdot (0.0299)^1 \\ &= 5 \cdot 10^{-10} m/min \end{aligned}$$

A set of temperature and supersaturation values are specified and the growth rate calculated for the different initial concentrations. The calculated values are specified in Table 4.1 and a plot of the resulting growth rates is shown in Figure 4.4:

Table 4.1: *Sucrose growth function responding to temperature and saturation*

Known		Unknown				
T	$x_{sucrose}$	γ_{eq}	x_{eq}	$\gamma_{sucrose}$	X	$G_{sucrose}$
K	-	-	-	-	-	nm/min
300	0.061	0.3205	0.0601	0.3254	0.0299	0.5
300	0.063	0.3205	0.0601	0.3371	0.1017	1.8
300	0.066	0.3205	0.0601	0.3545	0.2138	3.8
300	0.069	0.3205	0.0601	0.3718	0.3310	5.9
300	0.071	0.3205	0 0.0601	0.3833	0.4118	7.4
300	0.073	0.3205	0.0601	0.3947	0.4948	8.9
300	0.076	0.3205	0.0601	0.4117	0.6232	11.2
320	0.073	0.3832	0.0712	0.3937	0.0540	3.1
320	0.076	0.3832	0.0712	0.4107	0.1446	8.3
320	0.079	0.3832	0.0712	0.4274	0.2385	13.7
320	0.082	0.3832	0.0712	0.4440	0.3354	19.3
320	0.085	0.3832	0.0712	0.4604	0.4353	25.0
320	0.088	0.3832	0.0712	0.4765	0.5380	30.9
320	0.091	0.3832	0.0712	0.4924	0.6434	37.0
340	0.090	0.4771	0.0883	0.4862	0.0390	6.3
340	0.093	0.4771	0.0883	0.5019	0.1083	17.4
340	0.096	0.4771	0.0883	0.5173	0.1792	28.8
340	0.100	0.4771	0.0883	0.5375	0.2762	44.4
340	0.103	0.4771	0.0883	0.5523	0.3507	56.4
340	0.106	0.4771	0.0883	0.5668	0.4265	68.6
340	0.113	0.4771	0.0883	0.5995	0.6084	97.8

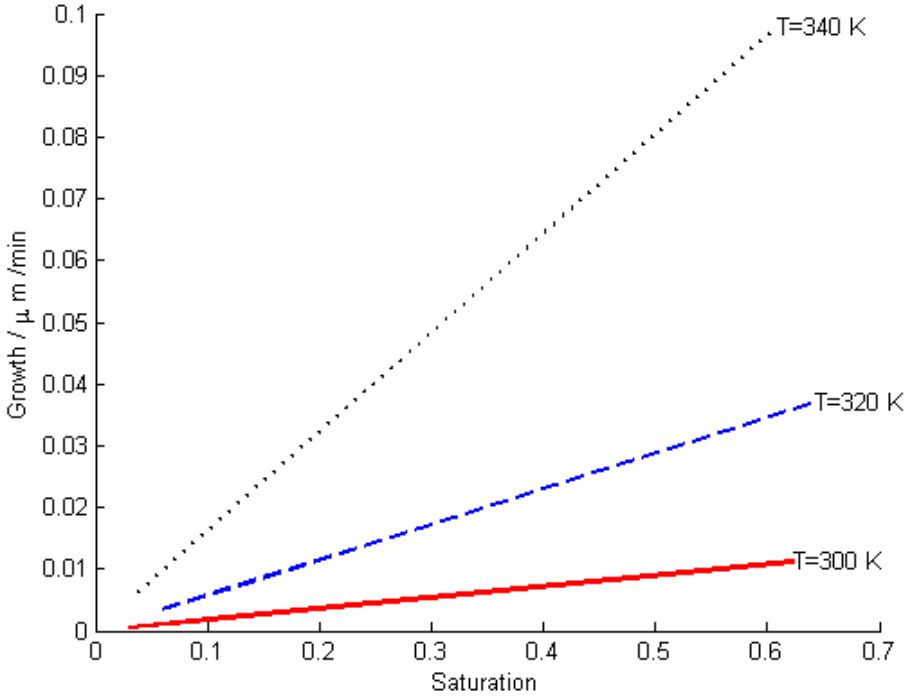

Figure 4.4: *Plot of the growth function for different temperatures as function of supersaturation. The plots are based on the conditions presented in table 4.1*

As illustrated in Figure 4.4 the growth response to increased supersaturation in the growth model is linear due to the assumed growth order of $g = 1$. The assumption is based on the diffusion of solute being the dominant effect for transport of material to the crystal surface as discussed in section 4.1.1. From the model, the order of growth is low and with common values for a nucleation order, the nucleation would be dominant at increased supersaturation. Extrapolation of the model to increased values of supersaturation not encountered in the original experiment should be done with utmost care and rather a new growth model should be derived with evaluation of the assumption of linear ($g = 1$) growth.

The response to change in temperature is an exponential decrease due to the Arrhenius expression used for the temperature dependence. This shows that the kinetic constant ($k_g = k_{g0} \cdot e^{\left(-\frac{Ea}{RT}\right)}$) will increase with increased temperature. This increase in growth will for a realistic process be counteracted by a decrease in supersaturation as the saturation concentration is increased at increased temperatures.

Population Balance for Growth of Sucrose

A series of distributions of particles, for which the growth is applied, is defined. This allows the kinetic model to be visualized with a distribution. Selecting the kinetic model and calculating the growth for a distribution defined in 25 classes with particles in class [10;14]:

$$N(10) = 50$$
$$N(11) = 60$$
$$N(12) = 70$$
$$N(13) = 60$$
$$N(14) = 50$$

The distribution grows as illustrated in Figure 4.5

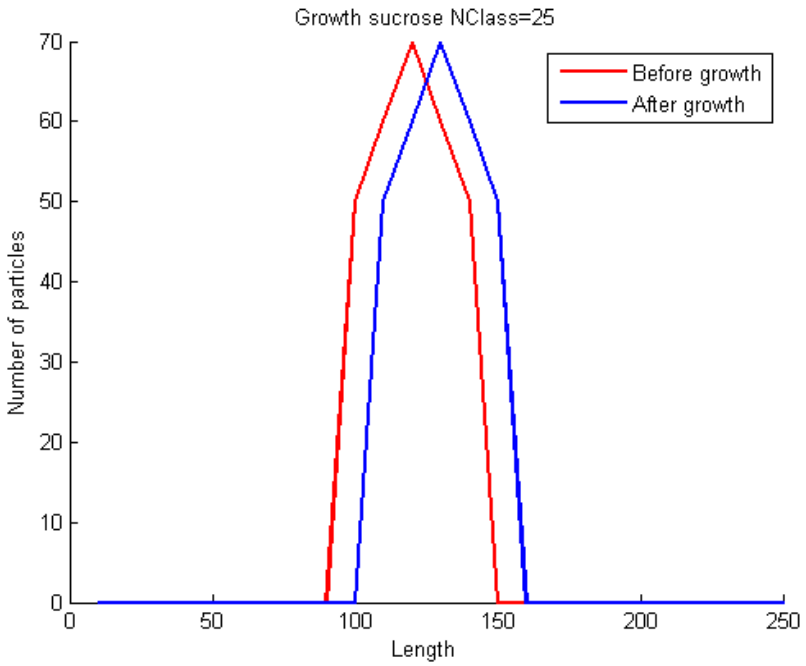

Figure 4.5: *The sucrose water system and a growth model. The distribution is moving as a result of the growth. Kinetic model* $G = k_g \cdot e^{\frac{-E_a}{RT}} \cdot S^g$

Example 2: Paracetamol

This example is based on Worlitschek and Mazzotti (2004).

System The chemical system under study is the paracetamol-ethanol system. The equipment used is a stirred batch vessel with a jacket to control the temperature in the system. The supersaturation is modeled as the absolute supersaturation.

Model Objective The objective of the model is to describe growth in a paracetamol cooling crystallization while accounting for temperature effects. The model should account for the saturation measured with the supersaturation ΔC, where a constant supersaturation is desired.

Assumptions Based on the model objective, a set of assumptions is made (Worlitschek and Mazzotti, 2004). These assumptions are formulated here as:

- Nucleation and growth are the dominant phenomena
- The growth is temperature dependent
- The growth is independent of size (no apparent size dependency)
- Transport phenomena are near constant and changes have neglectable effect

Kinetics The system under study is assumed to have nucleation and growth as dominant phenomena and other phenomena are not considered.

The growth kinetics are investigated. For this system temperature dependent growth is assumed. The crystals are assumed to grow independent of size (no apparent size dependency) and the effect of transport phenomena is not considered.

Phenomena	Model term	Used	Not used	
Temperature dependence	$e^{(\frac{-E_a}{RT})}$	$*$		(4.34)
Apparent Size dependency	$(1+\gamma_{size}L)^p$		$*$	(4.35)
Transport phenomena	ω^q		$*$	(4.36)
Supersaturation	ΔC	$*$		(4.37)

The general model is eq. (4.15) and under the stated assumptions it is reduced to:

$$G = k_{g0} \cdot e^{\left(\frac{-E_a}{RT}\right)} \cdot (\Delta C)^g \tag{4.38}$$

Supersaturation description The saturation model is taken from Worlitschek and Mazzotti (2004). According to this study the saturation C_{sat} in kg/kg can be described by

$$C_{sat} = a_1 \cdot e^{a_2 T} \tag{4.39}$$

Where

Parameter	Value	
a_1	$2.955 \cdot 10^{-4} kg/kg$	(4.40)
a_2	$2.179 \cdot 10^{-2} K^{-1}$	(4.41)

A plot of this supersaturation function is shown in figure 4.6.

Calculation Procedure The calculation procedure (section 4.1.2 is followed.

Variables and parameters Specifying the relevant parameters:

Parameter	θ	Value
k_{g0}	θ_1	$21 m/s(m^3/mol)^{1.9}$
R	θ_4	$8.314 J/(molK)$
E_a	θ_1	$41.6 kJ/mol$
g	θ_1	1.9

The growth is a function of the two variables concentration (C) and temperature (T).

The growth is calculated for varying temperatures and absolute supersaturations. The process variable temperature is set accordingly. The supersaturation is specified as well.

Calculation Example Temperature is specified at 280 K and the supersaturation is specified at 1.0 mol paracetamol/m^3 solution. The growth is calculated from Equation (4.38). At $T = 280K$ and $X = 1.0$ mol paracetamol/m^3

Temperature K	**Saturation concentration** kg paracetamol/ kg ethanol
280	0.1319
285	0.1471
290	0.1640
295	0.1829
300	0.2040
305	0.2274
310	0.2536
315	0.2828
320	0.3154
325	0.3517
330	0.3921
335	0.4373
340	0.4876
345	0.5437
350	0.6063

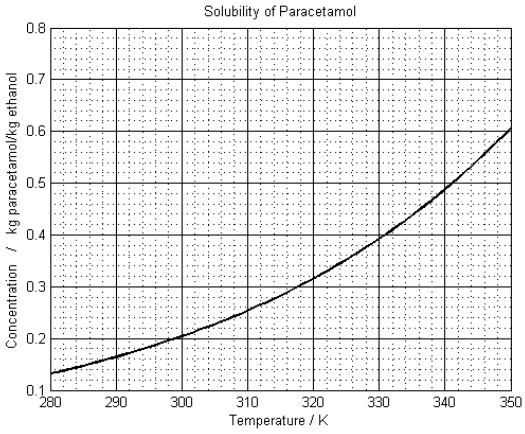

Figure 4.6: *The solubility of paracetamol in ethanol as function of temperature. The plot follows Equation* (4.38) *for temperatures specified next to the plot*

$$
\begin{aligned}
G_{Paracetamol} &= k_{g0} \cdot e^{\left(\frac{-E_a}{RT}\right)} \cdot X^g \\
&= 21 m/s (m^3/mol)^{1.9} \cdot e^{\left(\frac{-41.6 \cdot 10^3}{8.314 J/(mol \cdot K) 280 K}\right)} \cdot (1.0 mol/m^3)^{1.9} \\
&= 3.64 \cdot 10^{-7} m/s
\end{aligned}
$$

Using this procedure a set of values can be calculated as shown in Table 4.2:

Table 4.2: *Paracetamol growth values as function of temperature and supersaturation*

Known		Unknown	
T	C	C_{sat}	$G_{Paracetamol}$
K	mol/m^3	mol/m^3	$\mu m/min$
280	1.132	0.1319	0.3642
290	1.164	0.164	0.6745
300	1.204	0.2040	1.199
310	1.254	0.2536	2.053
320	1.315	0.3154	3.400
330	1.392	0.3921	5.461
340	1.488	0.4876	8.530
350	1.6063	0.6063	12.99
280	2.132	0.1319	1.359
290	2.164	0.164	2.517
300	2.204	0.2040	4.474
310	2.254	0.2536	7.663
320	2.315	0.3154	12.69
330	2.392	0.3921	20.38
340	2.488	0.4876	31.83
350	2.6063	0.6063	48.47
280	3.132	0.1319	2.937
290	3.164	0.164	5.439
300	3.204	0.2040	9.667
310	3.254	0.2536	16.56
320	3.315	0.3154	27.42
330	3.392	0.3921	44.03
340	3.488	0.4876	68.78
350	3.6063	0.6063	104.7

Plotting the growth expression under these conditions the effect of the changing variables (Temperature, concentration) can be seen. This is shown in Figure 4.7.

The growth expression of paracetamol includes an exponent $g = 1.9$, which is near second order growth. For the high supersaturation values, this results in high growth rates, however, nucleation could well take place here and the validity of the growth rate model in this area should be explored

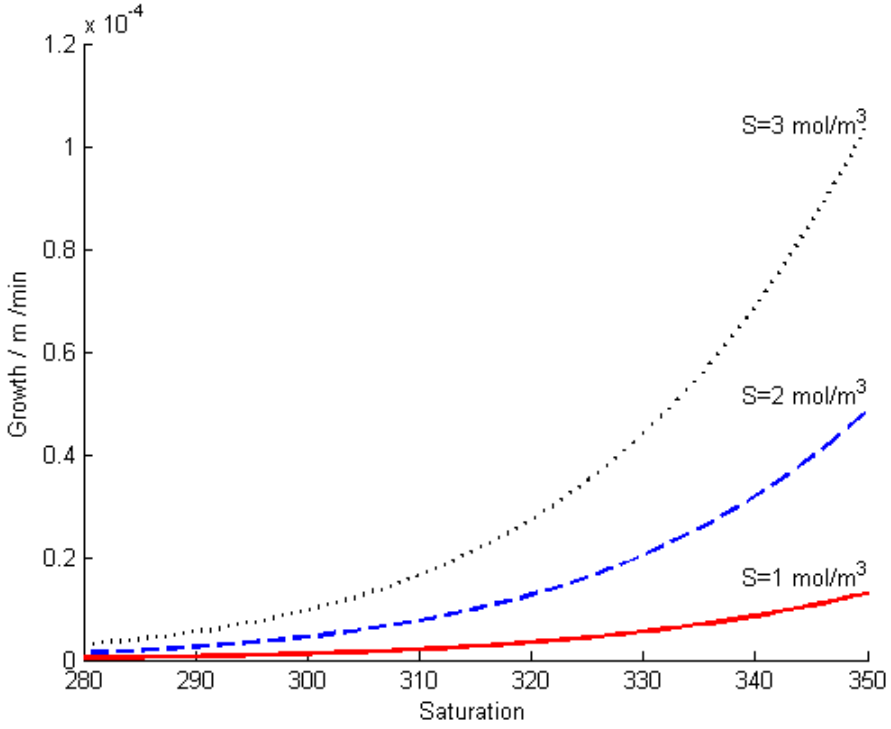

Figure 4.7: *The growth rate expression of paracetamol in ethanol at different conditions. The growth rate expression is plotted alone and no competing phenomena are considered. The growth expression of paracetamol includes an exponent* $g = 1.9$*, which results in high growth rate at increased supersaturation. Nucleation could well take place here and the validity of the growth rate model in this area should be explored*

Example 3: DL-threonine

This example is based on Angelov et al. (2008).

System The chemical system under study is the DL-threonine-water system. The equipment used is a stirred batch vessel with a jacket to control the temperature in the system. The supersaturation is modeled as the relative supersaturation based on mass.

Model Objective The objective of the model is to describe growth in a DL-threonine cooling crystallization accounting for temperature effects and transport phenomena. Specifically transport phenomena are investigated at different conditions.

Assumptions Based on the model objective, a set of assumptions is made (Worlitschek and Mazzotti, 2004). These assumptions are formulated here as:

- Nucleation and growth are the dominant phenomena
- The growth is temperature and transport phenomena dependent
- The growth is independent of size (no apparent size dependency)
- Transport phenomena can be modeled through the stirring

Kinetics The system under study is assumed to have nucleation and growth as dominant phenomena and other phenomena are not considered.

The growth kinetics are investigated. For this system temperature dependent growth is assumed and the effect of transport phenomena is considered. The crystals are assumed to grow independent of size (no apparent size dependency).

Phenomena	Model term	Used	Not used	
Temperature dependence	$e^{(\frac{-E_a}{RT})}$	$*$		(4.42)
Apparent Size dependency	$(1+\gamma_{size}L)^p$		$*$	(4.43)
Transport phenomena	ω^q	$*$		(4.44)
Supersaturation	σ	$*$		(4.45)

Supersaturation model The supersaturation parameters are not given specifically in the study. Rather, a mass balance is calculated assuming a subcooling of the system. From this a numerical study is performed with the supersaturation held at $\sigma = 0.2$.

The general model is Equation (4.15) and under the stated assumptions it is reduced to:

$$G_{DL-threonine} = k_{g0} \cdot e^{\left(\frac{-E_a}{RT}\right)} \cdot \sigma^g \cdot \omega^q \tag{4.46}$$

Calculation procedure The calculation procedure (section 4.1.2 p. 27) is followed. First the parameters are specified:

Parameters and Variables The necessary parameters are specified

Parameter	θ	Value
k_{g0}	θ_1	$1.1375 \cdot 10^7 m/min^{0.54}$
R	θ_4	$8.314 J/(molK)$
E_a	θ_1	$75.6 kJ/mol$
g	θ_1	1.9
q	θ_1	0.46

The growth is function of the variables supersaturation (σ), temperature (T) and stirring rate ω. The supersaturation is specified as constant, whereas the temperature and stirring are varied.

Calculation Example Temperature is specified at 300 K and the supersaturation is specified at $\sigma = 0.2$. The stirring rate is held at $\omega = 100 rpm$. At $T = 300K$, $\omega = 100 rpm$ and $\sigma = 0.2$:

$$\begin{aligned} G_{DL-threonine} &= k_{g0} \cdot e^{\left(\frac{-E_a}{RT}\right)} \cdot \sigma^g \cdot \omega^q \\ &= 1.1375 \cdot 10^7 m/min^{0.54} \cdot e^{\left(\frac{-75.6 \cdot 10^3}{8.314 J/(mol \cdot K) 300K}\right)} \cdot 0.2^{1.9} \cdot (100 min^{-1})^{0.46} \\ &= 1.30 \cdot 10^{-6} m/s \end{aligned}$$

Using this procedure a set of values can be calculated as shown in Table 4.3:

Table 4.3: *DL-threonine growth values as function of temperature and stirring at a supersaturation of* $\sigma = 0.2$

Known			Unknown
T	ω	σ	$G_{DL-threonine}$
K	min^{-1}	-	$\mu m/min$
300	100	0.2	1.30
300	200	0.2	1.79
300	300	0.2	2.15
300	400	0.2	2.46
300	500	0.2	2.72
300	600	0.2	2.96
300	700	0.2	3.18
300	800	0.2	3.38
320	100	0.2	8.63
320	200	0.2	11.9
320	300	0.2	14.3
320	400	0.2	16.3
320	500	0.2	18.1
320	600	0.2	19.7
320	700	0.2	21.1
320	800	0.2	22.5
340	100	0.2	45.9
340	200	0.2	63.2
340	300	0.2	76.1
340	400	0.2	86.9
340	500	0.2	96.3
340	600	0.2	105
340	700	0.2	112
340	800	0.2	120

The stirring rate influences the growth rate of the crystals as the diffusion through the boundary layer and subsequent integration of material into the crystal is dependent on the conditions in the crystallizer. The tendency for crystal growth to approach a steady rate as the velocity of the crystallization medium is increased is approximated through the power expression for the effect of stirring where the exponent is 0.46, resulting in a flattening curve for the effect. Figure 4.8 shows this effect as the curves flatten.

Growth of single particles

The growth of single particles where a single particle is assigned to each class is investigated with the model. In this case the model describes how the particles move and can ultimately end

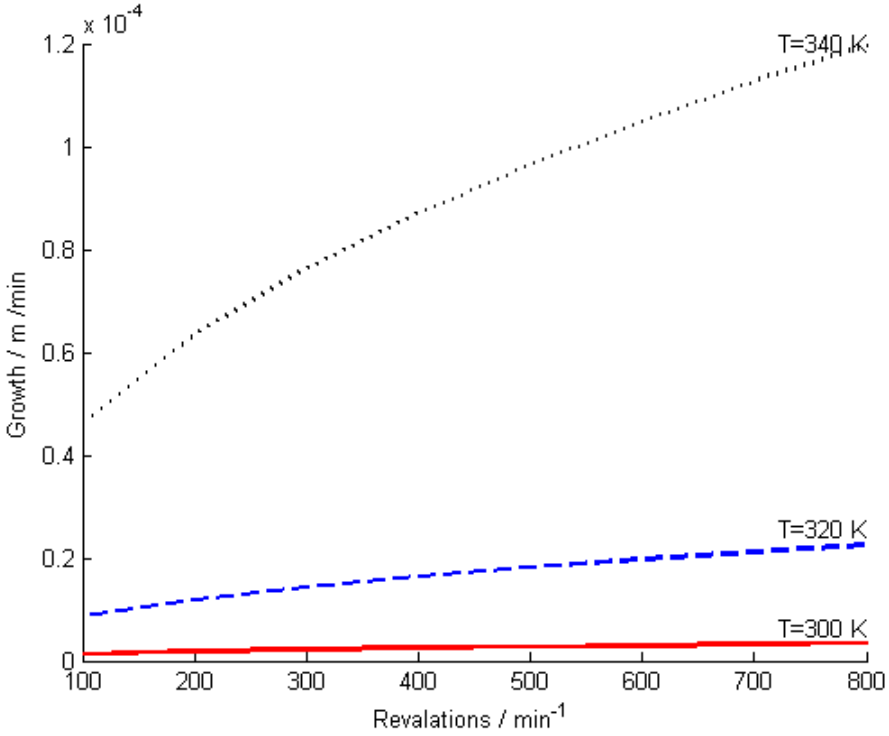

Figure 4.8: *The growth of DL-threonine as function of stirring rate. The tendency for crystal growth to approach a steady rate as the velocity of the crystallization medium is increased is approximated through the power expression for the effect of stirring where the exponent is* 0.46*, resulting in a flattening curve for the effect. Temperature dependence is included in the model and the distance between the curves for 340 K and 320 K compared to the distance between 300K and 320 K increases notably*

in the final bin. An example with a single particle is shown in Figure 4.9

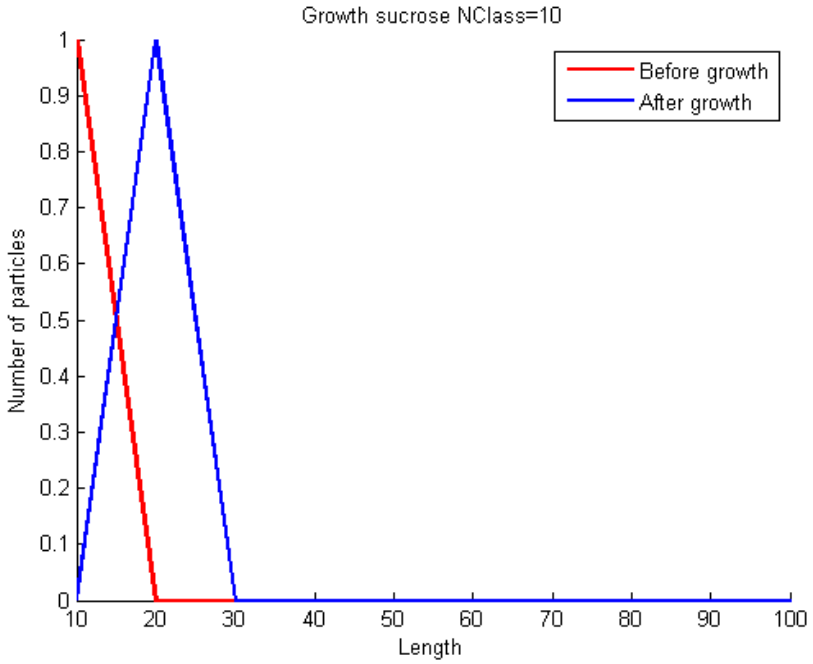

Figure 4.9: *Growth of single particle. A single particle moves from one bin to another as it grows. This behavior can be seen with multiple particles as well. Growth of multiple particles is shown in figure 4.10. Here, the particles are initially distributed in the size range and grow. The limited range of classes results in multiple particles being caught in the final bin.*

Here, a single particle moves from one bin to another as it grows. This behavior can be seen with multiple particles as well. Growth of multiple particles is shown in figure 4.10. Here, the particles are initially distributed in the size range and grow. The limited range of classes results in multiple particles being caught in the final bin.

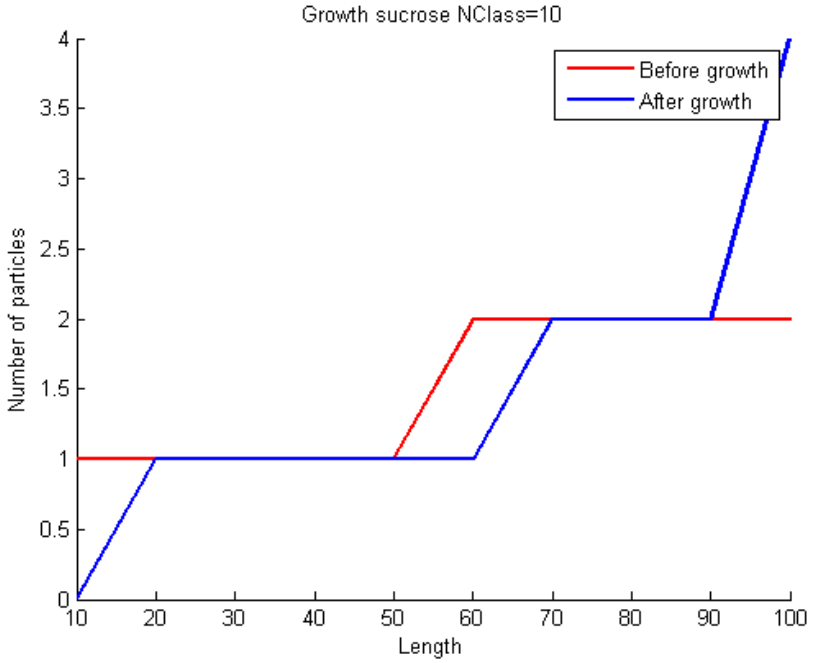

Figure 4.10: *Particles assigned in each class grow to larger classes. The class system captures the movement of particles to larger classes, but may capture all particles in the final bin.*

4.2 Nucleation Models

Nucleation is the formation of a new nucleus, which can involve several mechanisms. The nucleation types can be divided into primary and secondary nucleation depending on whether other crystals are involved or not. The absence or presence of crystals can occasionally be difficult to detect and apparent heterogenous nucleation can be secondary nucleation (Nývlt et al., 1985). There is no general agreement on nomenclature for the nucleation terms, the use of primary and secondary here is following the definitions set by Mullin (2001).

4.2.1 Nucleation Theory

The nucleation phenomena have been studied by authors in the 1930's and 1940's where a classical nucleation theory has been formulated (Mullin, 2001). This theory has been developed on the basis of condensation of vapour, however, the treatment is extended to a solute forming solid in solution. In this theory a small spherical particle is assumed to form from solution and the energy change associated with this is an increase of surface energy associated with the interaction between solid and solution and a decrease of volume free energy. The theory can be formulated as (Mullin, 2001) $\Delta\hat{G}_{Nucleation} = \Delta\hat{G}_{Surface} + \Delta\hat{G}_{Volume}$, where $\Delta\hat{G}_{Surface} = 4\pi r^2\gamma$ and $\Delta\hat{G}_{Volume} = \frac{4}{3}\pi r^3\Delta\hat{G}_v$ leading to:

$$\Delta\hat{G}_{Nucleation} = \Delta\hat{G}_{Surface} + \Delta\hat{G}_{Volume} = 4\pi r^2\gamma + \frac{4}{3}\pi r^3\Delta\hat{G}_v \tag{4.47}$$

The first term on the right hand side is associated with the surface energy. This is a positive quantity with $4\pi r^2$ representing the surface of the sphere and γ the surface tension between solid and solute. The second term represents the energy from formation of solid with $\frac{4}{3}\pi r^3$ being the volume of the particle and $\Delta\hat{G}_v$ being the free energy pr. volume. The former term is positive, whereas the latter is negative in a supersaturated solution. From this theory the nucleation can be seen as a competition between two mechanisms: The formation of small unstable nuclei and dissolution of these. A critical size $r_{crit.}$ can be defined for a given system where the nuclei achieve a size large enough to grow and through the Gibbs-Thompson relation a critical supersaturation can be defined Mullin (2001). From this relationship a nucleation flux can be defined as

$$J = A \cdot e^{\left(-\frac{\Delta\hat{G}_{critical}}{kT}\right)} \tag{4.48}$$

Introducing the Gibbs-Thomson relationship $\ln(S) = \frac{2\gamma v}{kTr}$ Mullin derives the relation for the critical energy (Mullin, 2001)

$$\Delta\hat{G}_{critical} = \left(-\frac{16\pi\gamma^3 v^2}{3k^2T^2(\ln S)^2}\right) \tag{4.49}$$

which substituted into Equation (4.48) leads to:

$$J = A \cdot e^{\left(-\frac{16\pi\gamma^3 v^2}{3k^3T^3(\ln S)^2}\right)} \tag{4.50}$$

The expression is of an Arrhenius type and A is the an energy constant, v is the molecular volume, k is the Boltzmann constant, T the temperature and S the supersaturation ratio. The equation indicates that surface tension, γ, Temperature, T and supersaturation, S are dominant factors in the nucleation.

As with growth kinetics, theoretical equations have been used with limited success. A problem arises from defining the surface tension γ for nuclei of near-critical size (Mullin, 2001). Though theoretically possible, it is argued that the term has no meaning at this size range.

4.2.2 General Nucleation Model

It has proven difficult to estimate the interfacial tension, which is necessary for the calculations of the nucleation flux. For practical purposes an empirical relations as

$$J = k_b \Delta C^b_{maximum} \tag{4.51}$$

is used to describe the rate of nucleation, J. k_b is the rate constant, $\Delta c_{maximum}$ is the *metastable zone* width and b is the *apparent order of nucleation*, which does not indicate the number of species involved Mullin (2001) but rather an apparent nucleation order similar to a reaction order. The expression is described as empirical in the literature but can be derived from (a simplified) nucleation theory as discussed by Myerson (2002)

The primary nucleation can be described by the power law model

$$B = k_b \Delta C^b \tag{4.52}$$

The birth rate of nuclei from nucleation, B, is driven by supersaturation Δc. b is a parameter known as the nucleation order and has no direct physical meaning. k_b is the nucleation rate constant and phenomena can be included in this description. The model is used to describe both primary nucleation and primary and secondary nucleation together. The included phenomena are shown in Figure 4.11

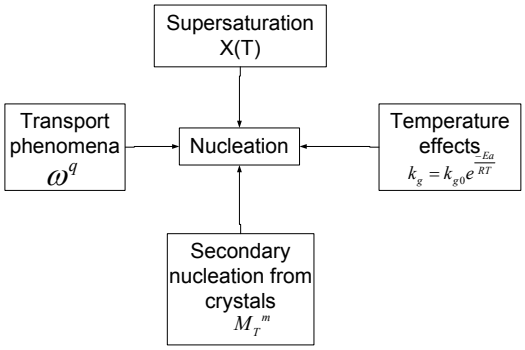

Figure 4.11: *Phenomena influencing nucleation. The supersaturation is the driving force and temperature effects, Secondary nucleation from crystals and transport phenomena may be included to account for observed growth rates when modelling.*

4.2.3 Specific Terms of the Nucleation Model

The nucleation models can be categorized into models, which include relevant phenomena and mechanisms for a given type of nucleation (primary, secondary) or for total nucleation.

An overall general model can be set up combining the phenomena-descriptions employed by different authors under their assumptions. This section covers the terms for describing the phenomena that are included in the nucleation models.

Supersaturation

The driving force for the nucleation is, similar to growth, the supersaturation. The supersaturation description is equivalent to the description given in section 2.1.1 p. 6.

Specific Term: Temperature Dependence of Nucleation Kinetics

Similar to growth, the nucleation model can have temperature dependence directly in the nucleation equation. The employed temperature description for the models is often encountered in the form of an Arrhenius equation:

$$k_b^{'} = k_{b0} \cdot e^{\left(\frac{-E_a}{RT}\right)} \tag{4.53}$$

E_a is the activation energy, R the gas constant and T the absolute temperature.

Specific Term: Transport Phenomena

Transport phenomena are relevant in the consideration of the nucleation models, where they can be used to describe several nucleation events relevant for growth. For the primary nucleation the increased energy of the solute molecules can serve as activation energy and increase the rate of nucleation. The secondary nucleation is often related to the phenomena as the shearing forces on the crystals are affected by the fluid transport in the crystallization vessel. This description, however, is covered in section 4.2.3. Similarly to growth the transport phenomena are often described by a power expression of the stirring rate or other measureable variable linked to the transport phenomena in the crystallization vessel:

$$\tau_b = \omega^q \tag{4.54}$$

An alternative correlation between the stirring rate and nucleation is used by Angelov et al. (2008). The authors use:

$$\tau = e^{\left(-\frac{n_b}{\omega}\right)} \tag{4.55}$$

where n_b is a parameter and ω is the stirring rate. With this expression the secondary nucleation is described through a relation where the stirring destroys crystals acting as nucleation generator.

Specific Term: Magma Density

The magma density in the system is relevant for the secondary nucleation occurring when crystals lose material acting as seeds for the crystallization operation. The model includes a description of the magma density M_T, which describes the amount of crystals present in the crystallization operation. This magma density is used in an empirical power expression to quantify the material formation from secondary nucleation:

$$\eta_b = {M_T}^j \tag{4.56}$$

Here j is a value which can be interpreted as a reaction order. According to Garside (1985) j is often close to unity suggesting collisions with walls rather than other crystals.

The amount of crystals can be described through the third moment when the method of moments is used for solution of a population balance model. With this procedure, the growth and nucleation of the crystals are tightly interwoven in the mass, energy and population balances.

General Nucleation Model with Specific Terms

Collecting the terms describing the different phenomena yields a general model:

$$N = (k_b^{'})(X^{'})(\eta_b)(\tau_b) \tag{4.57}$$

Substituting each term on the right hand side of Equation (4.57) the following is obtained:

$$N = k_{b0} \cdot e^{(\frac{-E_a}{RT})} \cdot (X(T))^b \cdot M_T^j \omega^q \tag{4.58}$$

The function $X(T)$ is given in different forms. This general model combines the phenomena related models and can be adapted to describe the nucleation involving each of the phenomena models for a desired application.

Model analysis

Similar to the growth model section 4.15, the general nucleation model Equation (4.58) has a set of process variables and parameters. This set is categorized in $\underline{\theta} = (\underline{\theta_1}, \underline{\theta_2}, \underline{\theta_3}, \underline{\theta_4})$ and subsets are characterized by the variable type as

System parameters	$\underline{\theta_1}$	(4.59)
Process variables	$\underline{\theta_2}$	(4.60)
Model parameters	$\underline{\theta_3}$	(4.61)
Universal Constants	$\underline{\theta_4}$	(4.62)

Using the above variable classification the model parameters of the nucleation model Equation (4.58) are listed as:

Known variable	$\in \theta_i$	Description	Unit
k_{b0}	θ_1	Rate constant	Number pr. unit time
b	θ_1	Nucleation exponent	–
E_a	θ_1	Activation energy	$\frac{J}{mol}$
j	θ_1	Magma density exponent	
q	θ_1	Stirring rate exponent	–
M_T	θ_2	Magma density	kg pr. unit volume
T	θ_2	Absolute temperature	K
ω	θ_2	Stirring rate	Revolutions pr. time
R	θ_4	Universal gas constant	$\frac{J}{mol \cdot K}$

The system parameters $\underline{\theta_1}$ and model parameters $\underline{\theta_3}$ need to be known before the nucleation model can be used. Thus, these parameters need to be regressed with suitable experimental data before the growth model can be used.

The process variables define the condition at which the crystallizer is operated, and thus, the conditions at which the growth must be determined.

Calculation Procedure

The calculation procedure for the nucleation model is given as follows:

1. Specify (retrieve from library) the nucleation model with appropriate phenomena from eq. (4.58)
2. Specify (retrieve from library) system parameters $\underline{\theta_1}$ and universal constants $\underline{\theta_4}$
3. Specify process variables $\underline{\theta_2}$
4. Specify (retrieve from library) model parameters $\underline{\theta_3}$
5. Calculate supersaturation X at relevant temperature and composition using the appropriate equation (2.2) - (2.4). If the saturation model is explicit X is calculated directly (equilibrium composition is initially unknown). If the model involves an implicit saturation model, such as an activity coefficient model, X is calculated through an iterative procedure where X satisfies the SLE condition (activity coefficients and equilibrium composition are initially unknown).

6. For all datapoints repeat from step 3 with new values of θ_2, then new values of θ_3 for step 4 until all datapoints are calculated.
7. Calculate nucleation N through specified model from Equation (4.58)

The procedure for this calculation is similar to the procedure in section 4.1.2 p. 27

4.2.4 Generation of Nucleation Models

The general model Equation (4.58) combines the different phenomena with the relevant terms. For a given application the relevant terms are selected by the modeler. The selection procedure is shown in the diagram in Figure 3.2.

Example 1: Sucrose

This example is based on Ouiazzane et al. (2008) and relates to the growth as discussed in Example 1: Sucrose p. 30.

System The chemical system under study is the sucrose-water system. The equipment used is a stirred batch vessel with a jacket to control the temperature in the system. A saturated solution is cooled from 70 °C to 40 °C. The supersaturation is modeled as the thermodynamical supersaturation.

Model Objective The objective of the model is to describe the secondary nucleation in a sucrose cooling crystallization with thermodynamical driving force, accounting for temperature effects.

Assumptions Based on the model objective, a set of assumptions is made (Ouiazzane et al., 2008). These assumptions are formulated here as:

- Nucleation and growth are the dominant phenomena
- The growth is temperature dependent
- The growth is independent of size (no apparent size dependency)
- Transport phenomena are near constant and changes have neglectable effect
- Nucleation is secondary only due to generous seeding

Kinetics The model for nucleation kinetics is investigated. For this system only secondary nucleation is assumed as the system is seeded generously. The effect of transport phenomena is not considered and the variation of transport properties is neglected. From the above phenomena descriptions model terms can be included to generate the appropriate model. The phenomena model terms are:

Phenomena	Model term	Used	Not used	
Temperature dependence	$e^{(\frac{-E_a}{RT})}$	$*$		(4.63)
Crystal mass	M_C^j	$*$		(4.64)
Transport phenomena	ω^q		$*$	(4.65)
Supersaturation	$\left(\frac{\gamma x - \gamma_{eq} x_{eq}}{\gamma_{eq} x_{eq}}\right)$	$*$		(4.66)

The selected path in diagram 3.2 is shown in 4.12 .

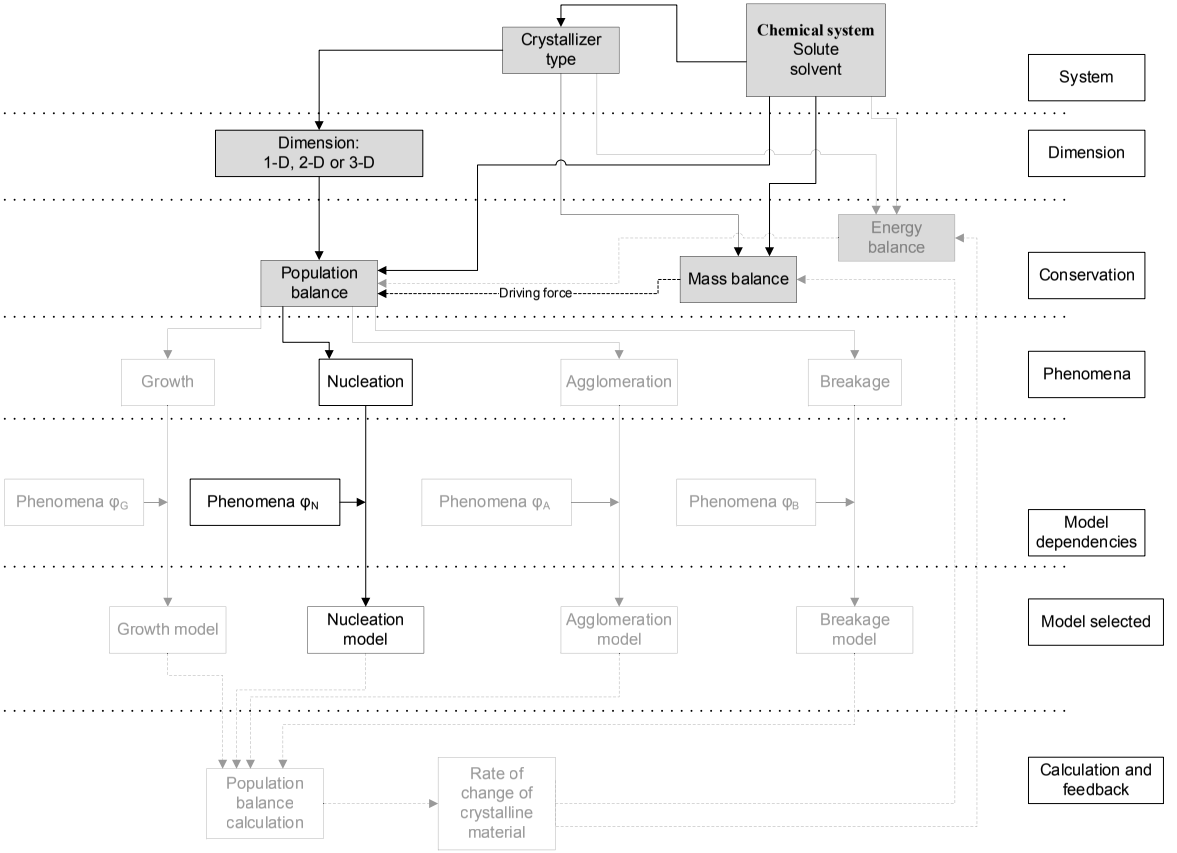

Figure 4.12: *The procedure for model generation and use highlighted from figure 3.2. Following the path, the nucleation model including the relevant phenomena ϕ_i (temperature effects, apparent size dependency and transport phenomena) may be generated*

The supersaturation condition depends on thermodynamic effects, which is described by Peres and Macedo (1996) and investigated by Ouiazzane et al. (2008). The system is bi-component and no subscript is used to indicate the solute compound. The description of the thermodynamic model and the calculation procedure are given by (Peres and Macedo, 1996) and discussed in section 4.1.3

As the equilibrium conditions have been calculated in Equation 4.32 it is possible to define the supersaturation as

$$X = \left(\frac{\gamma x - \gamma_{eq} x_{eq}}{\gamma_{eq} x_{eq}} \right) \tag{4.67}$$

The general nucleation model is (4.58) and under the stated assumptions it is reduced to:

$$N = k_{b0} \cdot e^{\left(\frac{-E_a}{RT}\right)} \cdot \left(\frac{\gamma x - \gamma_{eq} x_{eq}}{\gamma_{eq} x_{eq}} \right)^b \cdot M_C^j \tag{4.68}$$

This model describes the secondary nucleation of the crystals as a function of the thermodynamic supersaturation accounting for temperature dependence. For this example the nucleation at high magma density is investigated.

Calculation Procedure The calculation procedure (section 4.2.3 p. 55) is followed.

Initially all system parameters ($\underline{\theta_1}$) and universal constants $\underline{\theta_4}$ are specified.

Variables and Parameters The nucleation is function of the three variables composition (X), temperature (T) and crystal mass M_C. A set of parameters are needed as well. These are:

Parameter	θ	Value
k_{b0}	θ_1	$3.15 \cdot 10^{13} g^{-0.4136} min^{-1}$
E_a	θ_1	$78.8 kJ/mol$
b	θ_1	1.5
j	θ_1	0.4136
R	θ_4	$8.314 J/(molK)$

The nucleation is calculated for varying temperatures and initial concentrations at specified

magma densities. The process variables temperature and initial concentration $\underline{\theta_2}$ are set accordingly.

The supersaturation is calculated next. For this procedure the equilibrium is initially calculated using the modified UNIQUAC equation using the calculation in the growth example in paragraph 4.1.3, p. 32.

The activity coefficients are calculated through the modified UNIQUAC model (4.24). With this model implemented the growth expression becomes explicit and the growth can be calculated.

Calculation Example The secondary nucleation of a crystal in a supersaturated sucrose solution at $T = 300K$ with crystal mass $1.2 \cdot 10^2 g$ is calculated. The models for activity (4.24) and (4.31) are used. Error is specified as $error = 0.01$ in x_{eq}. An initial estimate of the equilibrium is given as $x_{sucrose,eq} = 0.1$, from which $\gamma_{sucrose} = 0.539$ is calculated and an activity of $activity_{sucrose,eq} = 0.019$ through SLE-equation (4.31). A new estimate of $x_{sucrose,eq}$ is set by $\alpha = 0.5$: $x^{new}_{sucrose,eq} = 0.1 + 0.5(0.035 - 0.1) = 0.068$ At this point the process is automated and $x_{sucrose,eq}$ converges to $x_{sucrose,eq} = 0.0601$ With this $\gamma_{sucrose,eq} = 0.3205$ is calculated. The solution is assumed to be supersaturated at 1.5% increase in $x_{sucrose}$. $x_{sucrose} = 1.015 \cdot x_{sucrose,eq} = 0.061$. At this point the activity coefficient is calculated as $\gamma_{sucrose} = 0.3254$. The supersaturation is calculated from (4.32). At $T = 300K$, $x_{sucrose} = 0.061$ and $M_C = 1.2 \cdot 10^2 g$

$$X = \left(\frac{\gamma x - \gamma_{eq} x_{eq}}{\gamma_{eq} x_{eq}} \right) = \left(\frac{0.3254 \cdot 0.061 - 0.3205 \cdot 0.0601}{0.3205 \cdot 0.0601} \right) = 0.0299$$

Using the parameters, the nucleation is calculated from (4.68). At $T = 300K$, $x_{sucrose} = 0.061$ and $M_C = 1.2 \cdot 10^2 g$

$$\begin{aligned} N_{sucrose} &= k_{b0} \cdot e^{\left(\frac{-E_a}{RT}\right)} \cdot (X)^b \left(1.2 \cdot 10^2 g\right)^{(0.4136)} \\ &= 3.15 \cdot 10^{13} g^{-0.4136} \cdot e^{\left(\frac{-78.8 \cdot 10^3 J/mol}{8.314 J/(mol \cdot K) 300K}\right)} \cdot 0.0299^{1.5} \cdot \left(1.2 \cdot 10^2 g\right)^{0.4136} \\ &= 8.75 \cdot 10^3 min^{-1} \end{aligned}$$

A set of temperature and supersaturation values are specified in accordance with changing initial concentration in table 4.1:

Table 4.4: *Sucrose nucleation function responding to Temperature and saturation*

Known			Unknown				
T	$x_{sucrose}$	M_C	γ_{eq}	x_{eq}	$\gamma_{sucrose}$	X	$N_{sucrose}$
K	-	g	-	-	-	-	$number/min$
300	0.061	$1.2 \cdot 10^2$	0.3205	0.0601	0.3254	0.0299	$8.75 \cdot 10^3$
300	0.063	$1.2 \cdot 10^2$	0.3205	0.0601	0.3371	0.1017	$5.50 \cdot 10^4$
300	0.066	$1.2 \cdot 10^2$	0.3205	0.0601	0.3545	0.2138	$1.67 \cdot 10^5$
300	0.069	$1.2 \cdot 10^2$	0.3205	0.0601	0.3718	0.3310	$3.23 \cdot 10^5$
300	0.071	$1.2 \cdot 10^2$	0.3205	0 0.0601	0.3833	0.4118	$4.47 \cdot 10^5$
300	0.073	$1.2 \cdot 10^2$	0.3205	0.0601	0.3947	0.4948	$5.90 \cdot 10^5$
300	0.076	$1.2 \cdot 10^2$	0.3205	0.0601	0.4117	0.6232	$8.33 \cdot 10^5$
320	0.073	$1.2 \cdot 10^2$	0.3832	0.0712	0.3937	0.0540	$6.81 \cdot 10^4$
320	0.076	$1.2 \cdot 10^2$	0.3832	0.0712	0.4107	0.1446	$2.99 \cdot 10^5$
320	0.079	$1.2 \cdot 10^2$	0.3832	0.0712	0.4274	0.2385	$6.32 \cdot 10^5$
320	0.082	$1.2 \cdot 10^2$	0.3832	0.0712	0.4440	0.3354	$1.05 \cdot 10^6$
320	0.085	$1.2 \cdot 10^2$	0.3832	0.0712	0.4604	0.4353	$1.56 \cdot 10^6$
320	0.088	$1.2 \cdot 10^2$	0.3832	0.0712	0.4765	0.5380	$2.14 \cdot 10^6$
320	0.091	$1.2 \cdot 10^2$	0.3832	0.0712	0.4924	0.6434	$2.80 \cdot 10^6$
340	0.090	$1.2 \cdot 10^2$	0.4771	0.0883	0.4862	0.0390	$1.17 \cdot 10^5$
340	0.093	$1.2 \cdot 10^2$	0.4771	0.0883	0.5019	0.1083	$5.41 \cdot 10^5$
340	0.096	$1.2 \cdot 10^2$	0.4771	0.0883	0.5173	0.1792	$1.15 \cdot 10^6$
340	0.100	$1.2 \cdot 10^2$	0.4771	0.0883	0.5375	0.2762	$2.20 \cdot 10^6$
340	0.103	$1.2 \cdot 10^2$	0.4771	0.0883	0.5523	0.3507	$3.15 \cdot 10^6$
340	0.106	$1.2 \cdot 10^2$	0.4771	0.0883	0.5668	0.4265	$4.23 \cdot 10^6$
340	0.113	$1.2 \cdot 10^2$	0.4771	0.0883	0.5995	0.6084	$7.21 \cdot 10^6$

Plotting the nucleation expression under these conditions the effect of the changing variables can be seen. This is shown in figure 4.13.

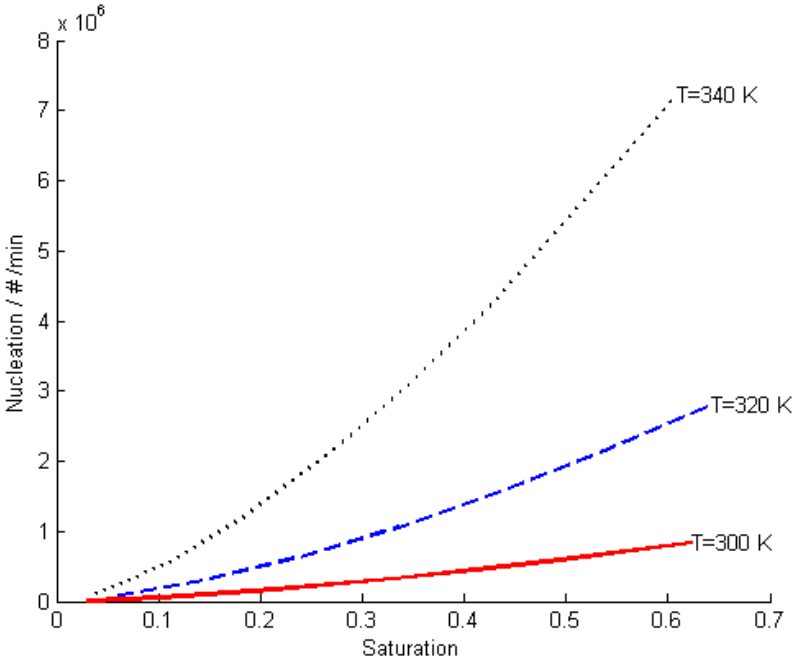

Figure 4.13: *The nucleation rate of sucrose crystals in the sucrose-water system. The model suggests nucleation is increased rapidly with the temperature visualized as the distance between the curves from different temperatures. The supersaturation is increasing the high temperature nucleation rate, whereas lower temepratures with this model are unaffected.*

Example 2: Paracetamol

This example is based on Nagy et al. (2008).

System The chemical system under study is the paracetamol-water system. The equipment used is a stirred batch vessel with a jacket to control the temperature in the system. A saturated solution is cooled and the effect on the nucleation is discussed using the nucleation model proposed by Nagy et al. (2008).

Model Objective The objective of the model is to describe the nucleation in a paracetamol cooling crystallization with absolute saturation as driving force.

Assumptions Based on the model objective, a set of assumptions is made (Nagy et al., 2008). These assumptions are formulated here as:

- The nucleation is initially dominant for the unseeded solution
- The growth is neglected
- Transport phenomena are near constant and changes have neglectable effect
- Nucleation is primary

Kinetics The model for nucleation kinetics is investigated. For this system only primary nucleation is assumed as the system contains no crystal material. The effect of transport phenomena is not considered and the variation of transport properties is neglected. From the above phenomena descriptions model terms can be included to generate the appropriate model. The phenomena model terms are:

Phenomena	Model term	Used	Not used	
Temperature dependence	$e^{(\frac{-E_a}{RT})}$		$*$	(4.69)
Crystal mass	M_C^j		$*$	(4.70)
Transport phenomena	ω^g		$*$	(4.71)
Supersaturation	ΔC	$*$		(4.72)

The selected path in diagram 3.2 is similar to the path in example 1.

Supersaturation description The supersaturation description is the absolute supersaturation, ΔC. The saturation model is taken from Nagy et al. (2008). According to this study the saturation C_{sat} in $kg\ solute/kg\ solvent$ can be described by

$$C_{sat} = A_{1,paracetamol} \cdot T^2 + A_{2,paracetamol} \cdot T + A_{3,paracetamol} \tag{4.73}$$

Where

Parameter	Value	
$A_{1,paracetamol}$	$1.5846 \cdot 10^{-5} kg/(kgK^2)$	(4.74)
$A_{2,paracetamol}$	$-9.0567 \cdot 10^{-3} kg/(kgK)$	(4.75)
$A_{3,paracetamol}$	$1.3066 kg/kg$	(4.76)

For the driving force to this model, the solution is assumed to be cooled and nucleation to progress. Hence the curves for cooling of $T = 2K$ and $T = 3K$ are included in the plot shown in Figure 4.14. This driving force difference is discussed in the following.

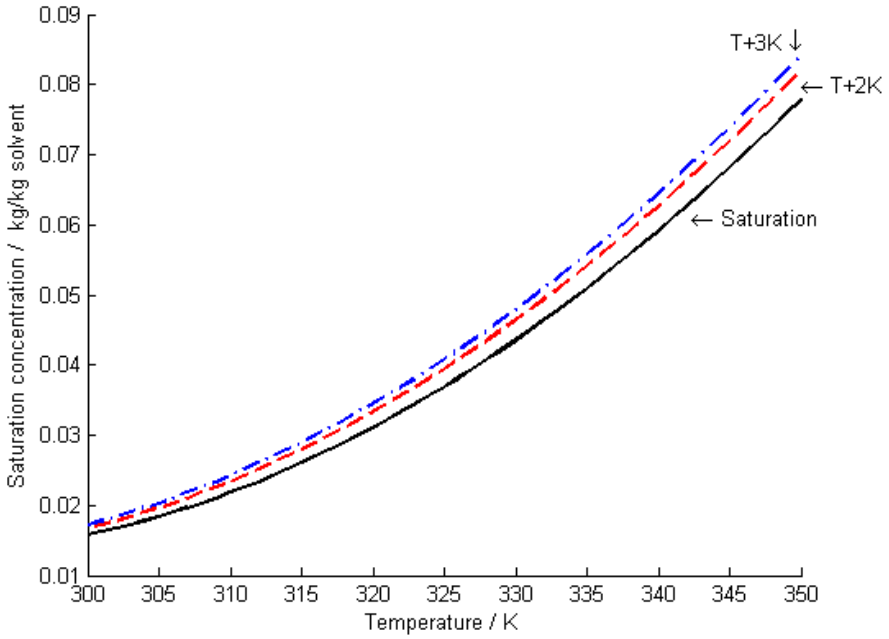

Figure 4.14: *The solubility of paracetamol in ethanol (saturation) as function of temperature (Nagy et al., 2008). The curves for cooling of $T = 2K$ and $T = 3K$ are included in the plot shown in Figure 4.14.*

The general nucleation model is Equation (4.58) and under the stated assumptions it is reduced to:

$$N = k_{b0} \cdot \Delta C^b \tag{4.77}$$

This model describes the primary nucleation of the crystals as a function of the absolute supersaturation accounting for temperature dependence.

Calculation Procedure The calculation procedure (section 4.2.3 p. 55) is followed.

Initially all system parameters ($\underline{\theta_1}$) and universal constants $\underline{\theta_4}$ are specified.

Variables and Parameters The nucleation is function of the variable composition (X) and temperature T (hidden in X) A set of parameters are needed. These are:

Parameter	θ	Value
k_{b0}	θ_1	$7.77 \cdot 10^{19} number/(min \cdot g_{water})$
b	θ_1	6.2

The nucleation is calculated for varying temperatures for the two sub-cooling scenarios. The process variables temperature and initial concentration $\underline{\theta_2}$ are set accordingly.

The supersaturation is calculated next from Equation (4.77) as the concentration difference between an initially saturated solution at temperature T_S and the saturated solution at T. The cooling of the system generates the supersaturation.

Initially T_S and T are specified. $C = C_{sat}$ is calculated from Equation (4.73) for T_S and C_{sat} is calculated for T. ΔC is then calculated as:

$$\Delta C = C - C_{sat}$$

The nucleation is calculated next as

$$\begin{aligned} N_{Paracetamol} &= k_{b0} \cdot (\Delta C)^b \\ &= 7.77 \cdot 10^{19} \cdot (0.084 - 0.779)^{6.2} \\ &= 1.68 \cdot 10^6 \end{aligned}$$

A set of temperature and supersaturation values are specified in accordance with changing initial concentration is specified in table 4.5:

Table 4.5: *Paracetamol nucleation function responding to temperature and saturation*

Known				Unknown
T	T_S	C	C_{sat}	$N_{paracetamol}$
K	K	kg/kg	kg/kg	$number/min$
300	302	$1.67 \cdot 10^{-2}$	$1.57 \cdot 10^{-2}$	15.7
305	307	$1.97 \cdot 10^{-2}$	$1.84 \cdot 10^{-2}$	91.2
310	312	$2.34 \cdot 10^{-2}$	$2.18 \cdot 10^{-2}$	$3.59 \cdot 10^{2}$
315	317	$2.80 \cdot 10^{-2}$	$2.61 \cdot 10^{-2}$	$1.10 \cdot 10^{3}$
320	322	$3.33 \cdot 10^{-2}$	$3.11 \cdot 10^{-2}$	$2.84 \cdot 10^{3}$
325	327	$3.95 \cdot 10^{-2}$	$3.69 \cdot 10^{-2}$	$6.47 \cdot 10^{3}$
330	332	$4.64 \cdot 10^{-2}$	$4.35 \cdot 10^{-2}$	$1.34 \cdot 10^{4}$
335	337	$5.41 \cdot 10^{-2}$	$5.09 \cdot 10^{-2}$	$2.56 \cdot 10^{4}$
340	342	$6.26 \cdot 10^{-2}$	$5.91 \cdot 10^{-2}$	$4.62 \cdot 10^{4}$
345	347	$7.19 \cdot 10^{-2}$	$6.81 \cdot 10^{-2}$	$7.90 \cdot 10^{4}$
350	352	$8.20 \cdot 10^{-2}$	$7.79 \cdot 10^{-2}$	$1.30 \cdot 10^{5}$
300	303	$1.72 \cdot 10^{-2}$	$1.57 \cdot 10^{-2}$	$2.37 \cdot 10^{2}$
305	308	$2.04 \cdot 10^{-2}$	$1.84 \cdot 10^{-2}$	$1.31 \cdot 10^{3}$
310	313	$2.43 \cdot 10^{-2}$	$2.18 \cdot 10^{-2}$	$5.00 \cdot 10^{3}$
315	318	$2.90 \cdot 10^{-2}$	$2.61 \cdot 10^{-2}$	$1.50 \cdot 10^{4}$
320	323	$3.45 \cdot 10^{-2}$	$3.11 \cdot 10^{-2}$	$3.83 \cdot 10^{4}$
325	328	$4.08 \cdot 10^{-2}$	$3.69 \cdot 10^{-2}$	$8.63 \cdot 10^{4}$
330	333	$4.79 \cdot 10^{-2}$	$4.35 \cdot 10^{-2}$	$1.77 \cdot 10^{5}$
335	338	$5.57 \cdot 10^{-2}$	$5.09 \cdot 10^{-2}$	$3.37 \cdot 10^{5}$
340	343	$6.44 \cdot 10^{-2}$	$5.91 \cdot 10^{-2}$	$6.03 \cdot 10^{5}$
345	348	$7.39 \cdot 10^{-2}$	$6.81 \cdot 10^{-2}$	$1.03 \cdot 10^{6}$
350	353	$8.41 \cdot 10^{-2}$	$7.79 \cdot 10^{-2}$	$1.68 \cdot 10^{6}$

Plotting the nucleation expression under these conditions the effect of the changing variables can be seen. This is shown in Figure 4.15.

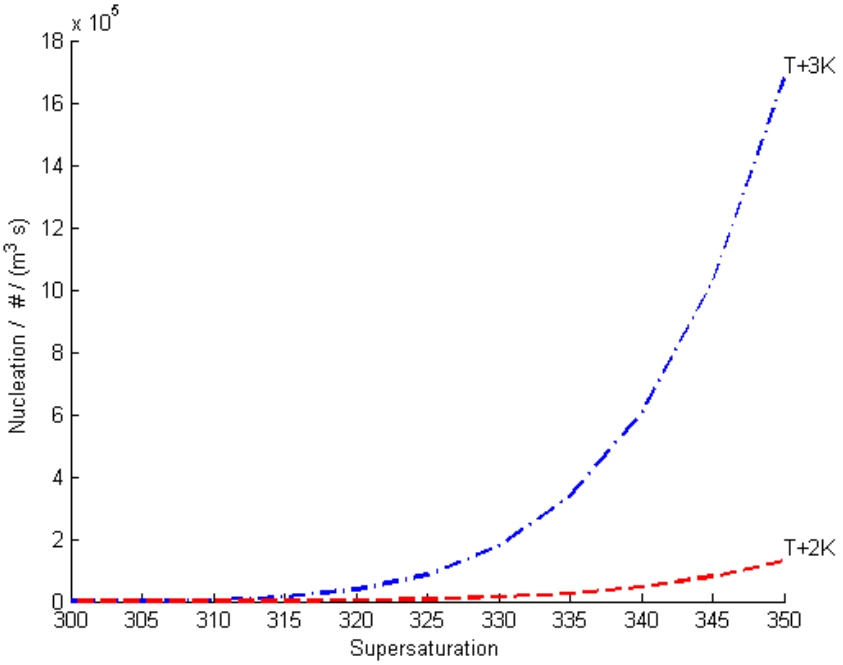

Figure 4.15: *The nucleation of paracetamol in ethanol at the two driving forces. The model suggests that the nucleation rate is increased steeply with at higher temperatures, suggesting that nucleation is massively present if the system is cooled rapidly at elevated temperatures*

Example 3: Glutamine

This example is based on Alvarez and Myerson (2010).

System The chemical system under study is the glutamine-water-acetone system, where glutamine is the solute, water the solvent and acetone acts as antisolvent.The equipment used is a stirred batch vessel. A saturated solution is held at constant temperature and acetone is added as an antisolvent. The effect on the nucleation is discussed.

Model Objective The objective of the model is to describe the nucleation in a glutamine preciptation with absolute saturation as driving force.

Assumptions Based on the model objective, a set of assumptions is made (Alvarez and Myerson, 2010). These assumptions are formulated here as:

- The nucleation is initially dominant for the unseeded solution
- The growth is neglected
- Transport phenomena are near constant and changes have neglectable effect
- Nucleation is primary
- Temperature is constant

Kinetics The model for nucleation kinetics is investigated. For this system only primary nucleation is assumed as the system contains no crystal material. The effect of transport phenomena is not considered and the variation of transport properties is neglected. From the above phenomena descriptions model terms can be included to generate the appropriate model. The phenomena model terms are:

Phenomena	Model term	Used	Not used	
Temperature dependence	$e^{(\frac{-E_a}{RT})}$		$*$	(4.78)
Crystal mass	M_C^j		$*$	(4.79)
Transport phenomena	ω^q		$*$	(4.80)
Supersaturation	ΔC	$*$		(4.81)

The selected path in diagram 3.2 is similar to the path in example 1.

Supersaturation description The supersaturation description is the absolute supersaturation, ΔC. The saturation model is taken from Alvarez and Myerson (2010). According to this study the saturation C_{sat} in $kg\ solute/kg\ solvent$ can be described by

$$C_{sat} = A_{1,glutamine} \cdot e^{\left(A_{2,glutamine} \cdot V_{antisolvent,\%}\right)} \tag{4.82}$$

Where $A_{1,glutamine}$ and $A_{2,glutamine}$ are system parameters and $V_{antisolvent,\%}$ is the volume percent of antisolvent

Parameter	Value	
$A_{1,glutamine}$	$8.7 g/l$	(4.83)
$A_{2,glutamine}$	$-0.048/\%antisolvent$	(4.84)

For the driving force to this model, the solution is assumed to be added antisolvent which is perfectly mixed with the solvent. Nucleation occurs after mixing for the supersaturated solution. The SLE-curves with the antisolvent addition are shown in Figure 4.16. One curve shows the solubility of the acetone-water system and the curve "'no effect"' shows the effect on concentration if the solubility of the liquid was similar to that of the solvent from Equation (4.85).

$$C_{no\,effect} = \frac{m_{solute}}{V_{solvent} + V_{antisolvent}} \tag{4.85}$$

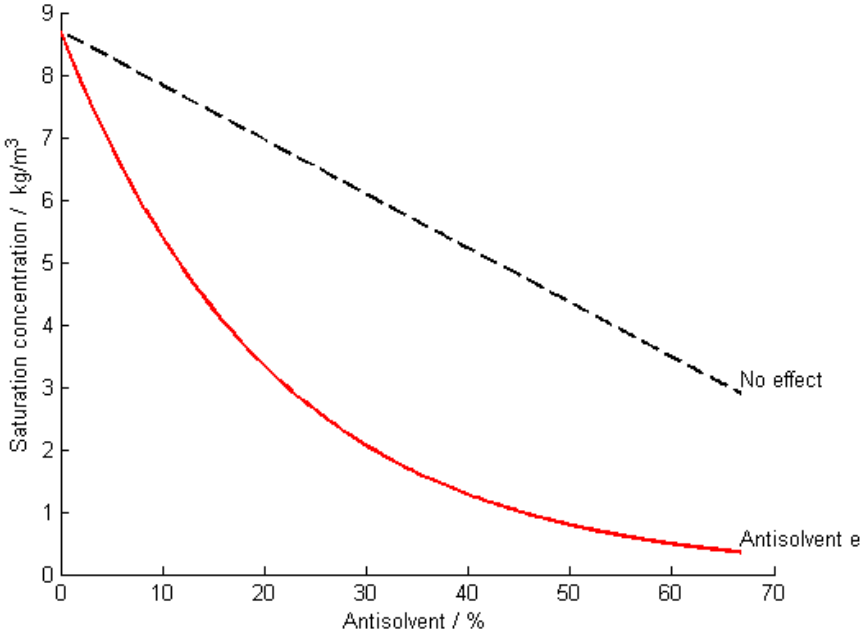

Figure 4.16: *The solubility of glutamine in water as function of acetone (antisolvent) addition at constant temperature of 298 K. The effect of mixing the solvents assuming perfect mixing would result in decreased solubility due to the differences in solubility in the two solvents alone (no effect). The antisolvent effect is seen as the curve for the mixed solvent is below that of the solvent (Antisolvent effect), which makes it possible to supersaturate the system through addition of acetone to the solution*

The general nucleation model is Equation (4.58) and under the stated assumptions it is reduced to:

$$N = k_{b0} \cdot \Delta C^b \tag{4.86}$$

This model describes the primary nucleation of the crystals as a function of the absolute supersaturation accounting for temperature dependence.

Calculation Procedure The calculation procedure (section 4.2.3 is followed.

Initially all system parameters ($\underline{\theta_1}$) and universal constants $\underline{\theta_4}$ are specified.

Variables and Parameters The nucleation is function of the variable composition (X) and temperature T (hidden in X). The temperature here is constant, however, X is affected by a change in the chemical system. A set of parameters are needed. These are:

Parameter	θ	Value
k_{b0}	θ_1	$1.7 \cdot 10^8 \#/(m^3 s)$
b	θ_1	1.8

The nucleation is calculated for varying addition of antisolvent. The process variables X and initial concentration and $\underline{\theta_2}$ are set accordingly. The initial concentration is set to $C_0 = 8.7 g/l$, which corresponds to saturated solution with no antisolvent added.

Next antisolvent is added and the saturation concentration for the amount of added antisolvent is calculated. As discussed above and shown in Equation 4.85 the dilution results in a lower concentration, however, the reduction in solubility is greater and supersaturation is achieved.

An amount of antisolvent corresponding to 10% of the original volume is added. The volume-% of antisolvent is

$$V_{antisolvent,\%} = 100\% \cdot \frac{V_{added}}{V_{initial} + V_{added}} = 9.09\% \tag{4.87}$$

The saturation concentration is calculated next from equation (4.86). At $V_{antisolvent,\%} = 9.09$

$$C_{sat} = A_{1,glutamine} \cdot e^{\left(A_{2,glutamine} \cdot 9.09\%\right)}$$
$$C_{sat} = 8.7 g/l \cdot e^{(-0.048/\% \cdot 9.09\%)} = 5.6238 g/l$$

The nucleation can now be calculated as:

$$N_{Glutamine} = k_{b0} \cdot (\Delta C)^b$$
$$= 1.7 \cdot 10^8 \cdot (8.7 g/l - 5.6238 g/l)^{1.8} \qquad = 1.47 \cdot 10^9$$

A set of temperature and supersaturation values are specified in accordance with changing initial concentration in table 4.6:

Table 4.6: *Glutamine nucleation function responding to temperature and saturation*

V_{added}	% Antisolvent	C	C_{sat}	$N_{glutamine}$
min^{-1}	-	g/l	g/l	
0	0	8.70	8.70	0
0.10	9.09	7.91	5.62	$7.53 \cdot 10^8$
0.20	16.7	7.25	3.91	$1.49 \cdot 10^9$
0.30	23.1	6.69	2.87	$1.90 \cdot 10^9$
0.40	28.6	6.21	2.21	$2.07 \cdot 10^9$
0.50	33.3	5.80	1.76	$2.10 \cdot 10^9$
0.60	37.5	5.43	1.43	$2.06 \cdot 10^9$
0.70	41.2	5.12	1.21	$1.98 \cdot 10^9$
0.80	44.4	4.83	1.03	$1.88 \cdot 10^9$
0.90	47.4	4.58	0.896	$1.78 \cdot 10^9$
1.0	50.0	4.35	0.789	$1.67 \cdot 10^9$
1.1	52.4	4.14	0.704	$1.57 \cdot 10^9$
1.2	54.5	3.95	0.634	$1.47 \cdot 10^9$
1.3	56.5	3.78	0.577	$1.38 \cdot 10^9$
1.4	58.3	3.63	0.529	$1.30 \cdot 10^9$
1.5	60.0	3.48	0.488	$1.22 \cdot 10^9$
1.6	61.5	3.35	0.454	$1.15 \cdot 10^9$
1.7	63.0	3.22	0.424	$1.08 \cdot 10^9$
1.8	64.3	3.11	0.398	$1.02 \cdot 10^9$
1.9	65.5	3.00	0.375	$0.966 \cdot 10^9$
2.0	66.7	2.90	0.355	$0.914 \cdot 10^9$

Plotting the nucleation expression under these conditions the effect of the changing variables can be seen in Figure 4.17.

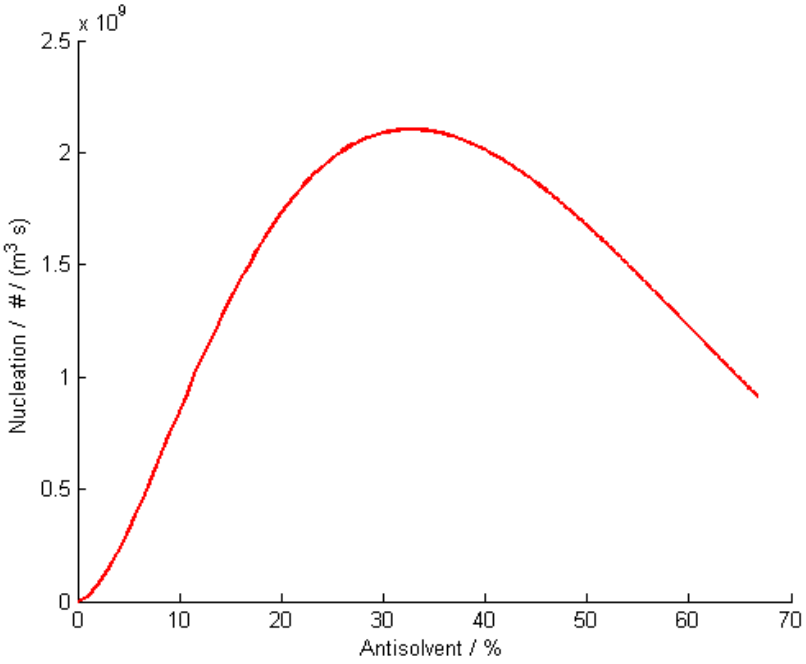

Figure 4.17: *The nucleation of glutamine in water as the acetone is added. Adding the antisolvent to the water resuslts in supersaturation, however, if a large proportion of undersaturated antisolvent is added, the dillution effect results in a relatively lower nucleation rate. Choosing the correct amount of antisolvent to achieve or avoid nucleation (depending on the process objective) is critical.*

4.3 Agglomeration models

Agglomeration is the clustering of particles. This clustering stems from collisions of smaller particles which form larger particles. The process can be viewed as collisions between two particles even when multiple particles collide to form large clusters. In this case a series of two-particle collisions can be used as a model.

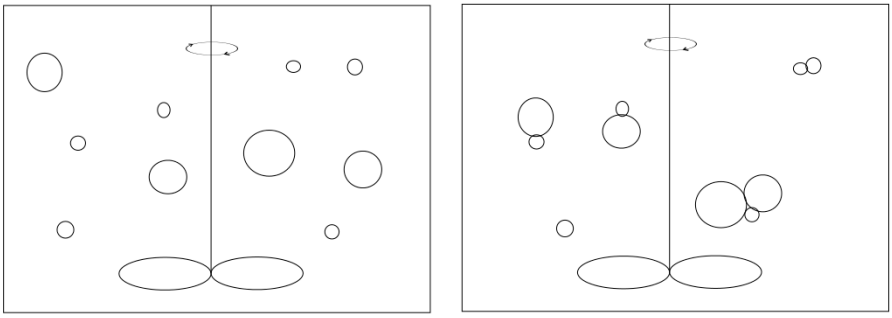

Figure 4.18: *The principle of agglomeration. Particles form clusters during the crystallization operation*

4.3.1 General Agglomeration Model

A general approach for the agglomeration describes how the number of particles changes through an agglomeration kernel. This kernel describes the frequency of agglomeration of two particles with specified volumes. Two particles colliding, forming a larger and smaller particle than the original particles can be seen as agglomeration followed by breakage of the agglomerate. The agglomeration results in the formation of one particle from two and hence the effect is seen in two terms of the population balance equation, Equation (2.7).

The contribution to the birth term stems from the production of one particle from two smaller particles. This contribution can be formulated as Equation (4.88)

$$B_{agglomeration} = \frac{1}{2}\int_0^v a(v-u,u)n(v-u)n(u)du \tag{4.88}$$

Here, the production of new particles $B_{agglomeration}$ of volume v from two particles of volume u and $v-u$, respectively, is described using the frequency kernel $a(v-u,u)$. The fraction $\frac{1}{2}$ ensures that only one particle is formed from the collision.

The contribution to the death term stems from the destruction of the two smaller particles. This contribution can be formulated as equation (4.89)

$$D_{agglomeration} = n(v)\int_0^\infty a(v,u)n(u)du \tag{4.89}$$

The term here is positive as the death contribution in equation (2.7) is considered negative

4.3.2 Agglomeration Phenomena

Supersaturation Dependence For some systems, the supersaturation has effect on the rate of agglomeration of particles in the system.

Temperature Dependence The agglomeration rate of the crystals has been found to exhibit temperature dependence. To take this into account, authors introduce temperature dependence in the kinetic model, often through an Arrhenius expression in the agglomeration kernel.

Transport Phenomena The collisions of crystals in the crystallizer and their subsequent agglomeration is dependent on the transport phenomena (Hill and Ng, 1996). This stems from the fact that the governing factor of the agglomeration is the number of collisions between particles.

Size Dependency The effect of the size of particles in the collision have been included by some authors in their kernels.

Agglomeration Kernels

The agglomeration kernel describes the probability of two particles colliding and forming a new particle through the agglomeration. This kernel can be derived from assumptions about the agglomeration mechanism and hence the effects included in the kernel play a significant role.

Table 4.7: *Agglomeration kernels*

Mechanism	Kernel	Author	Comment
Brownian motion	a_0	Scott	a_0 Can depend on phenomena
Turbulent diffusion	$a_0(u+v)$	Golovin	u and v volume of particles

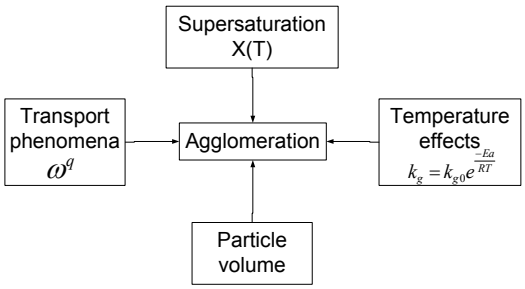

Figure 4.19: *Phenomena governing the agglomeration. The supersaturation is still considered the driving force and temperature effects, particle size and transport phenomena may be included to account for observed agglomeration rates when modelling.*

Effects included in kernels The value of the kernel is determining the rate of agglomeration.

An example illustrating this is the agglomeration shifting. A set of classes are defined as

$$Class_i = 7.81 \cdot \left(e^{\frac{ln(2)}{3}} \right)^{i-1} \tag{4.90}$$

These classes are initially seeded with a number of particles in class 15, 16 and 17 as:

$$Class_{15,0} = 100$$
$$Class_{16,0} = 50$$
$$Class_{17,0} = 20$$

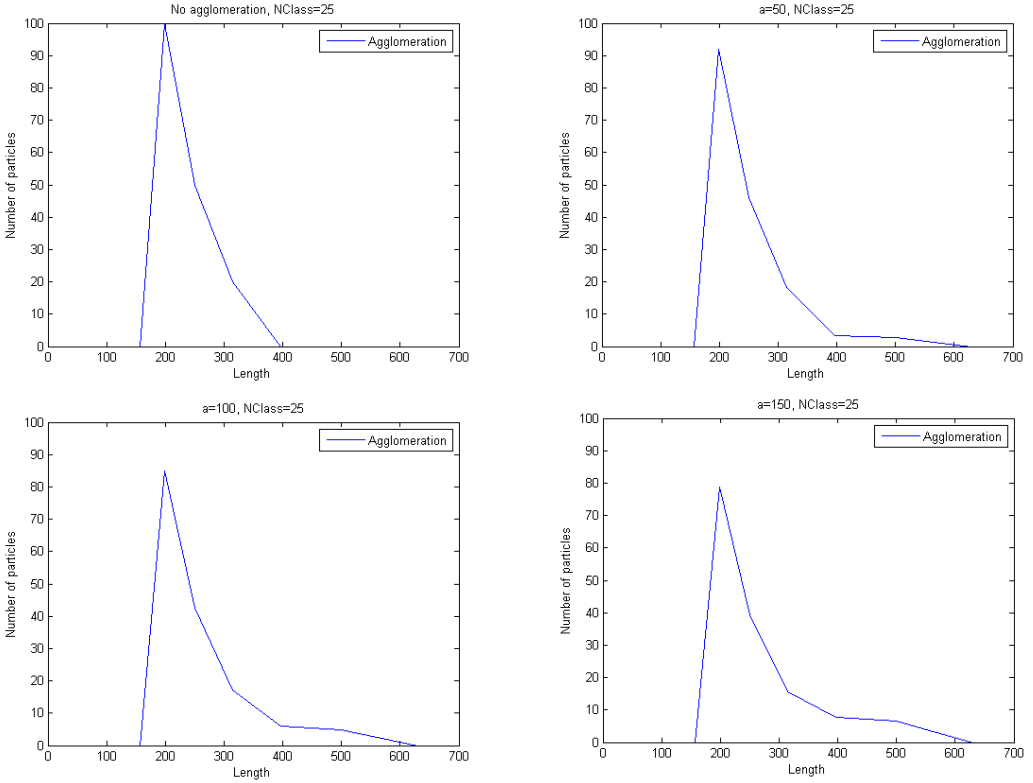

Figure 4.20: *Agglomeration with different values of the kernel a=0,50,100,150 in a system with 25 classes. Initially the classes 15, 16 and 17 are assigned 100, 50 and 20 particles, respectively and the result of a single step is seen.*

Example 1: Calcium oxalate

This example is based on Zauner and Jones (2000).

System The chemical system under study is the calcium oxalate - water system. The equipment used is a draft tube baffled crystallizer with a jacket to control the temperature in the system. The supersaturation is modeled as the relative supersaturation.

Model Objective The objective of the model is to describe agglomeration in a calcium oxalate crystallization and analyze the model kernel for this operation.

Assumptions Based on the model objective, a set of assumptions is made (Zauner and Jones, 2000). These assumptions are formulated here as:

- Temperature effects are not directly seen in the the agglomeration
- Transport phenomena are influencing the agglomeration

Kinetics The system under study is assumed to have nucleation and growth agglomeration and breakage.

The agglomeration kinetics are investigated. For this system, the transport phenomena are assumed to be affecting this along with the supersaturation.

Phenomena	Model term	Used	Not used	
Temperature dependence	$e^{(\frac{-E_a}{RT})}$		$*$	(4.91)
Size dependency		$*$		(4.92)
Transport phenomena	ω^q	$*$		(4.93)
Supersaturation	σ	$*$		(4.94)

The kernel model is

$$B_{agglomeration} = k_{agglomeration}(1 + a \cdot \omega^{0.5} + b \cdot \omega)\sigma^c \tag{4.95}$$

Supersaturation description The saturation model is taken from Zauner and Jones (2000). According to this study the saturation C_{sat} can be described by the solubility product

$$K_{SP} = 2.51 \cdot 10^{-9} mol^2 \cdot l^{-2} \tag{4.96}$$

Calculation Procedure Agglomeration data is taken from Zauner and Jones (2000). The data is provided in a graph, which is shown in figure 4.21

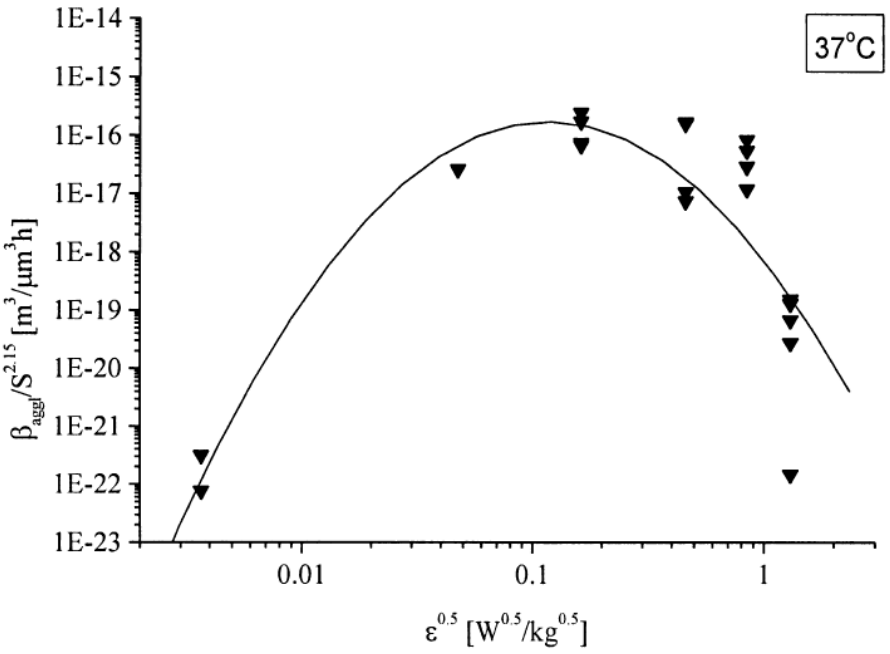

Figure 4.21: *The agglomeration data from Zauner and Jones (2000). The agglomeration is plotted as a function of the stirring rate,* ε *to the power of* 0.5 *and modelled. Figure adopted from Zauner and Jones (2000)*

The values for the variable ($\sqrt{\varepsilon}$) are given in Table 4.8.

Table 4.8: *Data from Zauner and Jones (2000) as taken from figure 4.21*

$\sqrt{\varepsilon}$	$\log_{10}\varepsilon$	$\beta_{agglomeration}$	$\log_{10}(average)$
$3.4 \cdot 10^{-3}$	-4.94	$\{7.0 \cdot 10^{-23}, 3.0 \cdot 10^{-22}\}$	$-2.18 \cdot 10^{1}$
$5.0 \cdot 10^{-2}$	-2.60	$\{2.2 \cdot 10^{-17}\}$	$-1.67 \cdot 10^{1}$
$1.6 \cdot 10^{-1}$	-1.59	$\{6.0 \cdot 10^{-17}, 1.5 \cdot 10^{-16}, 2.2 \cdot 10^{-16}\}$	$-1.59 \cdot 10^{1}$
$4.5 \cdot 10^{-1}$	$-6.93 \cdot 10^{-1}$	$\{8.0 \cdot 10^{-18}, 1.0 \cdot 10^{-17}, 1.5 \cdot 10^{-16}\}$	$-1.66 \cdot 10^{1}$
$8.4 \cdot 10^{-1}$	$-1.51 \cdot 10^{-1}$	$\{1.0 \cdot 10^{-17}, 3.0 \cdot 10^{-17}, 6.0 \cdot 10^{-17}, 8.0 \cdot 10^{-17}\}$	$-1.65 \cdot 10^{1}$
1.2	$1.58 \cdot 10^{-1}$	$\{1.2 \cdot 10^{-19}, 8.0 \cdot 10^{-20}, 3.0 \cdot 10^{-20}, 1.1 \cdot 10^{-22}\}$	$-1.99 \cdot 10^{1}$

Zauner and Jones (2000) argued that a second order polynomial is appropriate for describing the relation between the stirring power and the agglomeration kernel (β) function. Following this, an expression for the relation is regressed from the data provided by Zauner and Jones (2000). The regression results in

$$\log_{10}(\beta_{agglomeration}) = -0.6534(\log_{10}(\varepsilon))^2 - 2.4662\log_{10}(\varepsilon) - 18.206 \tag{4.97}$$

The R^2-value is calculated to be 0.8667. The data and function are plotted in figure 4.22. The $\beta_{agglomeration}$ is calculated in $m^3/\mu m^3$ and hence a factor of 10^{18} can be applied to investigate the agglomeration in consistent units.

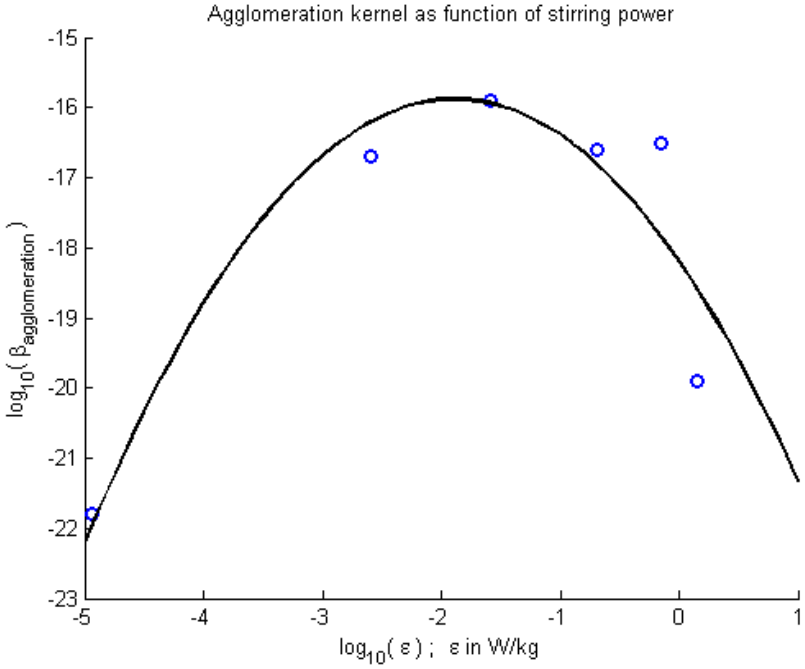

Figure 4.22: *The regressed function and data from Zauner and Jones (2000). The match is considered reasonable, though the R^2-value is calculated to be only 0.8667. The data uncertainty is not considered, but could be present.*

Zauner and Jones (2000) explored the agglomeration at a saturated condition, where the supersaturation does not affect the outcome of the agglomeration. With this kernel established, simulations of agglomeration of a population at a fixed temperature of 37°*C* and no supersaturation can be explored. For this purpose a particle distribution is defined in the class system.

$$Class_i = 7.81 \cdot \left(e^{\frac{ln(2)}{3}}\right)^{i-1} \tag{4.98}$$

These classes are initially seeded with a number of particles in class 12, 13 and 14 as:

$$Class_{12,0} = 20$$
$$Class_{13,0} = 50$$
$$Class_{14,0} = 40$$

Variables and Parameters The needed variables and parameters are listed.

Parameter	θ	Value
ε	θ_2	$10^{-4} - 1$

For the simulation the specification of the stirring rate power is sufficient as the agglomeration kernel function is calculated solely from this value through the prior regressed function. This value is specified at multiple values in the range $10^{-4} - 1$ to investigate the effect of the stirring on the agglomeration.

Calculation Example First, a stirring power is specified. Second the agglomeration kernel function is calculated. This is used to calculate the agglomeration of the specified population. A stirring power of $\varepsilon = 1.0 \cdot 10^{-2} W/kg$ is specified. Using Equation (4.97) an agglomeration kernel value is calculated. At $\varepsilon = 1.0 \cdot 10^{-2} W/kg$:

$$\log_{10}(\beta_{agglomeration}) = -0.6534(\log_{10}(1.0 \cdot 10^{-2}))^2 - 2.4662\log_{10}(1.0 \cdot 10^{-2}) - 18.206 \tag{4.99}$$

$$\beta_{agglomeration} = 129.7 \frac{\mu m^3}{\mu m^3 h} \tag{4.100}$$

Simulations of the agglomeration at values of $\varepsilon = \{1.0 \cdot 10^{-4}, 1.0 \cdot 10^{-3}, 1.0 \cdot 10^{-2}, 1.0 \cdot 10^{-1}, 1\} W/kg$ are carried out for the population. The results are shown in Figure 4.23

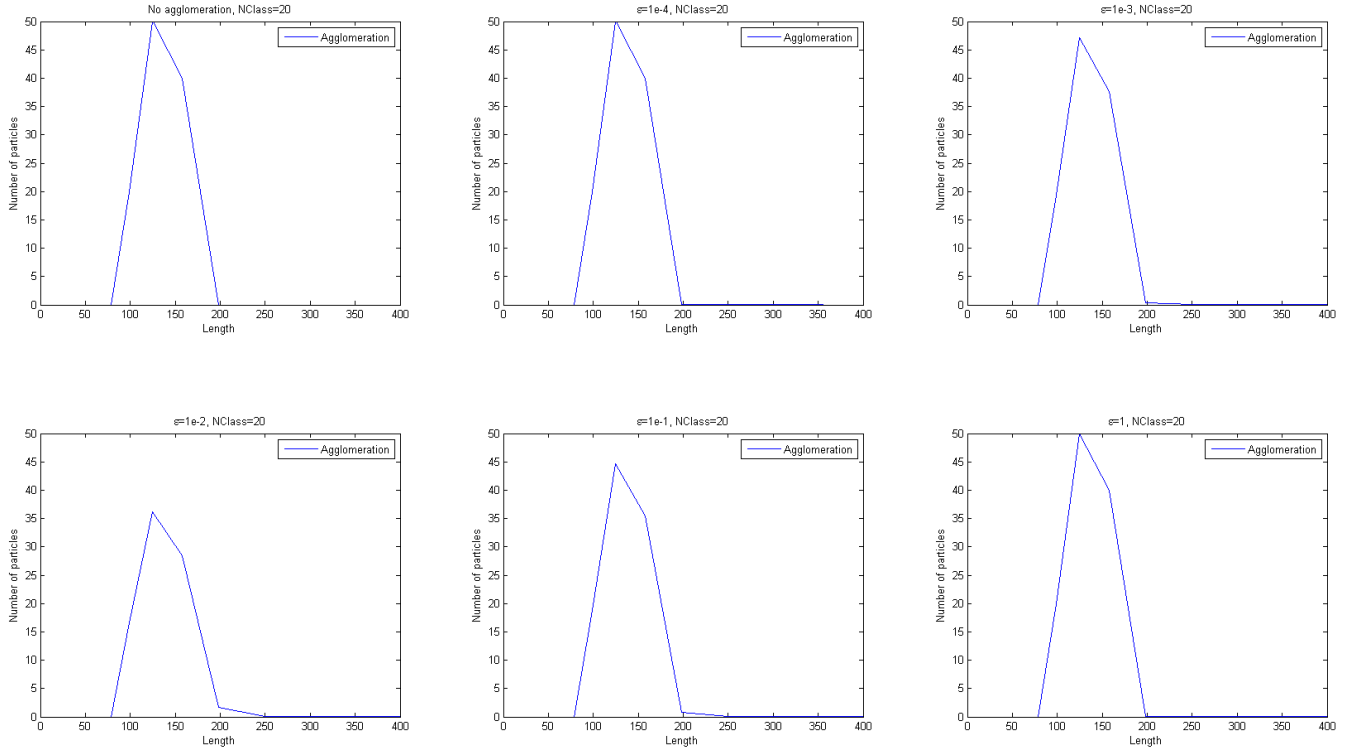

Figure 4.23: *Using 20 classes and a population distributed in class 12,13 and 14, as 20,50 and 40, respectively, agglomeration with variation in the stirring is investigated. Simulations of the agglomeration at values of* $\varepsilon = \{1.0 \cdot 10^{-4}, 1.0 \cdot 10^{-3}, 1.0 \cdot 10^{-2}, 1.0 \cdot 10^{-1}, 1\} W/kg$ *are carried out for the population.*

The effect of the stirring is seen as the agglomeration increases with the stirring in the region $\varepsilon = 1.0 \cdot 10^{-4} W/kg$ to $\varepsilon = 1.0 \cdot 10^{-2} W/kg$ and then decreases. This is attributed to the initial increase in particle energy facilitating collisions and contact between particles which lead to agglomeration. When the stirring becomes too powerful, the colliding particles will not stick together for sufficient time to form an agglomerate but rather collide and continue moving with fewer agglomerates forming as a result.

4.4 Growth and agglomeration models

With the agglomeration phenomena discussed, it is now possible to combine the agglomeration and growth as it was done with nucleation and growth. In this case the growth of particles occurs as well as the agglomeration resulting in a model where particles can increase in volume both because of growth as well as agglomeration. The combination of the growth and agglomeration models is highlighted through an example using the calcium oxalate system discussed in section 4.3.2.

System The chemical system under study is the calcium oxalate - water system. The supersaturation is modeled as the relative supersaturation.

Model Objective The objective of the model is to describe growth and agglomeration in a calcium oxalate crystallization and analyze the model kernel for this operation.

Assumptions Based on the model objective, a set of assumptions is made. These assumptions are formulated here as:

- Temperature effects are not directly seen in the the agglomeration
- Transport phenomena are influencing the agglomeration
- The growth is independent of temperature and modeled as $G = kg \cdot S^g$

Kinetics The system under study is assumed to have growth and agglomeration. The agglomeration kinetics are taken from the example in section 4.3.2.

For the growth model:

Phenomena	Model term	Used	Not used	
Temperature dependence			$*$	(4.101)
Size dependence			$*$	(4.102)
Transport phenomena			$*$	(4.103)
Supersaturation	σ	$*$		(4.104)

For the agglomeration model:

Phenomena	Model term	Used	Not used	
Temperature dependence	$e^{(\frac{-E_a}{RT})}$		*	(4.105)
Size dependence		*		(4.106)
Transport phenomena	ω^q	*		(4.107)
Supersaturation	σ	*		(4.108)

The kernel model is

$$B_{agglomeration} = k_{agglomeration}(1 + a \cdot \omega^{0.5} + b \cdot \omega)\sigma^c \tag{4.109}$$

Supersaturation description The saturation model is taken from Zauner and Jones (2000). According to this study the saturation C_{sat} can be described by the solubility product

$$K_{SP} = 2.51 \cdot 10^{-9} mol^2 \cdot l^{-2} \tag{4.110}$$

Here, the supersaturation is kept constant. The resulting distribution is shown in figure 4.24, where it is shown how the combination of particles and growth eliminates the particles in the smaller classes forming larger particles and clusters.

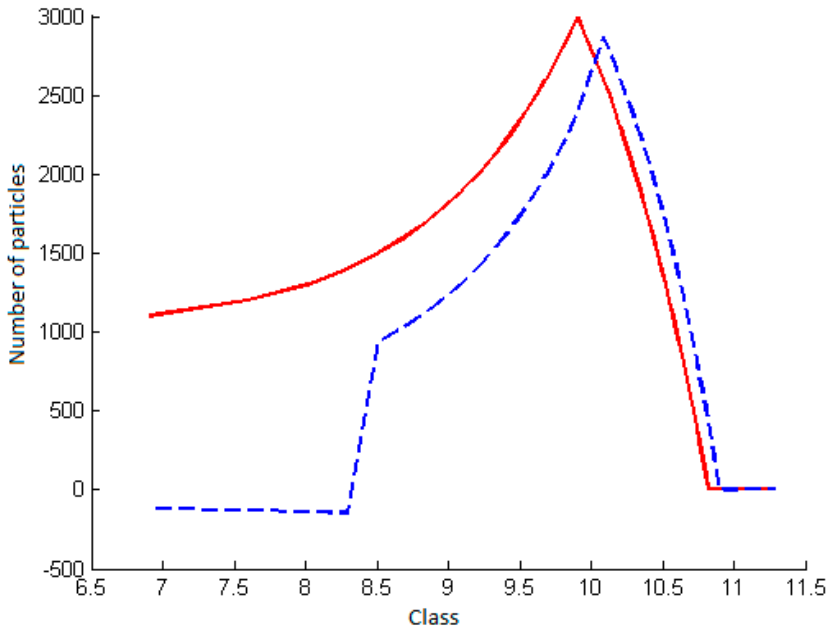

Figure 4.24: *The combination of growth and agglomeration in classes with increasing width. The initial distribution is shown in solid red, the resulting distribution in dashed blue. Some numerical uncertainty exists using this method and as the particles are eliminated from the smaller classes due to growth, small negative values are assumed*

4.5 Breakage models

Breakage is the destruction of particles. This destruction can stem from collisions of particles with other particles, the walls of the crystallization vessel, the stirrer or other objects in the crystallizer. The process can be viewed as breakage of one particle into two smaller particles even when a particle fractures into multiple pieces. In this case breakage is represented in the model as a series of breaking events where increasingly smaller particles break up.

4.5.1 General Breakage Model

A general approach for the breakage describes how the number of particles changes through a breakage kernel. This approach is similar to the approach in the agglomeration model. The kernel describes the distribution of new particles and a function simultaneously describes the frequency of particle breakage. A particle fracturing results in the formation of two particles from one and hence the effect is seen in two terms of the population balance equation, (2.7).

The contribution to the birth term stems from the production of two particles from a single larger particle. This contribution can be formulated as equation (4.111)

$$B_{breakage} = \int_{v}^{\infty} b(v,u)W(u)n(u)du \tag{4.111}$$

Here, the production of new particles $B_{breakage}$ of volume v from a particle of volume u is described using the breakage distribution kernel $b(v,u)$ and the breakage frequency $W(u)$. The integration over the volume range $[v;\infty]$ ensures that all produced particles are accounted for.

The contribution to the death term stems from the destruction of a breaking particle. This contribution can be formulated as Equation (4.112)

$$D_{breakage} = W(v)n(v) \tag{4.112}$$

$W(v)$ represents the brekage frequency for a particle of volume v. The term here is positive as the death contribution in Equation (2.7) is considered negative.

4.5.2 Breakage Phenomena

The breakage of particles appears to be dominated by mechanical phenomena in the crystallizer resulting in collisions of particles with other particles or equipment. Hence, transport phenomena are considered as well as temperature.

Temperature Dependence The breakage rate of crystals in some systems has been modelled to exhibit temperature dependence. Authors introduce temperature dependence in the kinetic model, often through an Arrhenius expression in the breakage frequency.

Transport Phenomena The crystal collisions in the crystallizer and is dependent on the transport phenomena (Hill and Ng, 1996). This stems from the fact that the governing factor of the breakage is the collisions between particles.

Size Dependence The effect of the size of particles in the collision have been included in the frequency function. This accounts for the observation that particles often need to reach a certain (system dependent) size before breakage occurs. The effect can be described by

$$W(v) = k_w \cdot v^w \tag{4.113}$$

Here $W(v)$ is the breakage frequency of a particle of size v, k_w is a rate constant and w weighs larger particles to break more often.

4.6 Growth, Breakage and Agglomeration models

A combination of breakage, agglomeration and growth is considered. For this consideration the calcium oxalate system is revisited. This system was discussed in 4.3.2 and used in section 4.6.

The system under study is briefly revisited. Zauner and Jones (2000) have provided kinetic data, which has been analyzed and models for the specific phenomena have been formulated. The specific phenomena included here are growth, agglomeration and breakage and the relevant parameters have been taken from the previous sections on these phenomena and the database.

System The chemical system under study is the calcium oxalate - water system. The equipment used is a draft tube baffled crystallizer with a jacket to control the temperature in the system. The supersaturation is modeled as the relative supersaturation.

Model Objective The objective of the model is to describe growth, breakage and agglomeration in a calcium oxalate crystallization and analyze a population distribution subjected to these phenomena.

Assumptions Based on the model objective, a set of assumptions is made (Zauner and Jones, 2000). These assumptions are formulated here as:

- Temperature effects are not directly seen in the kinetics
- Transport phenomena are influencing the kinetics

Kinetics The system under study is assumed to have growth, agglomeration and breakage.

Phenomena	Model term	Used	Not used	
Temperature dependence	$e^{(\frac{-E_a}{RT})}$		*	(4.114)
Size dependence		*		(4.115)
Transport phenomena	ω^q	*		(4.116)
Supersaturation	σ	*		(4.117)

The kernel model is

$$B_{agglomeration} = k_{agglomeration}(1 + a \cdot \omega^{0.5} + b \cdot \omega)\sigma^c \tag{4.118}$$

Supersaturation description The saturation model is taken from Zauner and Jones (2000). According to this study the saturation C_{sat} can be described by the solubility product

$$K_{SP} = 2.51 \cdot 10^{-9} mol^2 \cdot l^{-2} \tag{4.119}$$

As the saturation is fixed, this is simply substituted with $\sigma = 1.1$. As the models are not affected by temperature, it is not necessary to consider this directly. The temperature enters the equations through the kinetic definitions and parameter values. Stirring rate is fixed through $\varepsilon = 1 \cdot 10^{-2}$.

Parameters Growth equation:

$$G = k_g S^g \tag{4.120}$$

Agglomeration kernel:

$$\log_{10}(\beta_{agglomeration}) = -0.6534(\log_{10}(\varepsilon))^2 - 2.4662\log_{10}(\varepsilon) - 18.206 \tag{4.121}$$

Breakage rate: $R_{breakage} = k_{breakage} \cdot V_{particle}^{\alpha}$ Here, $k_{breakage}$ is the rate constant, $V_{particle}$ the particle volume and α the particle volume weighing factor. The breakage kernel is formulated as uniform.

The parameters for the system are shown in Table 4.9.

Table 4.9: *Parameters for the CaC_2O_4-water system*

Parameter	Value	$\in \underline{\theta_i}$
k_g	$1.33e-4$	$\underline{\theta_1}$
g	1	$\underline{\theta_1}$
$k_{breakage}$	$1e-20$	$\underline{\theta_1}$
α	1	$\underline{\theta_1}$

With these parameters it is possible to follow the evolution of the particle distribution if originally seeded in class 10 with 100 particles. The result is shown in Figure 4.25. The breakage dominates and the particles are moved to smaller classes

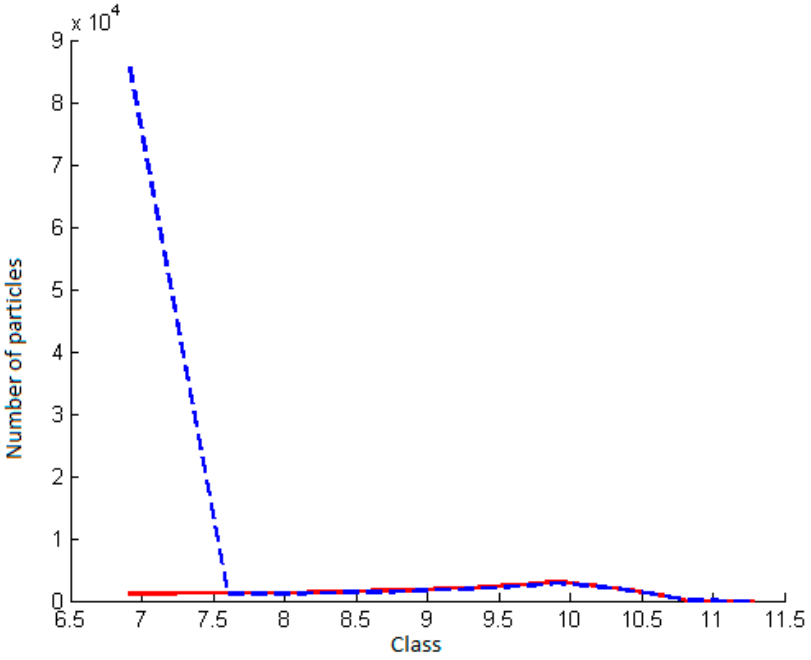

Figure 4.25: *The original distribution show in solid red, the resulting in dashed blue. The breakage dominates and the particles are moved to smaller classes*

4.7 Dissolution kinetics

Dissolution of crystals is the change of solid to liquid solute and the reverse of crystallization. The driving force for dissolution is the undersaturation. Similar to supersaturation, undersaturation can be described in multiple ways. For supersaturation Equation 2.2-2.4 describe possibilities, and furthermore the thermodynamical supersaturation can be used.

The absolute supersaturation expresses the difference in concentration, Δc as the difference between actual concentration c and equilibrium concentration c_{eq}, also known as saturated concentration c_{sat}. The relative supersaturation σ expresses the difference between actual concentration and equilibrium concentration, Δc, relative to the equilibrium concentration c_{eq} leading to numerical values near in the region [0;1] for most supersaturated systems. The supersaturation ratio has values in the region $[0;1[$ for undersaturated systems. An undersaturation described as $C_{sat} - C$ can be used as an absolute undersaturation or to calculate relative undersaturation $\frac{C_{sat}-C}{C_{sat}}$

The dissolution theory is related to work by Noyes and Whitney (1897), where the authors proposed the theory:

$$\frac{dC}{dt} = k(C_{sat} - C)$$

where k is the dissolution rate constant. This rate model is similar to the growth rate of crystals assuming the rate limitting step is the material transport through the diffusion layer surrounding the crystal. The theory was expanded by Dokoumetzidis and Macheras (2006), who included the dependency of the surface area and the dissolution media volume:

$$\frac{dC}{dt} = \frac{D \cdot A_{crystal}}{h \cdot V}(C_{sat} - C)$$

where D is the diffusivity, $A_{crystal}$ the surface area of the crystals releasing material, h the thickness of the diffusion layer and V the volume of the dissolution medium. The equation is similar to the equation proposed by Noyes and Whitney (1897), but includes the effect of the surface area releasing material and considers the volume of solvent. The driving force is described as the absolute supersaturation.

4.8 Database

The database is developed to contain the kinetic models used within crystallization sorted according to their kinetic phenomena.

4.8.1 Growth models

The growth models from the literature have been collected and are sorted based on system and model type.

Chemical system		Type	Model type						Remark	Reference
Solute	Solvent	Organic (O)/ Inorganic (I)	$k_g S^g$	$k_g S^g (1 + \gamma L)^p$	$k_{g0} \cdot e^{-\frac{E_a}{RT}} \cdot S^g$	$k_{g0} \cdot e^{-\frac{E_a}{RT}} \cdot S^g \cdot \omega^p$	$k_{g0} \cdot e^{-\frac{E_a}{RT}} \cdot S^g (1 + \gamma L)^p$	$k_g \cdot (\ln(S))^2$		
adipic acid	Water	O				*				David and Villermaux (1991)
Ammonium chloride	Water	I						X		Mohan and Myerson (2002)
Ammonium dihydrogenphosphate	Water	I						X		Mohan and Myerson (2002)
Ammonium oxalate	Water	O	X					X		Gherras and Fervotte (2012), Mohan and Myerson (2002)
Ammonium sulfate	Water	I	X							Abbas and Romagnoli (2007)
Barium sulphate	Water	I	X							Steyer, et al (2010)
Bisphenol A	Phenol	O			X					Alamdari et al (2010)
Borax Deca hydrate	Water	I	X							Akrap et al (2012)
Calcium flouride	Water	I							Special – model occuring once	Aldaco et al (2007)
Calcium oxalate	Water	O	X					X		Millan et al (1997) Mohan and Myerson (2002)
Citric acid monohydrate	Water	O						X		Mohan and Myerson (2002)
Dextrose	Water	O			X					Markande et al (2012)
dimethyl terephthalate	methanol	O							Special – model occuring once	Borissova (2009)

DL-threonine	Water	O			X	X	X			Czapla et al (2010) Angelov et al (2008) Qamar et al (2012)
D-Xylose	Water	O						X		Mohan and Myerson (2002)
flufenamic acid	ethanol	O	X							Alvarez and Myerson (2012)
Glutamic acid (L)	Water	O						X		Mohan and Myerson (2002)
Glycine	Water	O						X		Mohan and Myerson (2002)
hexamethylene tetramine	Water	O	X							Bourne and Davey (1976)
hexamethylene tetramine	ethanol	O	X							Bourne and Davey (1976)
Hexamine	Water	O						X		Mohan and Myerson (2002)
Hexamine	ethanol	O						X		Mohan and Myerson (2002)
Insulin	Solution	O	X							Hirata et al. (2012)
ketoconazole	methanol	O	X							Alvarez and Myerson (2010)
Lactose	Whey	O	X							Bund and Pandit (2007)
L-glutamic acid	Water	O	X							Alvarez and Myerson (2010)
L-threonine	Water	O			X	X				Bao et al (2006), Hofmann and Raisch (2012)
Magnesium hydroxide	Water	I	X							Alamdari et al (2008)
Mefenamic Acid	Water	O	X							Cesu and Yaylaci (2012)
Paracetamol	ethanol	O			X					Worlitschek and Mazzotti (2004)
Paracetamol	Water	O	X							Kadam et al 2012
Paracetamol	acetone	O						X		Mohan and Myerson (2002)

Phenytoin	Water	O						X		Mohan and Myerson (2002)
Phosphoric acid	Water	I							Special – model occuring once	Ma et al (2009)
Potassium alum	Water	I	X	X						Garside(1985), Nagy and Aamir (2012)
Potassium chloride	Water	I	X					X		Akl (1991) Mohan and Myerson (2002)
Potassium dichromate	Water	I		X						Aamir et al (2010)
Potassium nitrate	Water	I	X							Miller and Rawlings (1994)
Potassium sulphate	Water	I	X							Garside(1985)
Sea bittern	Water	I	X							Alamdari(2008)
Sodium bicarbonate	Water	I	X							Saberi et al (2009)
Sodium bromide dihydrate	Water	I						X		Mohan and Myerson (2002)
Sodium chlorate	Water	I	X							Bennema (1967)
Sodium chloride	Water	I	X					X		Mohan and Myerson (2002) Nowee et al (2008)
Struvite	Water	I	X							Ali and Schneider (2008)
Succinic acid (beta)	Water	O						X		Mohan and Myerson (2002)
Sucrose	Water	O	X		X			X	Special – model occuring once	Garside(1985) Faria et al (2008) Ouiazzane et al (2008) Mohan and Myerson (2002)
Triglycine sulfate	Water	O						X		Mohan and Myerson (2002)

CHAPTER 5

Process model

The systematic, generic approach to modelling is considered to save time in model development and recommended by Cameron and Gani (2011). Gernaey and Gani (2010) recommended that flexible frameworks with "'plug-and-play"' of knowledge-bases, models, methods (for design, analysis, control, etc.) and tools (simulation, model identification, product analysis, etc.) is developed and widely applied (Gernaey and Gani, 2010), and in this context Samad et al. (2011) proposed a generic multi-dimensional model-based system for batch cooling crystallization processes. The framework has been applied to multiple scenarios (Samad, 2012; Samad et al., 2012, 2013) and used for the study of the kinetics of crystallization (Samad et al., 2012; Meisler et al., 2013, 2014).

5.1 Modelling tool

The framework contains a generic modelling tool, which contains the equations for application of the mass and energy balances as well as population balances solved either through the method of moments (Hulburt and Katz, 1964) or the method of classes (Marchal et al., 1988) as formulated by Costa et al. (2005) and Puel et al. (2003) for the relevant scenarios (Samad, 2012).

5.1.1 Population balance

As shown in Figure 3.2, the kinetic phenomena interact with the balance equations through constitutive equations, which are included in the population balance equation. The population balance equation may be formulated in one dimension as equation (2.7). The equation can further be applied in two dimensions as

$$\frac{\partial n(L_1,L_2,t)}{\partial t} = -\frac{\partial\left[n(L_1,L_2,t)G(L,X,\phi)\right]}{\partial L_1} - \frac{\partial\left[n(L_1,L_2,t)G(L,X,\phi)\right]}{\partial L_2} + Birth - Death \quad (5.1)$$

$n(L,t)$ is the number of particles of size L for a given time t. This is a discrete number, but is often treated as a continuous variable. $G(L,X,\phi)$ is the growth function for a particle depending on size, supersaturation (X) and selected phenomena ϕ.

The population balance based model is solved using either the method of moments or the method of classes. For the method of moments the model is structured as highlighted by the equations given in table 5.1 (Randolph and Larson, 1971; Samad, 2012). It should be noted that the distributions can be considered per mass of solvent or total distribution across the crystallizer.

Table 5.1: *Model equations for the moment approach. The moments for the distribution and the concentration and energy balances*

0^{th} moment,μ_0	$\frac{d\mu_0}{dt} = B$
i^{th} moment, μ_i	$\frac{d\mu_i}{dt} = G\mu_{i-1}$
Concentration balance, solute	$\frac{dC}{dt} = -\rho_c \frac{k_v}{m_{solvent}}(3G\mu_2 + B \cdot L_0)$
Energy balance, crystallizer	$\rho V c_p \frac{dC}{dt} = -\Delta H_c \rho_c k_v V(3G\mu_2 + B \cdot L_0) - U_1 A_1 \Delta T$

B represents the nucleation, G the growth, C is the concentration, ρ_c is the crystal density, k_v is the shape factor, $m_{solvent}$ is the mass of solvent, L_0 is the size of a formed nucleus, V is the volume of the magma, c_p is the heat capacity of the magma, ΔH_c is the crystallization enthalpy, U_1 is the heat transfer across the side of the crystallization chamber, A_1 is the heat transfer area and ΔT is the temperature difference.

The overall model requires kinetic parameters, crystal properties, thermodynamic properties and operational variables as well as initial values for the differential equations.

For the method of classes (Marchal et al., 1988), the generic equations are given in Table 5.2

Samad (2012) implemented several variations of moment and method of class solutions, documented in Samad (2012). The framework approach allows modular modelling, in which model modules are connected to the framework. By extending the method of classes and method of moments with inflow, outflow and opportunities for classification of crystals, the framework has been extended with continuous and fed batch methods.

Table 5.2: *Model equations for the method of classes approach. The number of classes must be specified for the distribution. The concentration and energy balances are linked to the population balance. The equations are valid for size independent growth*

$Class_1$	$\frac{dN_1}{dt} = -\frac{G}{2\Delta Cl_1}N_1 + B - D$
$Class_i, 1 < i < End$	$-\frac{G}{2\Delta Cl_i}N_i + \frac{G}{2\Delta Cl_{i-1}}N_{i-1} + B - D$
$Class_End$	$\frac{G}{2\Delta Cl_{End-1}}N_{End-1} + B - D$
Concentration balance, solute	$\frac{dC}{dt} = -\rho_c \frac{k_v V}{m_{solvent}} \sum_{i=1}^{End}(Class_{Size}\frac{dN_i}{dt})$
Energy balance, crystallizer	$\rho V c_p \frac{dT}{dt} = -\Delta H_c - \rho_c k_v V \sum_{i=1}^{End}(Class_{Size}\frac{dN_i}{dt}) - U_1 A_1 \Delta T$

Continuous operation

Operating the crystallizer in continuous mode involves the connection of streams into and out of the crystallizer. With the connection of these, it is possible to provide a generic crystallization module with connections depending on the type of operation. Such an element is illustrated in figure 5.1. The crystallizer is shown with in- and outflows and a jacket for temperature regulation. The inflows are modelled as streams carrying relevant species, such as crystals or reactants for reactions. The outflow assumes the crystallizer module to be a well-mixed vessel and reflects the state of the crystallizer, however, multiple modules may be connected to simulate non-ideal mixing situations. Closing all valves, the crystallizer module simulates a batch operation.

The model forms the base for the case studies presented in chapter 7.

Seeding

Seeding the crystallizer provides an initial population of crystals in the crystallization operation, which should be considered. Using the moments approach, a population distribution (normal distribution, Γ-distribution) may be specified, for which the moments can be generated. The moment generating functions are:

$$\text{Normal distribution} \qquad e^{t\mu + \frac{1}{2}t^2\sigma^2} \tag{5.2}$$

$$\text{Gamma distribution} \qquad \left(1 - t \cdot \frac{\sigma^2}{\mu}\right)^{\left(-(\frac{\mu}{\sigma})^2\right)} \tag{5.3}$$

Specifying this with the desired distribution parameters (mean, μ, standard deviation, σ, crystal density, ρ_c, shape factor k_v and seed mass, m_{seed}) it is possible to generate the initial values for the crystallization operations problem.

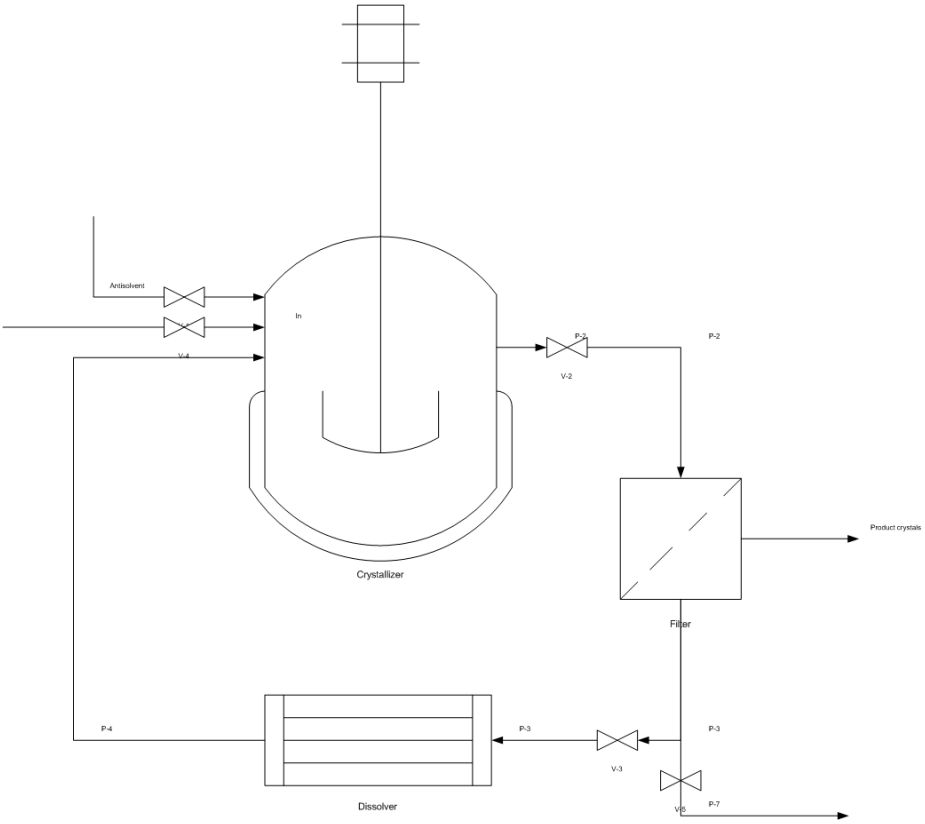

Figure 5.1: *The crystallizer module for continuous operation. Valves may be opened or closed depending on the situation allowing different configurations of the crystallizer. The corresponding model choices are made from the problem definition. The crystallizer module can be considered a basic module for modelling different crystallizer configurations as a single module or connected with other modules to include gradient effects ina crystallization operation. As discussed in the case studies, chapter 7, the module can connect to reaction modules*

CHAPTER 6

Model identification

Model identification requires data, which may be found in various forms. Concentration data for the solute may be monitored and scattering crystal size distributions may be estimated during a crystallization. in this chapter methods for acquiring data are discussed.

6.1 Focused Beam Reflectance Measurements

The focused beam reflectance measurements method is based on a scattering of light and can be characterized as a scattering technique.

6.1.1 Principle of FBRM

FBRM utilizes a probe which measures the reflected light from a monochromatic source. The probe combines the measuring unit and light source. The commercial probe (illustrated in Figure 6.1) produces a constant beam of monochromatic light at a specified wavelength, which is directed through a rotating optics module and the probe tip into the measured system. In a crystallization operation, the probe is placed in the magma chamber and the light is sent into the magma.

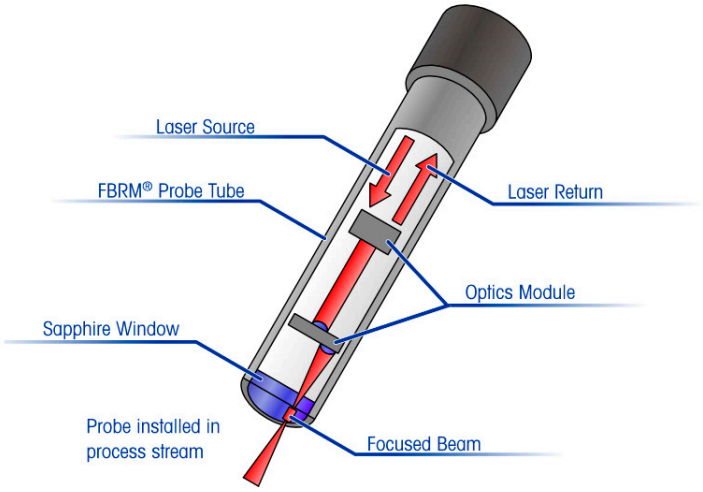

Figure 6.1: *Principle of FBRM. A light source is made monochromatic and sent into the measured vessel. The focus point can be varied and any object passing by the scanning area result in reflected light, which is returned as a signal to the probe. The probe rotates at a fixed speed and the signal time is combined with the velocity to give a chord length of the passing object. Figure adopted from Mettler-Toledo (Mettler-Toledo, 2013)*

The light interacts with the solution and any objects present in the magma chamber. Any reflection back to the source is detected and the duration of the signal Δt is registered. The scanning tip constantly rotates to eliminate error from stationary points and with this known velocity v, the size of the measured chord is calculated as $v \cdot \Delta t$. The chord length is assigned to a matching size bin and registered as a count. The bins are referred to as channels in the FBRM terms, and the number of counts in a specified measurement time interval is recorded and reported. The velocity of the probe is often in the range of meters pr. second, with 2 m/s being the default value (Mettler-Toledo, 2013).

As the light comes in contact with the media it interacts with the solution and any objects present in the solution depending on the properties of these.

Solution interaction

As light passes through the liquid solution, the light is subject to multiple effects from the interactions with the solution. The light is scattered from interactions with the particles and the backscatter which reaches the probe is registered as a signal. The properties of the light passing through the solution are closely related to the speed in the medium and hence the refractive index of the solution.

If the solution medium is changed in the process, for example through addition of a second solvent, this can affect the refractive index of the solution and related optical properties. This can affect the measured counts. The solvent effect is illustrated in Figure 6.2, where the actual focus shifts depending on the solvent. The impact of this is discussed in the chapter on application of FBRM.

The solution medium may also interact with the radiation in terms of absorbance. In the infrared spectrum, this absorbance is linked to the present bonds in the molecule, where the absorbance of the radiation will lead to increased amplitude in the bond vibration. For UV-visible radiation, the absorbance is linked to interaction with π-electrons, which can also produce undesired effects, which lead to wrong estimates of present particles(Loudon, 2002).

Particle interaction

The scatter type depends on the light type and size of particles. For the FBRM technology applied for crystallization purposes, the regime of scattering depends on the wavelength of the light and the medium As light interacts with a particle it can be absorbed, diffracted or reflected depending on the position of interaction.

$$\alpha = \frac{\pi D_{particle}}{\lambda} \tag{6.1}$$

Mie scattering: $\alpha \approx 1$

Geometric scattering $\alpha > 50$

The FBRM technology can be used at several wavelengths, the most common wavelength interval is the infrared. As an example for a spherical particle of size $10\mu m$ and light wavelength of $10\mu m$

$$\alpha = \frac{\pi \cdot 10\mu m}{1\mu m} = 31.4 \tag{6.2}$$

This value falls within the Mie - geometric scattering range, where none of the phenomena dominates the other. The Mie scattering theory assumes spherical particles, which in the case of crystallization is often not true and hence the direct measurements can be affected by this. Especially for smaller particles, Mie scattering is important and the shape of particles and properties need to match the assumptions in the translation theory or otherwise large deviations can be observed.

FBRM is a technique based on the count of backscattering areas versus non-backscattering areas. This is illustrated in Figure 6.3, where the path of the beam passes across an intersection of the

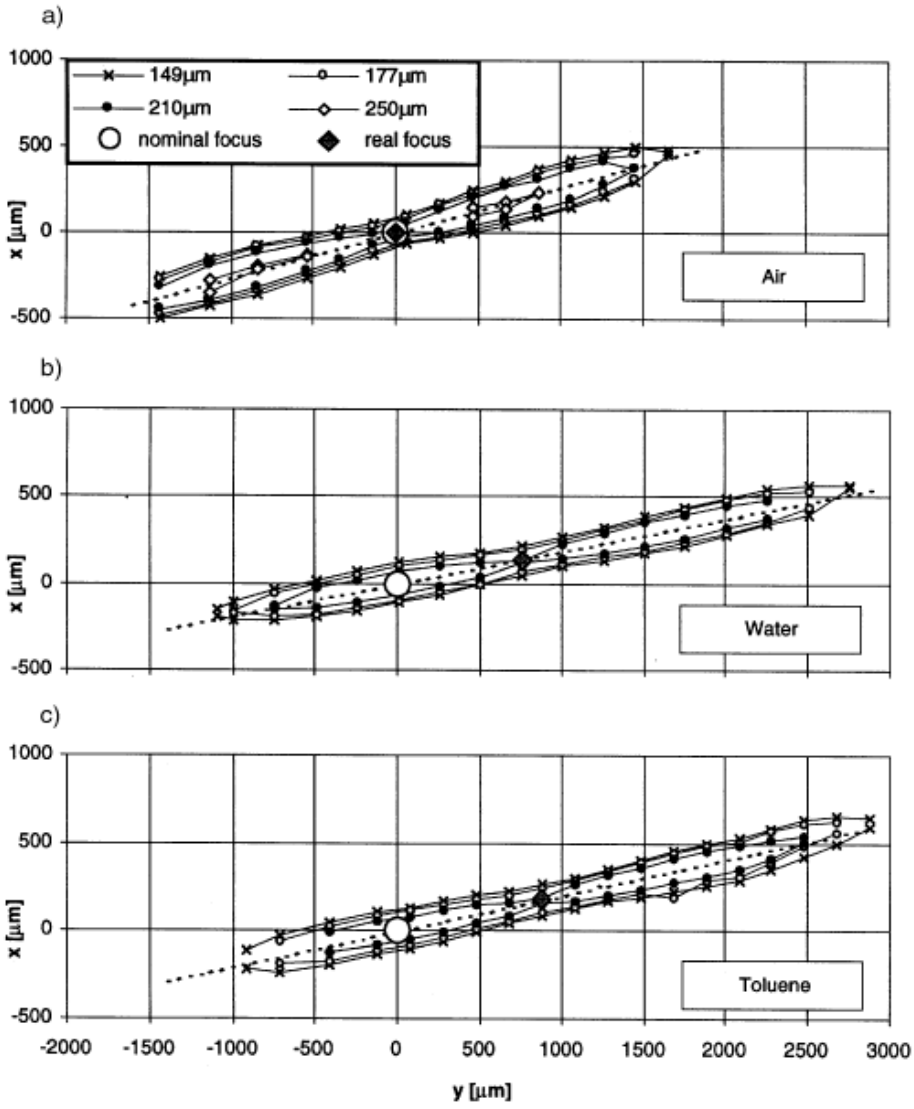

Figure 6.2: *The focus depends on the solution media and should be calibrated for the respective solution components. Light interacts with the solution as well as the objects, which can disturb the measurements adding uncertainty to the interpretation of the chord lengths Figure adopted from Ruf et al. (2000)*

solution.

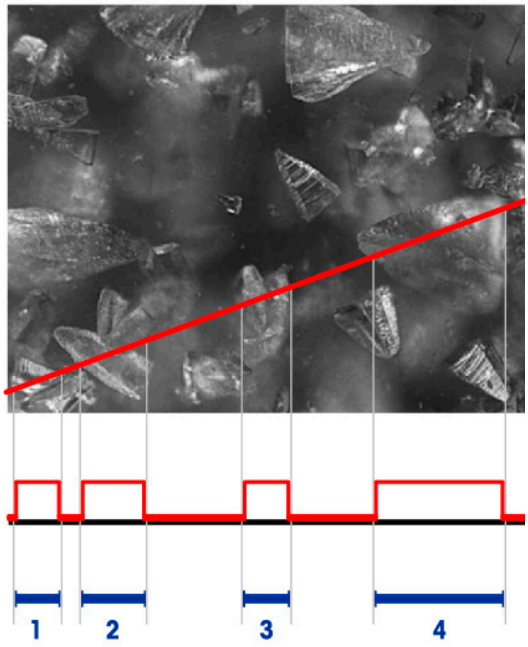

Figure 6.3: *The scanning of particles and corresponding counts. If any particles are close enough in the focus to cause a combined reflection, they are not individually counted. Figure adopted from Mettler-Toledo (2013)*

Note that the technique relies on the assumption that the beam is not backscattered in the intervals between particles. If the light is backscattered for example for solutions with large particle densities, it is not possible to directly distinguish between these particles. This situation is illustrated in Figure 6.4

6.1.2 Recreation of Particle Distribution from Chord Length Distribution

The reconstruction of the particle distribution from a chord length distribution has been the focus of multiple researchers (Ruf et al., 2000), (Chianese and Kramer, 2012). However, thus far no successful translation technique has been proposed in the literature (Chianese and Kramer, 2012). The comparison of FBRM data across different experiments have proven difficult, as FBRM can be considered a relative technique: The measurements are depending on the flow in the vessel where the FBRM is installed, and the objects present there. If the fluid with the objects is stirred at elevated speeds, the objects will pass the measuring point with higher frequency, and as such for the same solution an increase in chord length counts pr. time will often be observed when increasing the stirring rate. As the particles change during the crystallization operation, this effect can also be seen during the operation.

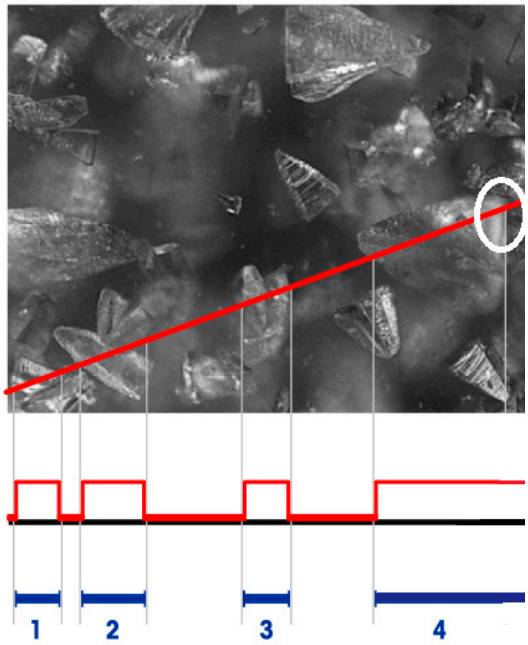

Figure 6.4: *The scanning of particles and corresponding counts similar to figure 6.3. Here, the overlapping particles are counted as one as the reflected signal is not cut off between particles. Original figure adopted from Mettler-Toledo (2013)*

6.1.3 Weighting of chord lengths

The chord lengths can be weighted for a chord length distribution and the weighing often makes use of the length of the chords. Possible weighing is shown in Table 6.1, where v_i is the size of the i^{th} channel, $n(v_i)$ is the number of counts in the respective channel. The weighing decides the area, where the FBRM has it greatest resolution.

Table 6.1: *Weighing of chord lengths. The chordlengths may be unweighed or weighed according to the size of the bin where a count is encountered. The weighing determines where the greatest resolution is found favouring smaller particles (unweighed) or larger particles (length weighed or square weighed), allowing focus on nucleation events or particle evolution*

Distribution type	Form
Unweighted	$\frac{n(v_i)}{\sum_{j=1}^{N_{Channel}} n(v_i)}$
Length weighted	$\frac{n(v_i)(v_i)}{\sum_{j=1}^{N_{Channel}} n(v_i)(v_i)}$
Square weighted	$\frac{n(v_i)(v_i)^2}{\sum_{j=1}^{N_{Channel}} n(v_i)(v_i)^2}$

The standard setup for the FBRM has 90 channels available. The size of each channel is shown in Figure 6.5. The channel setup corresponds to the logarithmic setup allowing different width of the channels. This allows the FBRM to capture both effects on small scale and larger scales. For these common values, it should be noted however, that the smaller channels are subject to Mie scattering rather than geometric scattering, in which the scatter signal is very sensitive to the particle shape. Care should be taken in interpretation of the signals from the smaller channels.

The channel size can generally be described as $[1.08^{i-1}; 1.08^{i}]$, where i is the channel number. This leads to a geometric mean channel size of $1.08^{i-\frac{1}{2}}$

6.1.4 Bi- and multimodal distributions

In case of bi- or multimodal distributions, the source of FBRM counts becomes difficult to identify. In combination with uncertainties on the source of signals stemming from larger particles out of focus and solvent effects, it becomes increasingly necessary to include other measurements and combine these with FBRM measurements. This is discussed in more detail in section 6.3.

Channel	Lower limit	Upper limit	Mean	Geometric mean	Channel	Lower limit	Upper limit	Mean	Geometric mean
1	0	1	0.5		46	29.286	31.623	30.4545	30.43207
2	1	1.08	1.04	1.03923	47	31.623	34.145	32.884	32.85981
3	1.08	1.166	1.123	1.122176	48	34.145	36.869	35.507	35.48087
4	1.166	1.259	1.2125	1.211608	49	36.869	39.811	38.34	38.31177
5	1.259	1.359	1.309	1.308045	50	39.811	42.987	41.399	41.36853
6	1.359	1.468	1.4135	1.412449	51	42.987	46.416	44.7015	44.66861
7	1.468	1.585	1.5265	1.525379	52	46.416	50.119	48.2675	48.23198
8	1.585	1.711	1.648	1.646795	53	50.119	54.117	52.118	52.07965
9	1.711	1.848	1.7795	1.778181	54	54.117	58.434	56.2755	56.23409
10	1.848	1.995	1.9215	1.920094	55	58.434	63.096	60.765	60.72027
11	1.995	2.154	2.0745	2.072976	56	63.096	68.129	65.6125	65.56422
12	2.154	2.326	2.24	2.238348	57	68.129	73.564	70.8465	70.79436
13	2.326	2.512	2.419	2.417212	58	73.564	79.433	76.4985	76.4422
14	2.512	2.712	2.612	2.610085	59	79.433	85.77	82.6015	82.54071
15	2.712	2.929	2.8205	2.818412	60	85.77	92.612	89.191	89.12537
16	2.929	3.162	3.0455	3.043271	61	92.612	100	96.306	96.23513
17	3.162	3.415	3.2885	3.286066	62	100	107.978	103.989	103.9125
18	3.415	3.687	3.551	3.548395	63	107.978	116.591	112.2845	112.2019
19	3.687	3.981	3.834	3.831181	64	116.591	125.893	121.242	121.1528
20	3.981	4.299	4.14	4.136946	65	125.893	135.936	130.9145	130.8182
21	4.299	4.642	4.4705	4.467209	66	135.936	146.78	141.358	141.254
22	4.642	5.012	4.827	4.823454	67	146.78	158.489	152.6345	152.5222
23	5.012	5.412	5.212	5.208161	68	158.489	171.133	164.811	164.6897
24	5.412	5.843	5.6275	5.623372	69	171.133	184.785	177.959	177.828
25	5.843	6.31	6.0765	6.072012	70	184.785	199.526	192.1555	192.0141
26	6.31	6.813	6.5615	6.556678	71	199.526	215.443	207.4845	207.3318
27	6.813	7.356	7.0845	7.079296	72	215.443	232.631	224.037	223.8721
28	7.356	7.943	7.6495	7.643867	73	232.631	251.189	241.91	241.732
29	7.943	8.577	8.26	8.253915	74	251.189	271.227	261.208	261.0158
30	8.577	9.261	8.919	8.912441	75	271.227	292.864	282.0455	281.8379
31	9.261	10	9.6305	9.623409	76	292.864	316.228	304.546	304.3219
32	10	10.798	10.399	10.39134	77	316.228	341.455	328.8415	328.5995
33	10.798	11.659	11.2285	11.22024	78	341.455	368.695	355.075	354.8137
34	11.659	12.589	12.124	12.11508	79	368.695	398.107	383.401	383.1189
35	12.589	13.594	13.0915	13.08185	80	398.107	429.866	413.9865	413.6818
36	13.594	14.678	14.136	14.12561	81	429.866	464.159	447.0125	446.6835
37	14.678	15.849	15.2635	15.25227	82	464.159	501.187	482.673	482.3178
38	15.849	17.113	16.481	16.46888	83	501.187	541.17	521.1785	520.7949
39	17.113	18.478	17.7955	17.78241	84	541.17	584.341	562.7555	562.3414
40	18.478	19.953	19.2155	19.20134	85	584.341	630.957	607.649	607.2018
41	19.953	21.544	20.7485	20.73324	86	630.957	681.292	656.1245	655.6416
42	21.544	23.263	22.4035	22.38701	87	681.292	735.642	708.467	707.9456
43	23.263	25.119	24.191	24.17319	88	735.642	794.328	764.985	764.422
44	25.119	27.123	26.121	26.10177	89	794.328	857.696	826.012	825.4041
45	27.123	29.286	28.2045	28.18376	90	857.696	926.119	891.9075	891.2511

Figure 6.5: *The channel size of each channel and its corresponding average size*

6.2 FBRM application

The application of FBRM to crystallization operations has become quite common. The FBRM technique is used to monitor the chord length distribution and often combined with other monitoring techniques to ensure a desired quality of a product. The FBRM has been used by several authors as a means to control the crystallization operation, specifying a desired target and controlling the supersaturation generation phenomenon to reach this.

6.2.1 FBRM for growth application

The FBRM application to growth is discussed using an example of FBRM applied to a crystallization of hydroquinone from water. The system hydroquinone-water was studied in four experiments. The purpose of these experiments was to follow the evolution in CLD along with analysis of the experimental outcome to see if agglomeration would be present in combination with other phenomena and if it could be quantified. For this purpose FBRM measurements as well as particle vision measurements (PVM) were intended, however due to faults in the particle vision measurements, end time microscopy was used solely to analyze for agglomeration.

Experimental plan

The experiment was planned for analyzing the agglomeration and to see if information could be extracted for the specific system. For this purpose, the experimental procedure was to charge the batch vessel with the material, dissolve it under heating and generate the seeds in-situ. After seed generation, the system was heated to equilibrium and cooled slowly to promote growth and possible agglomeration. This should be monitored through samples or PVM.

Experimental procedure

31 g of hydroquinone and 300 g of water was weighed out and mixed in the batch vessel. This mixture corresponds to a saturation temperature of 30 °C, as shown in Figure 6.6.

The stirring was started at the experimentally relevant value and the automatic control and data collection were initiated. The vessel was programmed to follow a predefined temperature curve shown in Figure 6.7. This temperature profile is composed of four ramps allowing the three intended phases of nucleation: An initial dissolution, subsequent nucleation generation and finally growth. In the initial stage, the system is heated to 40 °C, where the material is dissolved. This is 10 °C above the saturation temperature, and due to the rapid dissolution compared to crystallization (Mullin, 2001), it is reasonable to assume that all dissolvable material is dissolved at this temperature. The assumption was confirmed experimentally as the FBRM count came close to

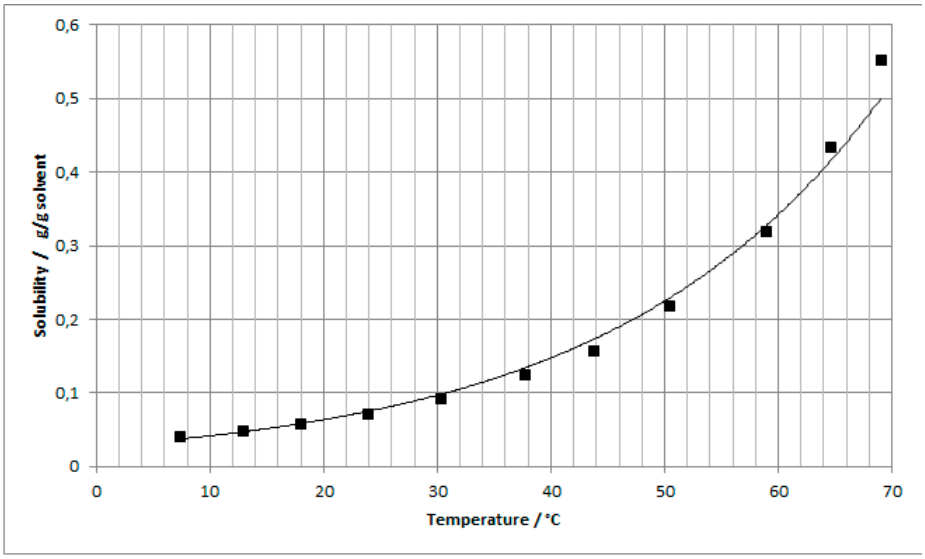

Figure 6.6: *The solubility of hydroquinone in water at temperatures from 7- 68 °C Li et al. (2006)*

zero. Following this dissolution step, a rapid cooling to 20 °resulted in nucleation. The induction time of this system is relatively short compared to the paracetamol-IPA system (see section 6.2.2) and during the 1000 seconds after being cooled below the equilibrium, the system nucleated and was brought back to equilibrium temperature at 30 °C. From this point, the system was slowly cooled to a final temperature of 20 °C.

Results

Crystal samples were taken from the crystallizer during the experiment, filtered and dried and analyzed under the microscope. Examples of the crystals are shown in Figure 6.8 and Figure 6.9. In Figure 6.8 the needle-shaped crystals are seen as the dominant crystals by mass. Several crystals are aligned and show indication of agglomeration through well-structured sharing of the longer edges. The present agglomeration distorts the growth estimations from size of the crystals. The agglomeration tends to occur along the longer facets of the crystals, and some of the counts from the FBRM in the higher bins can be assumed to be larger crystals measured along their length axis, however, this does not eliminate the possibility of this being in an agglomerate.

Figure 6.9 shows an indication of breakage or nucleation in the system resulting in a possible bimodal distribution as discussed in section 6.1.4. The smaller crystals have been highlighted in circles. Note that the shape of the crystals is closer to stout habit, where side lengths are close in size. This second population gives rise to smaller counts without the possibility of larger counts.

The FBRM count for the process was registered during the experiment and two views are shown

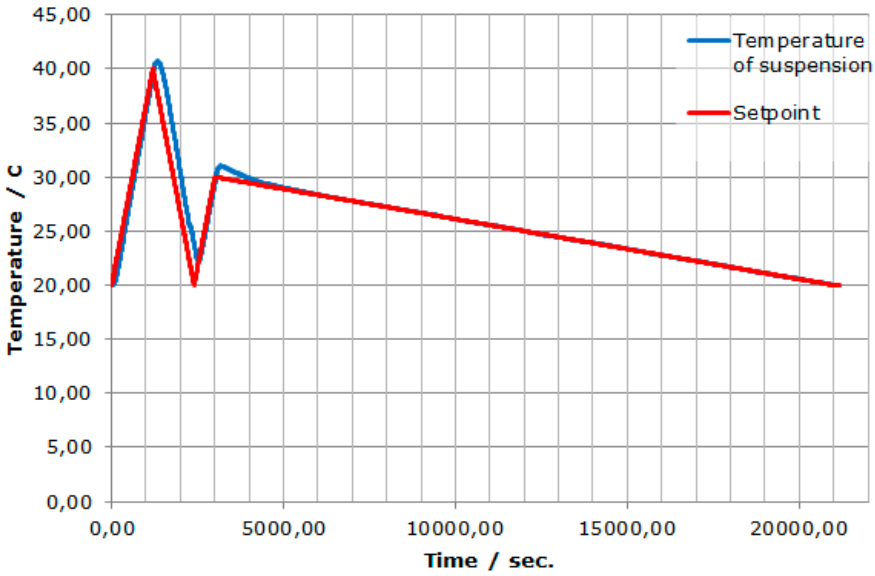

Figure 6.7: *The temperature profile for the hydroquinone-water experiments*

Figure 6.8: *Crystals showing agglomerated needles*

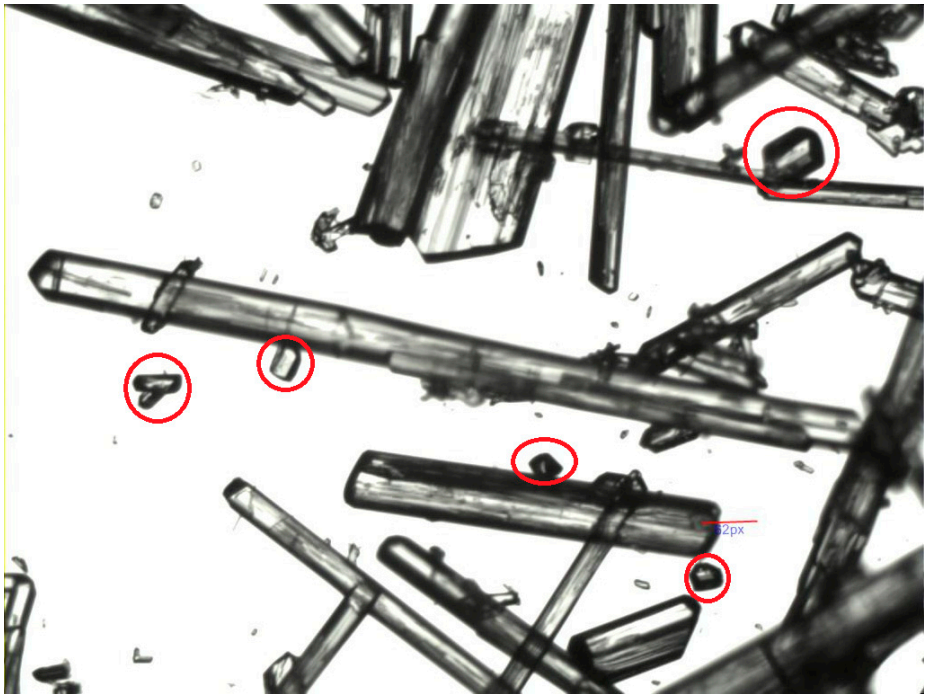

Figure 6.9: *Crystal sample from the hydroquinone-water experiments. Highlighted in the circles is the second population of crystals with different shapes than the larger needle-shaped crystals*

in Figure 6.10 and Figure 6.11. It was found that in the upper channels with channel size above $200\mu m$ no counts were registered, and these are not shown in the figures.

In Figure 6.10 the side view is shown. From this view it can be seen that the process follows the temperature curve well. Initially material is charged to the vessel and dissolved leading to very few counts across all channels. The seed generation leads to a rapid rise in the counts, which is eliminated in the reheating of the system which takes place from $2.5 \cdot 10^3$ to $3.0 \cdot 10^3$ seconds. The response in the FBRM indicates that this chemical system in the current technical system responds rapidly. From $10 \cdot 10^3$ seconds the system is steadier in count number and the system exhibits growth and agglomeration. This can be seen in Figure 6.11, where the maximum count in the channels from 50 to 200 increases. It should be noted that the counts in channels below $10\mu m$ are uncertain due to the Mie scatter effects as discussed in section 6.1.1. This count is partly due to the minor particles highlighted in Figure 6.9, partly due to the larger needle-shaped crystals that are intersected at angles near ortogonal values of their length direction.

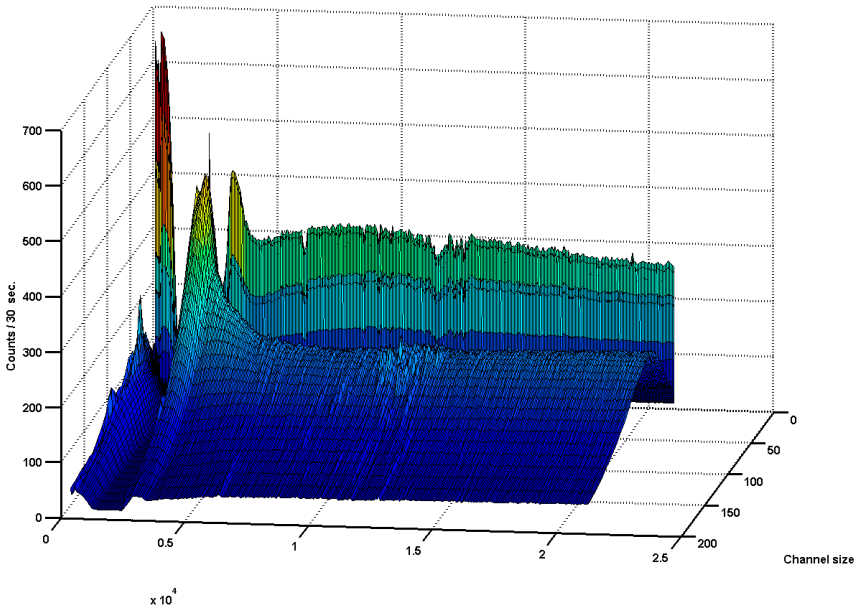

Figure 6.10: *FBRM count during crystallization in the lower channels*

6.2.2 FBRM for nucleation application

The FBRM application to nucleation is discussed using an example of FBRM applied to a crystallization of paracetamol from propan-2-ol (isopropyl alcohol, IPA). This system was studied using a combination of FBRM and Raman spectroscopy. The FBRM results are discussed in this chapter, the combined results are discussed in section 6.3.

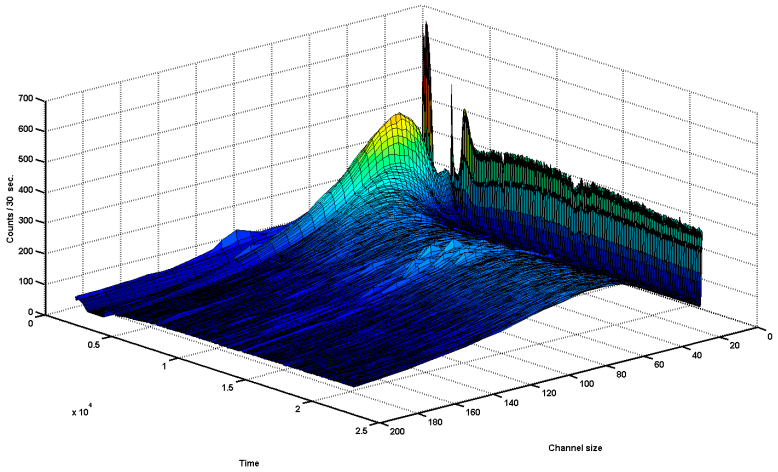

Figure 6.11: *FBRM count during crystallization in the lower channels*

Experimental plan

The experimental series was planned for analyzing the nucleation and to see if information could be extracted for the specific system. For this purpose, the experimental procedure was to charge the batch vessel with the material, dissolve it under heating and generate the seeds in-situ. The process was monitored using PVM. With FBRM for detection the induction time can be estimated for the system, and the induction time is estimated as a function of stirring and cooling rate.

Experimental procedure

For the experiments 62.1 g paracetamol and 300 g propan-2-ol were charged into the crystallization vessel. This corresponds to a saturation temperature of 50 °C.

The system was heated to 60 °C and kept at this temperature for 20 min. to ensure dissolution of the material charged into the crystallizer. Following this dissolution the system is cooled at a ramp of either 0.5 °C/min. or 2 °C/min. The system is cooled to the lowest possible temperature with the water-based cooling system, which corresponds to 5-6 °C under the temperature regime in the laboratory where the experiment took place. During the experiment stirring is applied in the vessel. The stirring rate is varied during the experimental series and for a given experiment it is fixed at 300, 450 or 600 rpm. Table 6.2 shows the variation in stirring and cooling rate along with measured variables. As nucleation was detected and the FBRM count increased, samples were withdrawn, filtered and analyzed under the microscope. When the FBRM count reached a plateau, the experiment was stopped and the crystals isolated.

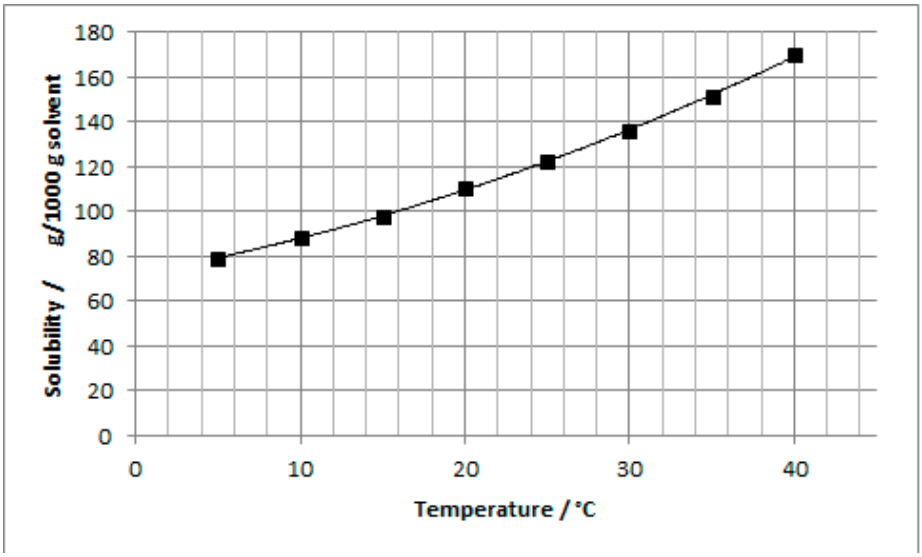

Figure 6.12: *The solubility of paracetamol in propan-2-ol. The relation is expressed as a second order polynomial (equation 7.1.3), which validity matches the range of operations (Saleemi, 2011)*

Results

The experimental series was carried out and an example of the obtained data is shown in Figure 6.13. All data from experiments are given in Appendix: Experimental results

The results are summarized in Table 6.2. The stirring rate seems to have significant influence on the total count number. This is to be expected as the stirring will determine how many objects will pass the measurement point pr. unit time. At elevated stirring rates, bubbles were observed in the PVM. These, along with large particles or artifacts, would result in decreased count as they block other particles.

The cooling rate affects the induction time and the slower the cooling, the longer the induction time.

The FBRM is very efficient at detecting the nucleation event, however, this should be correlated with the concentration measurements as discussed in section 6.3 in order to establish the nucleation parameters k_b and b used in the function $B = k_b \cdot S^b$. If the concentration is not measured, no mass balance can be completed, even with pictures of the crystals, as the deviation in size is to large.

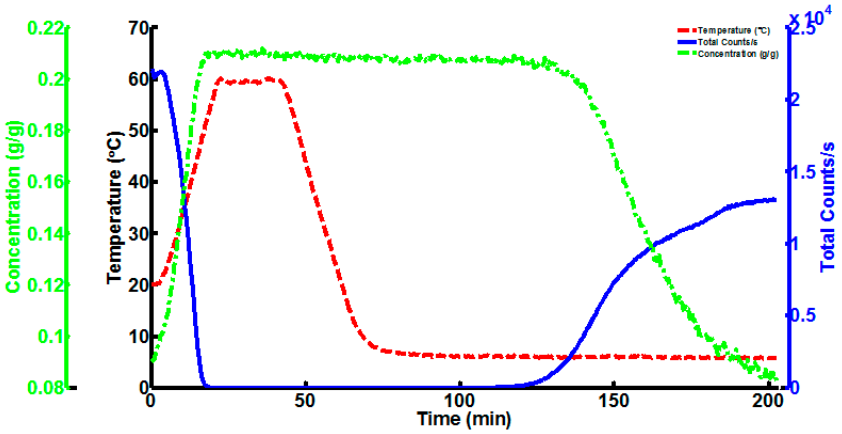

Figure 6.13: *Batch cooling of paracetamol in propan-2-ol. A jacketed vessel is charged with paracetamol and propan-2-ol and heated until the paracetamol is dissolved. The concentration (dashed green line), temperature (dashed red line) and chord length counts (solid blue line) are monitored. The saturation condition is matched to a solution saturated at 50 °C, and the crystallizer vessel is programmed to reach 60 °C, where it is kept for 20 min. The concentration of paracetamol in solution appears to reach a maximum. The temperature curve is pre-programmed to cool linearly at a cooling rate of 2.0 °C pr minute, and from the monitoring this curve is followed well, untill the final setting of the temperature is reached. The crystallizer is held at 7 °C and after 110 min, the total chord count increases and the concentration of paracetamol in solution decreases. The vessel is continuously stirred at 300 rpm*

Table 6.2: *Relation between final count, stirring and cooling rate for the experiments. The stirring rate influences the total count in the lower range. At 300 rpm, the maximum FBRM count is around 75% of the nearest higher stirring rate counts. The stirring affects how frequently a suspended particle will pass the measurement point, at elevated stirring larger bubbles may form, which are also counted as objects.*

Cooling rate degree C	Stirring rate rpm	maximum FBRM count -	Induction time sec.	Run number
2.0	300	13067	3110	1
2.0	450	18051	2180	5
2.0	600	17022	3240	6
0.5	300	13841	6270	2
0.5	450	19743	3150	4
0.5	600	17799	4710	3

6.3 Other monitoring techniques

FBRM can be combined with other measuring techniques, and for monitoring crystallization operations this is often the case. This section covers some of the possible combinations of measuring techniques, which can be used to compare results of FBRM and possibly gain more information from the data. The techniques are only covered briefly in this chapter with focus on how they are utilized along with the FBRM. The techniques are primarily for obtaining information on concentration and shape of the crystals.

6.3.1 Concentration measurements

Measuring the concentration in the crystallization operation allows concentration profiles with respect to time to be constructed. These profiles can be used to construct the concentration or mass balance for the operation with respect to time. From the reconstructed profile, a model can be identified to match this profile, and hence a set of parameters for the involved kinetic phenomena can be obtained. To match this profile, it is important to have a correct assumption of the involved kinetic phenomena growth and nucleation, which are the two concentration consuming phenomena. Agglomeration and breakage involve formed crystals getting in contact and forming agglomerates or formed crystals breaking, which does not contribute to the solution mass balance. However, these phenomena may alter the available surface area and hence contribute to the overall nucleation and growth rate of the system. Measuring the FBRM along with the concentration allows detection of the chord lengths and changes in the chord length distribution. The FBRM acts as a relative technique, and the measured chord length distribution is dependent on the flow in the crystallizer, as it counts the number of passing chords within the measurement area. Settings, such as the stirring rate, and the size of particles and objects in the crystallizer affect the measurements. This makes comparison of FBRM data from different experiments difficult as discussed in section 6.1.2. Assuming this effect is not important across a crystallization operation, where the growth and agglomeration is limited, the increase in count in upper channels can be taken as a measurement of the growth. This could lead to an estimate of the growth kinetics from the FBRM only, which would be compared with the concentration based kinetics.

Techniques for concentration measurements

Techniques that are compatible with FBRM and the crystallization operation can be used to measure the concentration of a solute in solution. Such techniques can be spectroscopy, which is treated here. The spectroscopy techniques rely on subjecting the chemical system to radiation at a certain frequency and observe the interaction of the radiation with the chemical system. When spectroscopy is used with FBRM for concentration measurements, the frequency of the used measurement devices should not coincide in order to avoid errors in the measurements. If the chemical system absorbs in the UV-visible spectrum, this can be used with the FBRM for concen-

tration measurements. In this case, a probe is mounted along the FBRM probe and a determined correlation used to calculate the concentration of solute in the magma. A second possibility is the utilization of Raman spectroscopy. This technique was utilized for the paracetamol - propan-2-ol system to measure the shift, and with the measured intensity, the concentration was calculated for the solution. The advantage of Raman spectroscopy is that unique shifts may be assigned to solvent, solute and solid in the system, respectively. This allows a combined measurement of the form of the crystals and the concentration of the solution. Raman spectroscopy utilizes the shifts connected to Raman, which are inelastic. The frequency of the shifts make Raman susceptible to fluoroscence and external sources of radiation such as light. For chemical systems exhibiting fluoroscence, Raman spectroscopy is problematic to use. In connection with the FBRM technique, the most important measure to take to avoid problematic interaction is to ensure that the techniques operate at different wavelengths and that the wavelengths are compatible with the chemical system in terms of obtaining the desired interaction.

6.3.2 Particle images

Shape assumptions can be analyzed in connection with the crystallization operation. This can be done through in-line monitoring through particle vision and measurements or off-line using taken samples under a microscope. Both techniques offer advantages and disadvantages and are treated below.

Particle vision and measurements

Particle vision and measurements utilize a probe placed in the crystallizer to take pictures of the system. These pictures are taken at specific intervals and can be analyzed through the crystallization. The pictures are taken using a limited light source, which needs to be directed away from the Raman and FBRM probe. The pictures can be analyzed using software for picture analysis and these results can be used for online optimization of the process. However, the technique is limited as the image separation in depth for computer analysis is limited and hence the possibilities of discriminating between artefacts, crystals, overlapping crystals and agglomerates are limited. This analysis is appropriate using a representative sample in a microscope.

Microscopy

Microscopy techniques for off-line sample analysis can be applied to the crystallization operation for obtaining shape factors for the crystals. If samples are taken during the operation, the sampling technique needs to provide limited disturbance to the system. Taking a representative sample can be difficult at these conditions and this should be considered when the sample results are discussed. Microscopy allows detailed analysis of the respective samples, which are used to

discuss the shape of the crystals, the size and size distribution and the degree of agglomeration of the system.

Figure 6.14: *Pictures of the crystals in the sample withdrawn from the operation. The crystals have been dried and some agglomeration may have occurred in the drying process. Signs of inclusion appear present. A similar sample was drawn 10 min. later. This sample is shown in Figure 6.15*

6.3.3 Combined measurements

The measurements of the chemical system paracetamol - propan-2-ol were taken using FBRM and Raman spectroscopy combined. The system was monitored through PVM and samples were taken at regular time intervals when nucleation had been detected as an increase in total FBRM count. In this section it is discussed how the combined measurements can be used for the identification of the model for the seed generation for this system and thus obtaining the nucleation kinetics.

The experiments and results were discussed in section 6.2 and the data was presented in Appendix: Experimental resultsand discussed in section 6.2.2. An example of the concentration, temperature and FBRM count profiles are shown in Figure 6.13

Using this data, the kinetics of the nucleation are estimated. For this purpose the concentration profile was matched to the obtained data. A moments model was built and used with the data for the error function. The shape factor was obtained from the microscope pictures. The specifications are shown in the calculation procedure below.

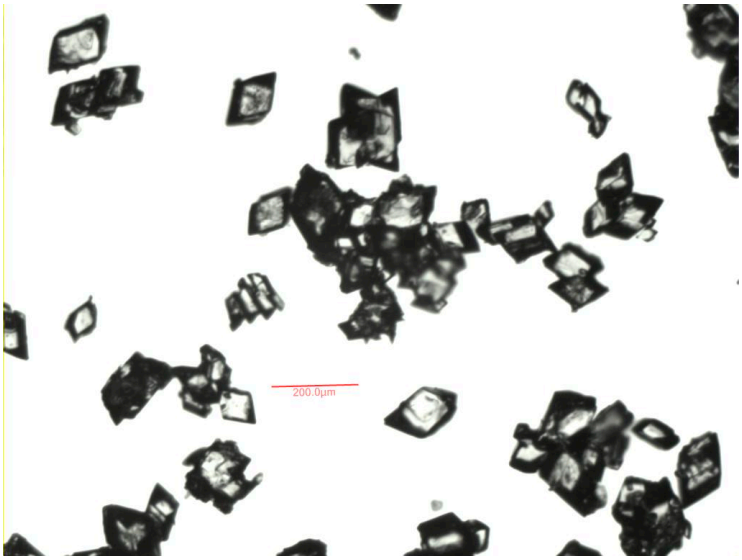

Figure 6.15: *Crystals withdrawn from the operation 10 min after the sample in figure 6.14. The size of the crystals varies, but the shape appaers to be similar. Some agglomeration has occurred in the drying process*

Calculation procedure

This section presents the model structure and the calculation procedure.

Model The model structure is given below:

saturation concentration	$C_{sat} = A_1 \cdot T^2 + A_2 \cdot T + A_3$	(6.3)
supersaturation	$S = C - C_{sat}$	(6.4)
zeroth moment	$\frac{d\mu_0}{dt} = k_b \cdot S^b$	(6.5)
first moment	$\frac{d\mu_1}{dt} = k_g \cdot S^g \cdot \mu_0$	(6.6)
second moment	$\frac{d\mu_2}{dt} = 2k_g \cdot S^g \cdot \mu_1$	(6.7)
third moment	$\frac{d\mu_3}{dt} = 3k_g \cdot S^g \cdot \mu_2$	(6.8)
concentration	$\frac{dC}{dt} = \frac{-\rho_c \cdot k_v}{M_{solvent}} \cdot 3k_g \cdot S^g \cdot \mu_2$	(6.9)

Variables The variables are categorized as given in Table 6.3:

Table 6.3: *Variables for the model classified as specified system parameters, known variables and calculated variables*

Specified system parameters	$A_1, A_2, A_3, \rho_c, k_v, k_g, g, k_b, b$
Known variables	$M_{solvent}, T$
Calculated variables	$C_{sat}, S, \mu_0, \mu_1, \mu_2, \mu_3, C$

The system parameters need to be specified for the calculations. Here A_1, A_2, A_3 are known from the supersaturation description and the plot of the saturation curve shown in Figure 6.12.

From the microscopy pictures shown in Figures 6.14 and 6.15, the form and shape factor are estimated. From the literature, ρ_c is known.

k_g, g, k_b, b are all estimated using the concentration, temperature and FBRM data and the model with the model equations 6.3 - 6.9.

$M_{solvent}$ is known from the experiment.
T and C are known from the data.

The estimation of the parameters is discussed in chapter 7.

Part III

Application of Modeling framework

CHAPTER 7

Case studies

Selected case studies are presented to discuss the versatility of the generic modelling framework and the developed procedures. Initially case studies on the identification of a model from concentration profiles in batch mode for the chemical systems paracetamol-ethanol and paracetamol propan-2-ol are discussed in section 7.1 and section 7.1.3, respectively. This is followed by an extension to continuous mode of operation for the paracetamol-ethanol system (section 7.2) and a study on reactive crystallization (section 7.3). The chapter is finished with a deeper discussion of the model identification procedure (section 7.4).

7.1 Parameter estimation for paracetamol-ethanol

The chemical system paracetamol-ethanol is known from the literature and parameters for the associated kinetic phenomena have been estimated previously (Worlitschek and Mazzotti, 2004; Mitchell and Frawley, 2010; Frawley et al., 2012). The saturation curve is known as well and an expression (7.1) has been found in the literature (Mitchell and Frawley, 2010).

$$C_{sat} = 2.955 \cdot 10^{-4} \cdot e^{2.179 \cdot 10^{-2} T} \tag{7.1}$$

The relation is for temperatures in Kelvin. A plot of the corresponding saturation in the range

of 2-60 °C is shown in Figure 7.1. From the relation it is found that in a cooling crystallization from 50 to 10 °C, 58 % of the material can be crystallized (not considering the kinetics). The solubility points are shown in Table 7.1

Table 7.1: *Solubility of paracetamol in ethanol at 10 and 50°C*

Temperature / °C	Solubility / g/g
10	0.14
50	0.34

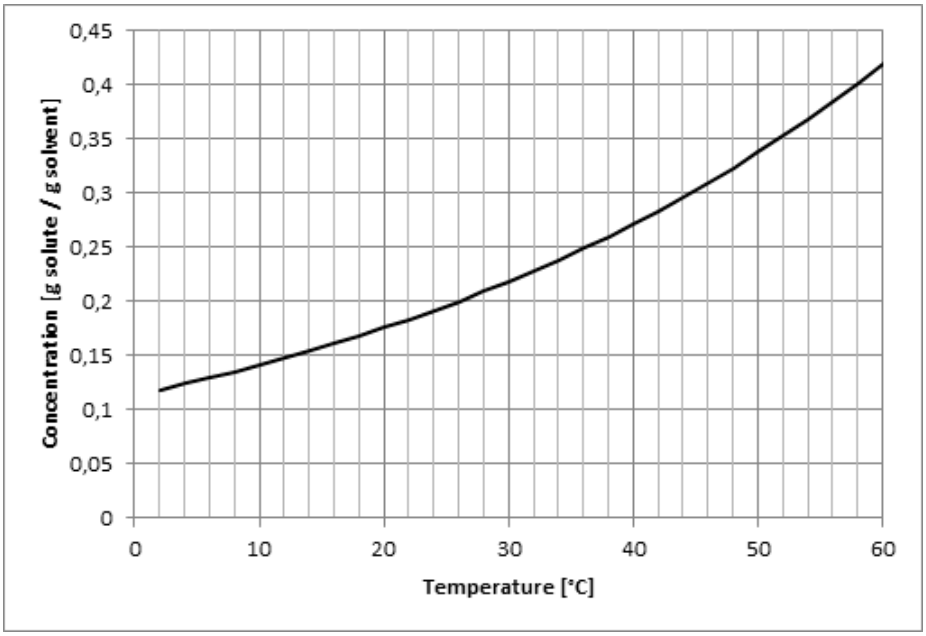

Figure 7.1: *The solubility of paracetamol in an ethanol solution in the temperature interval 2-60 °C. The relation is given as equation* (7.1) *(Mitchell and Frawley, 2010)*

7.1.1 Model

For the parameter estimation, a mass, energy and population balance are needed, although perfect temperature control is assumed and the crystallizer temperature will follow a linear cooling curve. The moment approach was applied due to its speed of solution. The moments approach is established in the framework and a function for describing a seed distribution was written. The moment approach can give the kinetics for growth and nucleation for a system with solution of few equations and can give a fast solution within the overall parameter estimation problem. The equations are shown in Table 7.2

Table 7.2: *Model equations for the moment approach*

Model element	Model equation
0^{th} moment,μ_0	$\frac{d\mu_0}{dt} = k_{b1} \cdot S^{b1} + k_{b2} \cdot S^{b2}\mu_3$
1^{st} moment,μ_1	$\frac{d\mu_1}{dt} = k_g \cdot S^g \mu_0$
2^{nd} moment,μ_2	$\frac{d\mu_2}{dt} = 2k_g \cdot S^g \mu_1$
3^{rd} moment,μ_3	$\frac{d\mu_3}{dt} = 3k_g \cdot S^g \mu_2$
Concentration balance, solute	$\frac{dC}{dt} = -\rho_c \frac{k_v}{m_{solvent}} 3k_g \cdot S^g \mu_2$
Supersaturation definition	$S = C - C_{sat}$
Saturation relation	$C_{sat} = a_1 \cdot e^{a_2 T}$ (eq. (7.1))
Temperature relation	$\frac{dT}{dt} = D$

Data required The overall model requires kinetic parameters, crystal properties, thermodynamic properties and operational variables as well as initial values for the differential equations. The kinetic parameters, crystal properties, thermodynamic properties and operational variables are shown in Table 7.3. The initial conditions for the differential equations are discussed below in section 7.1.2.

Table 7.3: *Kinetic parameters, properties and operational variables needed for the moment approach*

Kinetic parameters	$k_{b1}, b_1, k_{b2}, b_2, k_g, g$
Crystal properties	ρ_c, k_v
Thermodynamic relation	a_1, a_2
Operational variables	$m_{solvent}, D$

Kinetic phenomena

The model includes the kinetic phenomena growth and nucleation. The growth is assumed constant across crystal size and properties. The nucleation is split into primary $k_{b_1} S^{b_1}$ and secondary nucleation $k_{b_2} S^{b_2} \mu_3$. The secondary nucleation is assumed to be based on the volume of crystals and includes the total volume factor μ_3. Primary nucleation is assumed to be possible to dominate through seeding. The secondary nucleation is present due to the crystals in the system and may not be possible to dominate depending on the chemical and technical system and their properties.

7.1.2 Initial conditions

The initial conditions for the differential equations are related to the moments, the initial concentration and initial temperature of the system. The initial moments are derived from the initial crystal distribution seed and discussed below in Seeding. The initial concentration C_0 is defined from the amount of solute pr unit solvent, the initial temperature T_0 is specified for the system as well as the operation considers temperature change and hence change in saturation and

thermodynamical potential.

Seeding

The seeding is specified for the moment equations as moments of a distribution. The normal distribution is chosen and the moment generating function is within the framework (Equation (5.3)) Specifying this with the desired distribution parameters (mean, μ, standard deviation, σ, crystal density, ρ_c, shape factor k_v and seed mass, m_{seed}) it is possible to generate the initial values for the crystallization operations problem. According to experimentalists, the crystallization seeding mass is often taken to be 5% solute, or if the final solution contains a significant amount of solute as 5% of $m_{solute,initial} - m_{solute,final}$.

Within the functions a seed of 5% solute mass was specified and the problem simulated with and without nucleation, assuming that this phenomenon can be dominated.

6 simulations are made using different conditions. 2 sets of 3 simulations are used for parameter estimation, a short set with simulation time {120, 130, 140} minutes and a longer set with simulation times {600, 660, 720} minutes. Using the generated data points, a parameter estimation is undertaken, and a set of parameters estimated on the basis of the simulated data. Uncertainties are estimated using the approach of Sin et al. (2010). The returned parameter set from the estimation is different from the set used for data generation, however, the fit is good. From visual inspection of the plot, the model and simulated points are in agreement as seen in Figure 7.2, where the data points and the models are matching.

Table 7.4: *Parameters used for data generation and estimated parameters*

Parameter	Data generation	Estimate
k_{b1}	$2.024 \cdot 10^7$	$3.897 \cdot 10^4 \pm 1.230 \cdot 10^4$
b_1	4	2.286 ± 0.083
k_{b2}	$2.656 \cdot 10^7$	$1.878 \cdot 10^8 \pm 4.619 \cdot 10^7$
b_2	2.232	$3.228 \pm 9.36 \cdot 10^{-2}$
k_g	$8.45 \cdot 10^3$	$1.967 \cdot 10^4 \pm 1.107 \cdot 10^3$
g	1.602	$1.793 \pm 1.14 \cdot 10^{-2}$
E_a	4.056e4	$4.021 \cdot 10^4 \pm 1.40 \cdot 10^2$

Only one specified parameter is within the 95% confidence interval of the estimated parameters as seen in Table 7.4. This indicates that the identifiability of the model is problematic. The consequences of this is initially investigated adding noise to the data set. Using a random number generator, white noise with a standard deviation of $\sigma = 1\%$ of the final concentration value in a simulated experiment is added to each of the six experiments and the parameter estimation is repeated. The result of the parameter estimation is given in Table 7.18. As expected, the parameters are highly uncertain with some having 95% confidence intervals larger than the absolute value of the parameter. Plotting the noisy data in Figure 7.3, the fit appears good from visual

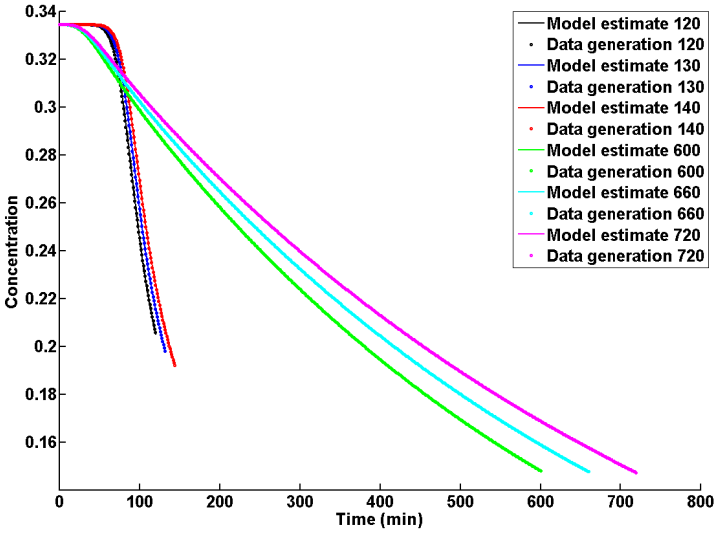

Figure 7.2: *Data points generated with one set of parameters (Data generation in table 7.4) and the model shown in table 7.2 with a second set of parameters (Estimate) in table 7.4. The fit is good, and parameters may be accepted for system description, however, the large uncertainties point towards an identifiability problem.*

inspection

Table 7.5: *Parameters used for data generation and parameters estimated for the data with added noise. Compare to table 7.4. The parameters relating to the nucleation are highly dubious as their 95% confidence intervals are very large compared to the absolute parameter value*

Parameter	Data generation	Noisy estimate
k_{b1}	$2.024 \cdot 10^7$	$1.77 \cdot 10^9 \pm 4.44 \cdot 10^9$
b_1	4	5.00 ± 0.704
k_{b2}	$2.656 \cdot 10^7$	$3.6 \cdot 10^8 \pm 2.30 \cdot 10^9$
b_2	2.232	2.84 ± 2.71
k_g	$8.45 \cdot 10^3$	$4.22 \cdot 10^4 \pm 2.84 \cdot 10^4$
g	1.602	1.39 ± 0.105
E_a	4.056e4	$4.75 \cdot 10^4 \pm 1.1 \cdot 10^3$

The identifiability is explored further in section 7.4

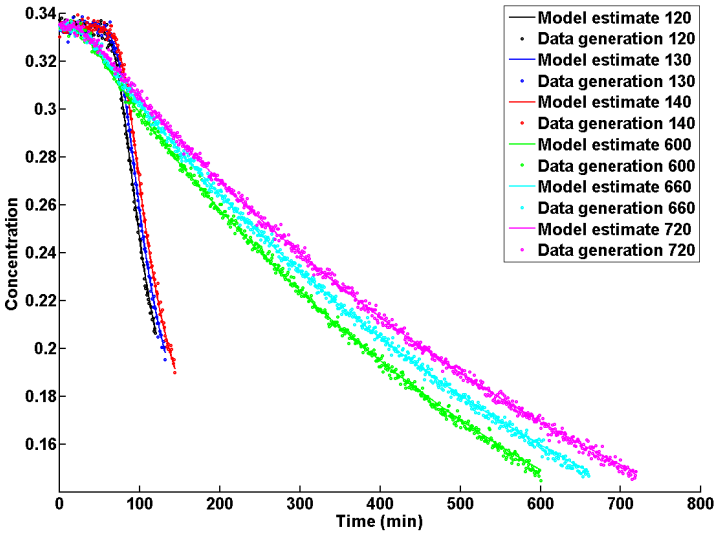

Figure 7.3: *Noisy data and the model with estimated parameters as shown in table 7.5. The noisy data were generated using the data set generated previously and normal distributed white noise with a standard deviation of $\sigma = 1\%$ of the final concentration value in a simulated experiment was added to each of the six experiments. From visual inspection, the plotted curves match the data*

Overlap of growth models

As indicated above, multiple regressed parameter sets for the model may match the data points. For the paracetamol-ethanol system, two parameter sets for the growth rate model (Equation (7.1.2)) are given in Table 7.6. The kinetic model parameters are k_g, E_a and g, S represents the supersaturation. In Figure 7.4, it is seen that for the lower supersaturations, where the growth may be a dominating phenomenon, the growth rates predicted from the models are close to each other in terms of numerical values.

$$G = k_g \cdot e^{\frac{-E_a}{RT}} S^g$$

Table 7.6: *Parameters for the growth rate model for paracetamol-ethanol from Mitchell and Frawley (2010) and Worlitschek and Mazzotti (2004). The parameter sets are notably different, however, similar values are obtained when the growth rate models are plotted together as seen in figure 7.4*

Parameter	Mitchell and Frawley (2010)	Worlitschek and Mazzotti (2004)
k_g	$8.45 \cdot 10^3$	$1.78 \cdot 10^4$
g	1.602	1.9
E_a	$4.056 \cdot 10^4$	$41.6 \cdot 10^4$

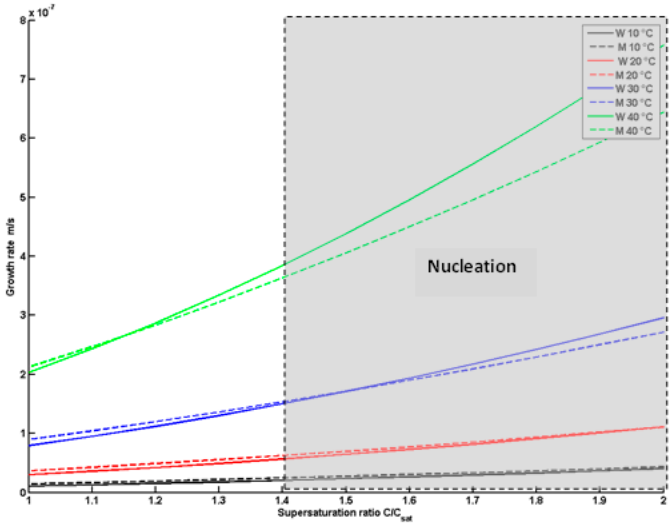

Figure 7.4: *The growth models are close at low supersaturations and deviate only at increased temperature and supersaturation. In this are nucleation can well take place disturb the estimation of the growth model parameter. The relation within the growth model suggests, that at low supersaturation, where growth can be dominating the nucleation phenomena, the growth models may be difficult to identify reliably, whereas at increased supersaturation nucleation will interfere*

7.1.3 Parameter estimation for paracetamol - propan-2-ol

The parameters are needed to simulate the systems but the estimates come with a high uncertainty. A scenario with parameter estimation for the paracetamol propan-2-ol system has been established. In this scenario, a model similar to the model employed in section 7.1 is employed and the parameters estimated again. The overall model requires kinetic parameters, crystal properties, thermodynamic properties and operational variables as well as initial values for the differential equations.

Chemical system

The chemical system is paracetamol - propan-2-ol and the saturation curve is known from the literature. The equilibrium relation can be described as a second-order polynomial expression (Equation (7.1.3)) (Saleemi, 2011):

$$C_{sat} = 2.78 \cdot 10^{-2} T^2 + 1.32T + 72.1$$

where C_{sat} is the solubility of paracetamol in g pr. kg propan-2-ol at the temperature T in $°C$. The equilibrium curve is plotted in figure 7.5.

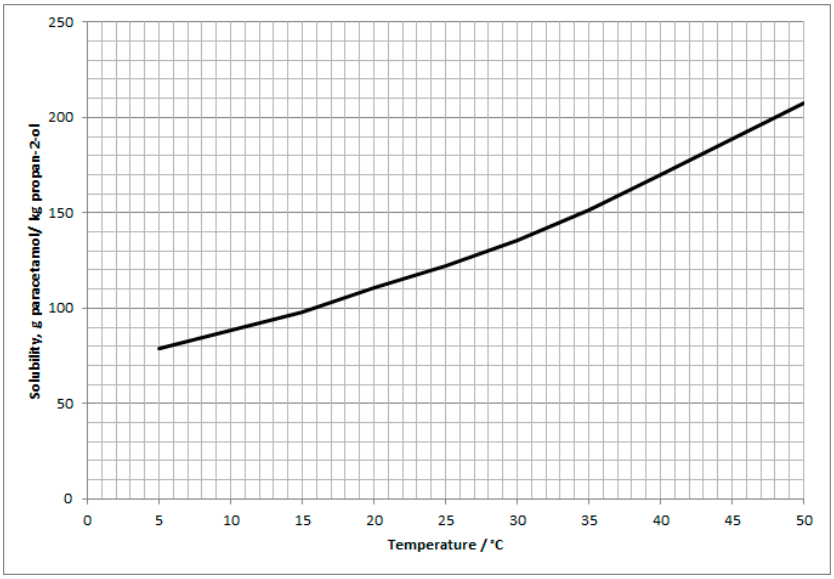

Figure 7.5: *The solubility of paracetamol in propan-2-ol in g/kg solvent in the range 5-50 °C. The relation is expressed as a second order polynomial (equation 7.1.3), which validity matches the range of operations (Saleemi, 2011)*

The kinetic parameters, crystal properties, thermodynamic properties and operational variables are similar to those for the paracetamol-ethanol case shown in Table 7.3, except the crystallizer

is pre-programmed to follow a temperature trajectory and follows this well. Furthermore, the crystallizer is assumed to reach thermal equilibrium internally (no temperature gradient within the crystallizer), and as such the measured temperature data is used rather than a correlation.

A similar parameter estimation has been carried out for the chemical system paracetamol - propan-2-ol. For this system a set of experimental data providing the concentration profile under known operating conditions is necessary. This is obtained through a series of experiments as discussed in 7.1.3.

Available data

The available data for the parameter estimation originates from a series of experiments, where paracetamol has been crystallized through batch cooling. The available data from an experiment is shown in Figure 7.6. A vessel is charged with paracetamol and propan-2-ol at an amount corresponding to equilibrium at 50 $°C$ and heated to 60$°C$. It is kept at this temperature for 20 min. and monitored though FBRM. The FBRM count decreases significantly during the heating phase and a low count from the FBRM indicates that all crystals are dissolved, which also is the impression from visual inspection. The vessel is then slowly cooled and crystallization occurs. A concentration and temperature profile is obtained and from this, the parameters for the mode can be obtained. For this purpose a moments model is used, similar to the model given in Table 7.2.

Parameter estimation

Using the available data parameter estimations are performed to obtain the parameter values for the model. The parameters $k_{b1}, b_1, k_{b2}, b_2, k_g, g, E_a$ are estimated from the concentration curve using a least squares approach and it is found that multiple parameter sets can be used to represent the data. Two sets of estimated parameters are given in Table 7.7. The corresponding model fit to the data is shown in Figure 7.7. It can be seen that the models match the data well.

It is possible to describe the obtained data well, using the model. The estimated parameters are stored in the database, as they can be useful for the future model based studies of this system. However, a note is added that the parameters should not be assigned the physical meaning built into the structure.

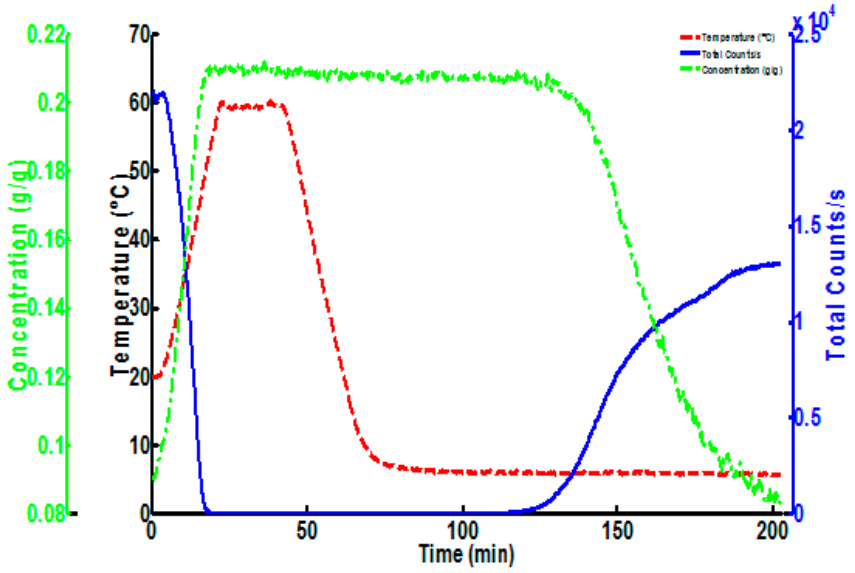

Figure 7.6: *Batch cooling of paracetamol in propan-2-ol. A vessel is charged with paracetamol and propan-2-ol and heated until the paracetamol is dissolved. The temperature (red dashed line), concentration (green dashed line) and chord length counts (blue solid line) are monitored (spectroscopy is used for the concentration, which is translated to the concentration). The saturation condition is matched to a solution saturated at 50 °C, and the crystallizer vessel is programmed to reach 60 °C, where it is kept for 20 min. teh concnetration of paracetamol in solution appears to reach a maximum. The temperature curve is pre-programmed to cool linearly at a cooling rate of 2.0 °C pr minute, and from the monitoring this curve is followed well, untill the final setting of the temperature is reached. The crystallizer is held at 7 °C and after 110 min, the total chord count increases and the concentration of paracetamol in solution decreases. At this stage, the crystallization of the paracetamol is initiated and continues. The operation is stopped as the chord length count levels off and a concentration of paracetamol in solution comes close to the equilibrium (83g paracetamol/kg solvent from eqation* (7.1.3)).

Table 7.7: *Estimated parameters from two least-squares estimations for the paracetamol-propan-2-ol case. The parameters are found using two different starting points for the estimation and several parameters differ. Both parameter sets can be used to represent the data as illustrated in figure 7.7, where the resulting model fits are plotted with the data. The curves for the model overlap*

Parameter	Estimate 1	Estimate 2
k_{b1}	$8.7 \cdot 10^3$	$8.4 \cdot 10^4$
b_1	4.1	4.9
k_{b2}	$2.1 \cdot 10^7$	$4.6 \cdot 10^6$
b_2	1.2	1.1
k_g	$8.2 \cdot 10^3$	$1.6 \cdot 10^4$
g	1.3	1.3
E_a	$4.0 \cdot 10^4$	$4.0 \cdot 10^4$

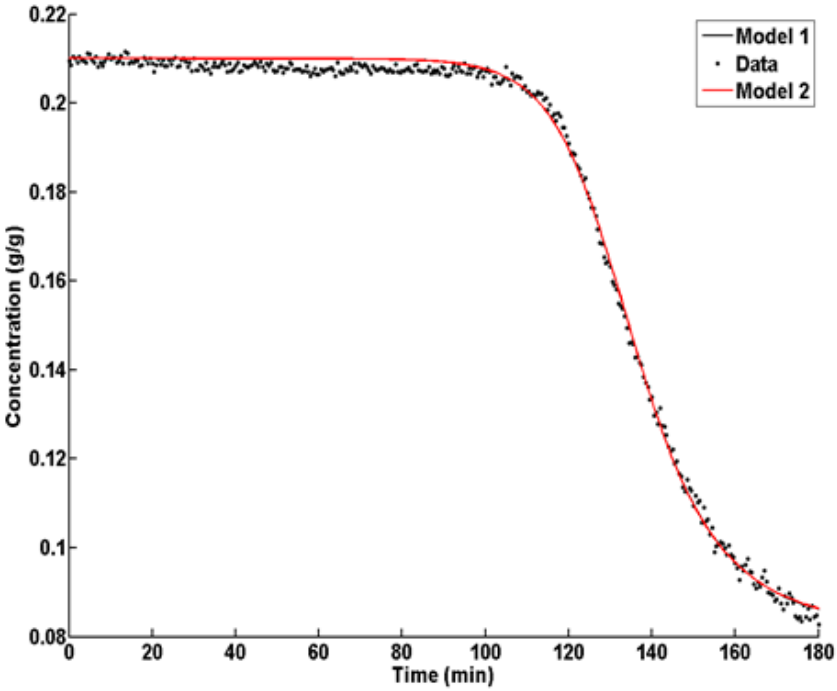

Figure 7.7: *Estimated parameters from two least-squares estimations (sets seen in table 7.7) for the paracetamol-propan-2-ol case. The parameters are found using two different starting points for the estimation and several parameters differ. Both parameter sets can be used to represent the data, as the curves for the model overlap and only the red curve can be seen, as the curves are on top of each other.*

7.2 Continuous crystallization of paracetamol

A continuous operation for the crystallization of paracetamol from an ethanol solution is investigated. For this operation, the vessel is initially filled with solution saturated at 50°C, and an inflow with this condition is maintained. The vessel is assumed to hold 1000 g solvent initially and the inflow and outflow are 1 g/min.

7.2.1 Model criteria

The model will follow the population of the crystals and a population balance is necessary. Nucleation and growth phenomena are assumed to be present and the mass balance will have to include the cooling of the crystallizer as well as the in-flow and out-flow of the liquid. It is assumed that the crystallizer is well-mixed in the liquid phase and classification occurs, so no crystals leave in the out-flow. The mass balance must account for this. It is assumed that a crystallizer of this size can be controlled well enough so that the temperature profile can be assumed to be linear.

7.2.2 Model equations

The model equations are taken from the generic modelling tool. The necessary equations for the method of classes are listed in Table 5.2. Furthermore, constitutive relations are necessary. These involve a saturation relation, which was presented in Equation (7.1) and kinetic relations. For the kinetic relations, the involved equations are listed in Table 7.9

Table 7.8: *Model equations for the continuous crystallization of paracetamol using the method of classes approach from the modelling tool. The number of classes is 400. The concentration balance is linked to the population balance. The energy balance is assumed independent and reduced to a constant for linear cooling*

Model element	Model equation
$Class_1$	$\frac{dN_1}{dt} = -\frac{G}{2\Delta Cl_1}N_1 + B - D$
$Class_i, 1 < i < End$	$-\frac{G}{2\Delta Cl_i}N_i + \frac{G}{2\Delta Cl_{i-1}}N_{i-1} + B - D$
$Class_End$	$\frac{G}{2\Delta Cl_{End-1}}N_{End-1} + B - D$
Concentration balance, solute	$\frac{dC}{dt} = -\rho_c \frac{k_v V}{m_{solvent}} \sum_{i=1}^{End}(Class_{Size}\frac{dN_i}{dt}) + \frac{\mathbf{FC_i}}{m_{solvent}}$
Energy balance, crystallizer	$\rho V c_p \frac{dT}{dt} = -\Delta H_c - \rho_c k_v V \sum_{i=1}^{End}(Class_{Size}\frac{dN_i}{dt}) - U_1 A_1 \Delta T$

The model equations need parameters and variables supplied. The necessary parameters and variables are listed in Table 7.10. The kinetic parameters for the paracetamol-ethanol system are known from the literature. The parameter set from Table 7.4 used for data generation is used for this example, as well as the crystal properties. The thermodynamic relation is supplied in Equation (7.1). Several of the operational variables are specified from the problem definition requirements $m_{solvent} = 1000g, m_{in} = m_{out} = 1g/min$. The concentration is specified from the

Table 7.9: *Model equations for the kinetic relations needed for the method of classes approach*

Model element	Model equation
Nucleation	$B = k_{b1} \cdot S^{b1} + k_{b2} \cdot S^{b2} \sum_{i=1}^{End} \left(\frac{\Delta Cl_i}{2} \right)^3$
Growth	$G = k_g \cdot S^g$
Concentration balance, solute	$\frac{dC}{dt} = -\rho_c \frac{k_v}{m_{solvent}} \sum_{i=1}^{End} \left(\frac{\Delta Cl_i}{2} \right)^3 + \frac{C_{in} m_{in} - C m_{out}}{m_{solvent}}$
Supersaturation definition	$S = C - C_{sat}$
Saturation relation	$C_{sat}(T) = a_1 \cdot e^{a_2 T}$ (eq. (7.1))
Temperature relation	$\frac{dT}{dt} = E$

requirement of saturation at 50 °C: $C_{in} = C_{sat}(50)$. The cooling rate E is fixed at 0.06 °C/min, resulting in a cooling of the crystallizer from 50 to 20 °C over 500 min.

Table 7.10: *Kinetic parameters, properties and operational variables needed for the method of classes approach*

Kinetic parameters	$k_{b1}, b_1, k_{b2}, b_2, k_g, g$
Crystal properties	ρ_c, k_v
Thermodynamic relation	a_1, a_2
Operational variables	$m_{solvent}, E, C_{in}, m_{in}, m_{out}$

The concentration profile, resulting supersaturation and temperature profile are shown in Figure 7.8. The supersaturation is changing little during the process and the crystals grow.

As the inflow and outflow are similar, the solvent volume is assumed unchanged. The growth of these crystals is followed and illustrated in Figure 7.9. It can be seen that the crystals gradually grow in size as new liquid is introduced and the vessel cools. Few new crystals are formed during the process.

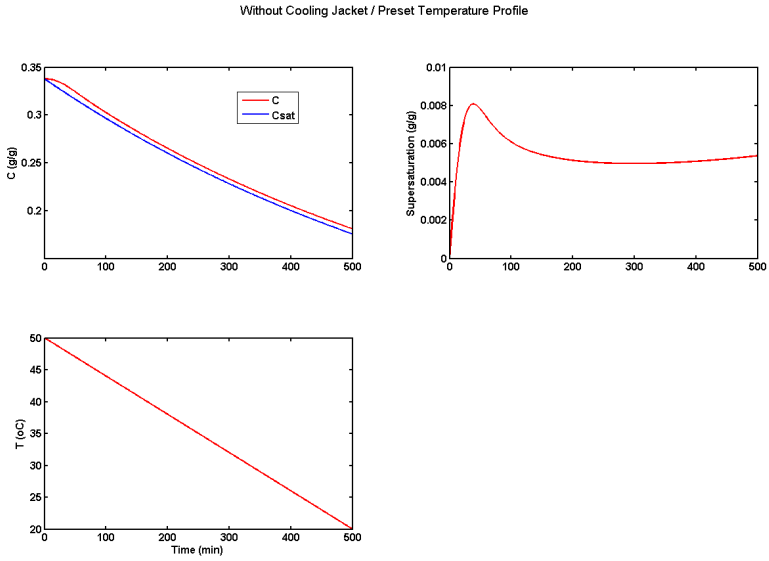

Figure 7.8: *The temperature and saturation profile for the continuous operation. The vessel is cooled linearly over 500 min. with a cooling rate of 0.06 °C/min. Initially the supersaturation increase, then decreases and remains around 0.006 g/g.*

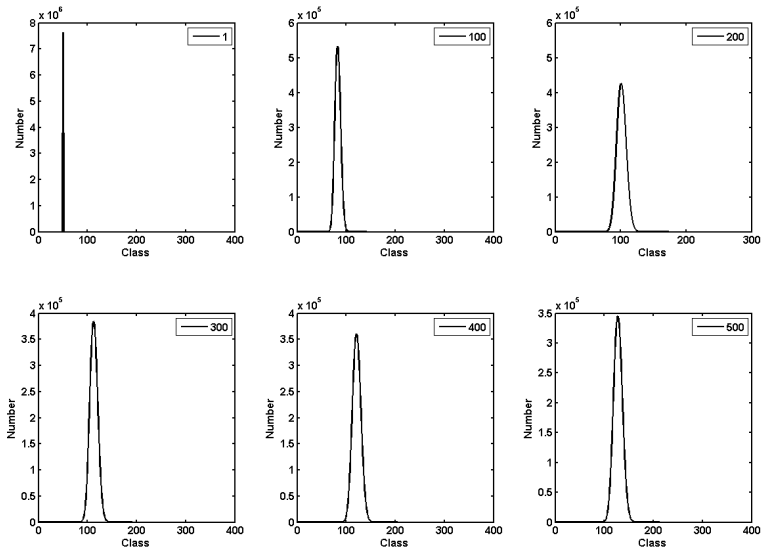

Figure 7.9: *Crystals growing in the continuous operation. The initial seeds grow into the larger classes absorbing the material and nucleation is insignificant with the level of seeding chosen*

7.3 Reactive crystallization

Reactive crystallization is a process in which a chemical reaction occurs and a crystallizing product forms. In this case, the vessel works as a reactor and a crystallizer in combination, and the dynamics of the reaction and crystallization can determine the characteristics of the crystalline product. Multiple reactions may occur simultaneously in the crystallizer, changing the conditions for the crystallization. The crystallizer may have equilibrium conditions for the reaction or be dynamic.

The framework has been extended with a reaction module. The process model remains the same, but involves a module, which describes reacting species and the evolution in the concentration of these as a consequence of reaction. Simultaneously the framework describes the crystallization taking the kinetics into account. Within this, it is possible to handle changes in composition of the chemical system due to reactions and changes in pH.

7.3.1 Example: Reactive Crystallization

Benzoic acid is part of the acid-base pair benzoic acid-benzoate. Sodium benzoate is more soluble in water than its corresponding acid in the temperature interval $20-45°C$ (more than twice the amount of benzoate can be dissolved). From a solution of sodium benzoate, benzoic acid may be crystallized through the addition of strong acid, lowering the pH. The investigation of a precipitation of benzoic acid crystals is desired.

Reactive properties Benzoic acid is part of the acid-base pair benzoic acid-benzoate. Sodium benzoate is more soluble in water than its corresponding acid in the temperature interval $20-45°C$ (more than twice the amount of benzoate can be dissolved). The acid-base reaction can be described as:

$$C_6H_6COOH \rightleftharpoons C_6H_6COO^- + H^+; \qquad pKa = 4.2 \tag{7.2}$$

Model criteria and assumptions A fed-batch operation is desired, where a solution of sodium benzoate is kept in the vessel, and a solution of hydrochloric acid is added to the chamber. To describe the precipitation of benzoic acid, the model requires a population balance, mass and energy balances. The reactor here is assumed small and the temperature kept constant through a cooling jacket. No crystals are present in the inflow and nuclei are assigned no dimensions.

Model structure The method of moments is chosen as solution method and and the appropriate model equations generated through the generic modelling tool on basis of the criteria. Using the

model of table 5.1, the model is structured in table 7.11.

Table 7.11: *Model equations for the moment approach for reactive crystallization of benzoic acid. The term reacted refers to the amount formed from reaction 7.2*

0^{th} moment,μ_0	$\frac{d\mu_0}{dt} = B$
i^{th} moment μ_i	$\frac{d\mu_i}{dt} = G\mu_{i-1}$
Concentration balance, benzoic acid	$\frac{dC}{dt} = \frac{m_{in}C}{m_{solvent}} - \rho_c \frac{k_v}{m_{solvent}}(3G\mu_2) - Reaction_{forward}$
Concentration balance, benzoate	$\frac{dC}{dt} = \frac{m_{in}C}{m_{solvent}} - Reacted_{backwards}$
Energy balance, crystallizer	$T = E$

Kinetic relations are found in the database and specified. The kinetic expressions are found in Ståhl et al. (2001). With these, the growth and nucleation are specified. A saturation relation is needed for teh concentration. The chemical system benzoic acid - benzoate in sodium chloride solution is known from the literature and parameters for the associated kinetic phenomena have been estimated previously. The saturation curve for benzoic acid crystallization under these conditions is known as well and an expression (7.3) has been found in the literature (Ståhl et al., 2001).

$$C_{sat,\,benzoic\,acid} = 10^{-5.6329+0.0137T-0.1771C_{NaCl}} \tag{7.3}$$

The relation is for temperatures in Kelvin and the concentration of sodium chloride C_{NaCl} in moles/l . A plot of the corresponding saturation in the range of $20-45°C$ is shown in figure 7.10.

Table 7.12: *Model equations for the moment approach for reactive crystallization of benzoic acid written out with the relevant kinetic expressions. The term reacted refers to the amount formed from reaction 7.2*

Model element	Model equation
0^{th} moment,μ_0	$\frac{d\mu_0}{dt} = k_b \cdot e^{-\frac{b}{Ln^2(S)}}$
1^{st} moment,μ_1	$\frac{d\mu_1}{dt} = k_g \cdot (ln(S))^g \mu_0$
2^{nd} moment,μ_2	$\frac{d\mu_2}{dt} = 2k_g \cdot (ln(S))^g \mu_1$
3^{rd} moment,μ_3	$\frac{d\mu_3}{dt} = 3k_g \cdot (ln(S))^g \mu_2$
Concentration balance, benzoic acid	$\frac{dC}{dt} = \frac{m_{in}C}{m_{solvent}} - \rho_c \frac{k_v}{m_{solvent}} 3k_g \cdot (ln(S))^g \mu_2 - Reaction_{forward}$
Concentration balance, benzoate	$\frac{dC}{dt} = \frac{m_{in}C}{m_{solvent}} - Reacted_{backwards}$
Supersaturation definition	$S = \frac{C}{C_{sat}}$
Saturation relation	$C_{sat} = 10^{a_1+a_2T+a_3C_{NaCl}}$ (eq. (7.3))
Temperature relation	$\frac{dT}{dt} = D$
Acid base equilibirum	eq. (7.2)

The overall model requires kinetic parameters, crystal properties, thermodynamic properties and operational variables as well as initial values for the differential equations. The kinetic parameters, crystal properties, thermodynamic properties and operational variables are shown in table 7.13. The initial conditions for the differential equations are discussed below.

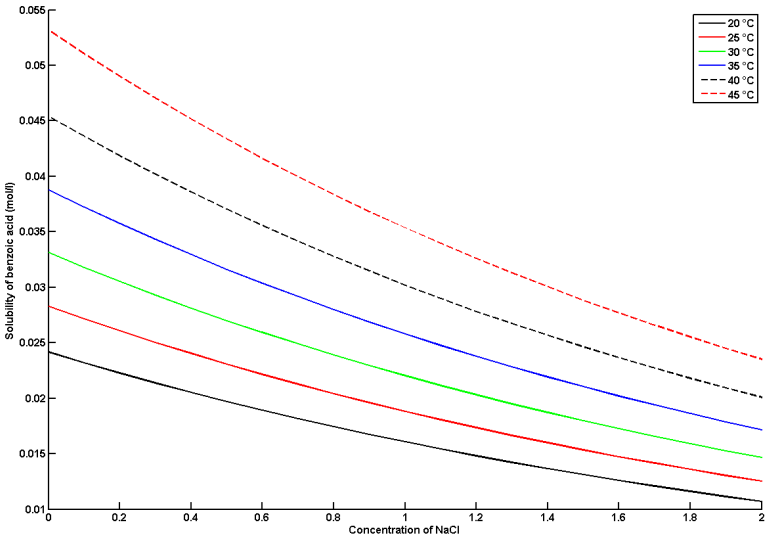

Figure 7.10: *The equilibrium for benzoic acid in water with sodium chloride present at temperatures 20-45 °C. The compounds interact and the solubility of benzoic acid is reduced as the sodium chloride concentration increases. The response to increases in temperature decreases (visualized as the smaller distance between the temperature curves) as well for increased sodium chloride content. The relation is presented as 7.3 (Ståhl et al., 2001)*

Table 7.13: *Kinetic parameters, properties and operational variables needed for the method of moments approach for benzoic acid*

Kinetic parameters	k_b, b, k_g, g
Crystal properties	ρ_c, k_v
Thermodynamic relation	a_1, a_2, a_3
Operational variables	$m_{solvent}, D, C_{acid,in}, m_{in}$

The initial conditions for the differential equations relate to the initial moments and initial concentration. No crystals are present, and thus the initial moments are 0, $\mu_i = 0, i = \{0,1,2,3\}$. The initial concentration of the benzoic acid is 0, $C_{Benzoic} = 0$, the initial concentration of sodium benzoate is 4.0 mol/l

The initial volume of the solution is 1.00 l and an inflow of $m_{in} = 1.00 \cdot 10^{-3}$ l/s hydrochloric acid solution with a concentration of $C_{acid,in} = 10\ mol/l$ (around 30% w/w) is used. The temperature is kept constant at 20 °C.

The kinetic parameters are located in the database and available from Ståhl et al. (2001). The parameters are shown in table 7.14.

Table 7.14: *Kinetic parameter values from the database used for the growth and nucleation models for benzoic acid (Ståhl et al., 2001)*

Kinetic parameters	Value	
k_b	$1.7 \cdot 10^9$	
b	17.5	
k_g	$1.4 \cdot 10^{-5}$	m/s
g	2.9	

With the kinetic model parameters, the necessary parameters and data have been acquired and the problem can be simulated. The results from the simulation are presented in figure 7.11 - 7.13. As the operation is initiated, no crystalline material is present in the crystallizer, as seen from the moments of the distribution. The concentration of benzoic acid increases as the hydrochloric acid is added, shifting the benzoate-benzoic acid equilibrium towards benzoic acid. The solution is supersaturated within few seconds of the operation (figure 7.11) and nucleation occurs (figure 7.13). As the crystals nucleate and grow, the benzoic acid is removed from solution and the solute concentration decreases (figure 7.11) for the rest of the process as the crystals grow (figure 7.13). Through the process, the sodium benzoate concentration steadily decreases and the sodium chloride concentration (in solution) increases. pH is evaluated based on the equilibirum. As the strong acid is added, the pH decreases, but increases as the crystallization set on and the equilibrium is shifted in the solution. In the t-mixer of Ståhl et al. (2001)

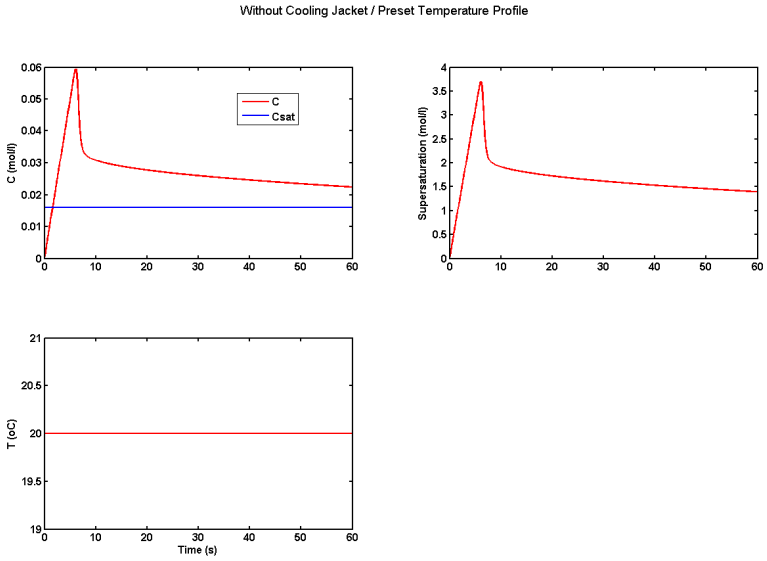

Figure 7.11: *The saturation and supersaturation profile for the crystallization*

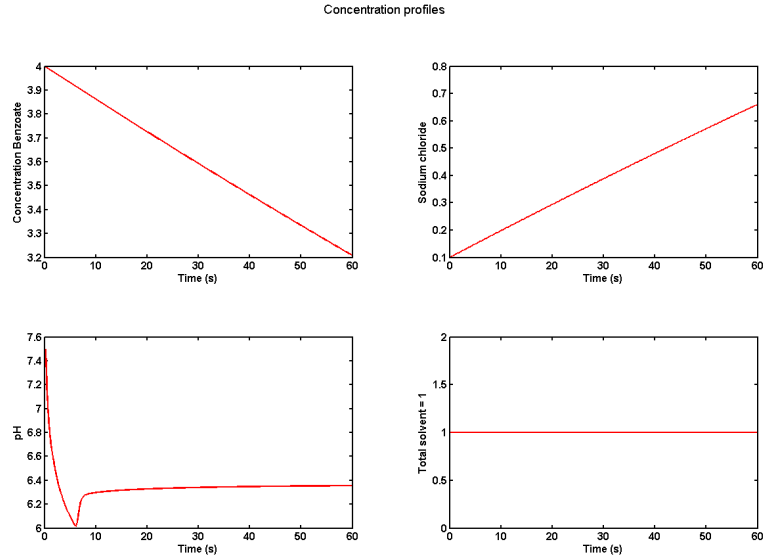

Figure 7.12: *The concentration profile for other present species*

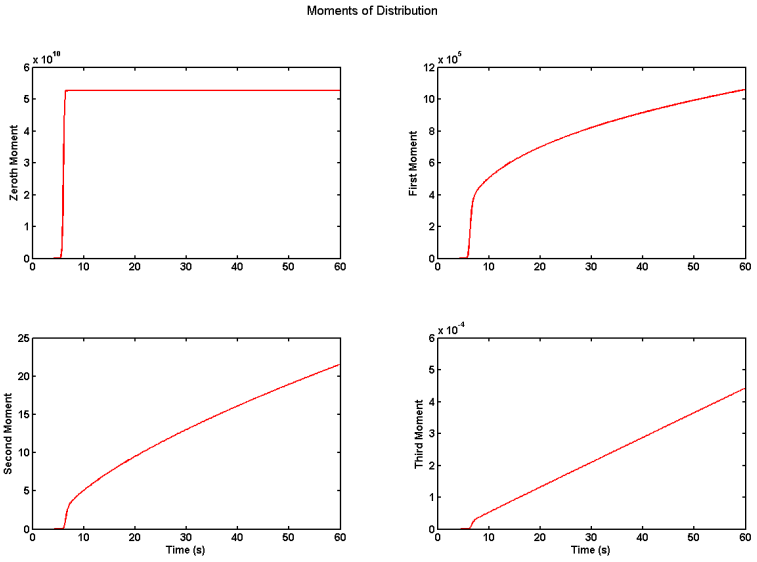

Figure 7.13: *The calculated moment of the distribution. As the operation is initiated, no crystalline material is present in the crystallizer, however, as the solution is supersaturated the crystals form and continue to grow while the supersaturation is depleted*

7.4 Model Identification

This section discusses the estimation of parameters for the models used in simulation of crystallization operations. Throughout the section a chemical system is used as an example for the estimation procedures. This system is introduced first. Secondly, the system identifiability is introduced and discussed. This is done, as it is recognized that in crystallization multiple kinetic phenomena (growth, nucleation, agglomeration, breakage) can occur simultaneously in a process depending on the conditions. Describing these with models can be challenging, as responses in measured variables can be similar for the respective phenomena. Following the theoretical discussion of identifiability, sensitivity methods are used to discuss the possibilities for achieving a more reliable parameter estimation.

7.4.1 Chemical system

The chemical system paracetamol-ethanol is known from the literature and parameters for the associated kinetic phenomena have been estimated previously (Worlitschek and Mazzotti, 2004; Mitchell and Frawley, 2010). As discussed initially in this chapter, several authors have studied the system and a saturation curve is known (Equation (7.1)). The solubility was shown in Figure 7.1

7.4.2 Model

For the parameter estimation, the moment approach was applied due to its speed of solution. The moments approach is established in the framework and a function for describing a seed distribution was written. The moment approach can give the kinetics for growth and nucleation for a system with solution of few equations and can give a fast solution within the overall parameter estimation problem. The equations are shown in Table 7.2 and 7.3

Kinetic phenomena

The model includes the kinetic phenomena growth and nucleation. The growth is assumed constant across crystal size and properties. The nucleation is split into primary $k_{b_1} S^{b_1}$ and secondary nucleation $k_{b_2} S^{b_2} \mu_3$. The secondary nucleation is assumed to be based on the volume of crystals and includes the total volume factor μ_3. Primary nucleation is assumed to be possible to dominate through seeding. The secondary nucleation is present due to the crystals in the system and may not be possible to dominate depending on the chemical and technical system and their properties.

7.4.3 Initial conditions

The initial conditions for the differential equations are related to the moments, the initial concentration and initial temperature of the system. The initial moments are derived from the initial crystal distribution seed and discussed below. The initial concentration C_0 is defined from the amount of solute pr unit solvent, the initial temperature T_0 is specified for the system as well as the operation considers temperature change and hence change in saturation and thermodynamical potential. Seeding is used and the seeding in the process is similar to the seeding described in 7.1.2

7.4.4 Model identifiability

Model identifiability addresses the question of whether a model can be identified. This question can be interpreted in several ways: From the model structure, a model may be globally identifiable and all parameters uniquely identifiable, the model may be locally identifiable under certain assumptions, or the model may have a structure that makes unique parameter identification impossible. The theoretical identifiability problem determines if and to which degree a model with specified in- and outputs can be identified under ideal circumstances, for example with error-free data (Jacquez and Greif, 1985). For practical purposes, it may not be possible to identify a model as certain information is not practically available or of a quality insufficient to reliably estimate parameters (Holmberg, 1982). Practical identifiability describes the possibility of identifying a specific model with a specified, real data set.

Currently, parameters for different crystallization phenomena are estimated together simultaneously for experiments assumed to have multiple phenomena present. Such phenomena are not always uniquely identifiable and parameters may be strongly correlated. As a consequence, multiple sets of parameters may be used to capture a response. This is illustrated in figure 7.14. A set of parameters are used to generated a set of data, which is described through the model with a different set of parameters.

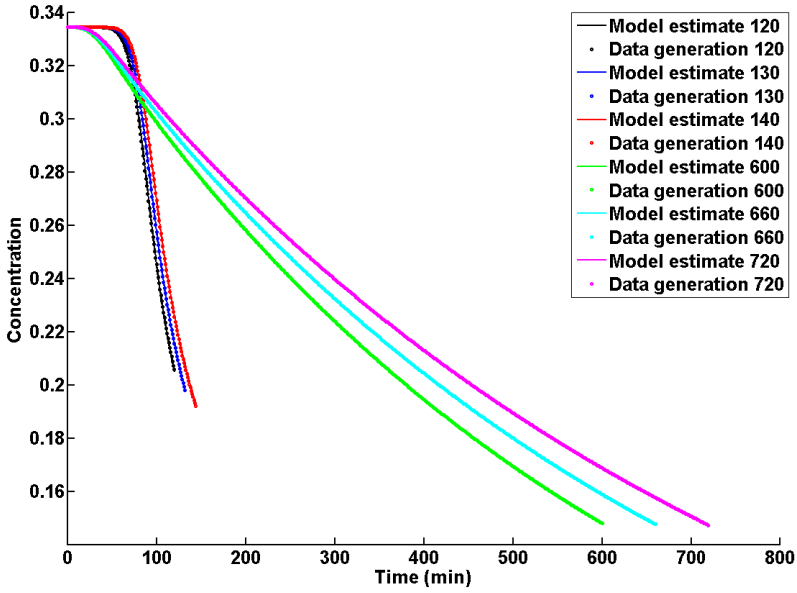

Figure 7.14: *Data points generated with one set table of parameters (Data generation) in table 7.15 and the model shown in table 7.2 with a second set of parameters (Estimate) in table 7.15. The fit is good, and parameters may be accepted for system description*

Only one specified parameter is within the 95% confidence interval of the estimated parameters as seen in table 7.15. This indicates that the identifiability of the model is problematic.

7.4.5 Theoretical identifiability

The problem of identifiability can be divided into different categories treating the theoretical problem as structural identifiability (Bellman and Åström, 1970) on a local or a global scale. Bellman and Åström (1970) provided a definition relating to the possibility of minimizing the function 7.4

$$V(\theta) = \int_0^1 (y(t) - y_m(t))^2 \, dt \tag{7.4}$$

If a local minimum exists, the structure under consideration is locally identifiable; if the local minimum is a global minimum, the structure is globally identifiable.

Table 7.15: *Parameters used for data generation and estimated parameters. Only one specified parameter is within the 95% confidence interval of the estimated parameters, indicating that the identifiability of the model is problematic*

Parameter	Data generation	Estimate
k_{b1}	$2.024 \cdot 10^7$	$3.897 \cdot 10^4 \pm 1.230 \cdot 10^4$
b_1	4	2.286 ± 0.083
k_{b2}	$2.656 \cdot 10^7$	$1.878 \cdot 10^8 \pm 4.619 \cdot 10^7$
b_2	2.232	$3.228 \pm 9.36 \cdot 10^{-2}$
k_g	$8.45 \cdot 10^3$	$1.967 \cdot 10^4 \pm 1.107 \cdot 10^3$
g	1.602	$1.793 \pm 1.14 \cdot 10^{-2}$
E_a	4.056e4	$4.021 \cdot 10^4 \pm 1.40 \cdot 10^2$

The theoretical problem has been under review for several years for multiple models of systems in various fields .

The identifiability of the models can be classified in several ways. Miao et al. (2011) review multiple forms of identifiability of models. Multiple identifiability studies have been carried out within studies of system control and are within a domain of linearized models. Within this domain, several methods have been proposed, and some have been expanded to cover non-linear systems. The notation used within several publications ((Jacquez and Greif, 1985),(Ljung and Glad, 1994)) are consistent with the notation used in Seborg et al. (2004) and will be followed here. A model is described as:

$$\dot{\mathbf{x}} = \mathbf{A}(\theta)\mathbf{x} + \mathbf{B}(\theta)\mathbf{u}, \qquad \mathbf{x}(0) = \mathbf{x}_0 \tag{7.5}$$

$$\mathbf{y} = \mathbf{C}(\theta)\mathbf{x} + \mathbf{D}(\theta)\mathbf{u} \tag{7.6}$$

Here $\mathbf{x}$ is the state variable vector, $\mathbf{y}$ the measurement output vector, $\mathbf{u}$ the (known) inputs vector and θ is the parameter vector. Ljung and Glad (1994) give an informal definition of identifiability based on the transfer function (7.8) and note that several definitions are consistent.

$$G(s,\theta) = G(s,\theta_*), \qquad \forall s \Rightarrow \tag{7.7}$$

$$\theta = \theta_* \tag{7.8}$$

A formal definition is similarly given by Ljung and Glad (1994): *A model structure $\mathcal{M}$ is said to be globally identifiable at θ_*, with respect to $\mathcal{D}_\mathcal{M}$ if there exists an input signal u_*, such that*

$$\bar{\mathbf{y}}(\theta_*, u_*) \neq \emptyset \tag{7.9}$$

$$\bar{\mathbf{y}}(\theta_*, u_*) \cap \bar{\mathbf{y}}(\theta, u_*) \neq \emptyset, \qquad \theta \in \mathcal{D}_\mathcal{M} \Rightarrow \theta_* = \theta \tag{7.10}$$

$$\tag{7.11}$$

$\mathcal{D}_\mathcal{M}$ is a subset of the complex parameters, where certain complex roots may be eliminated based on physical insight. From the definition globally identifiable, the local identifiability concept

is similarly introduced by Ljung and Glad (1994): *A model structure $\mathcal{M}$ is said to be locally identifiable at θ_*, if there exists an open neighbourhood $\mathcal{D}_\mathcal{M}$ of θ_*, such that $\mathcal{M}$ is globally identifiable at θ_*, with respect to $\mathcal{D}_\mathcal{M}$.*

Identifiability of non-linear systems

The theoretical approaches used above, such as definitions based on transfer functions work for linear systems. However, when non-linear systems are considered the above theory, which assumes linear equations must be expanded. Grewal and Glover (1976) claim that if a non-linear system's linearization around a point is identifiable, the corresponding non-linear system is identifiable as well through a sufficient condition. Vajda et al. (1989) state that the condition is sufficient but not necessary. Vajda et al. (1989) introduced a new method, and argues that it complements the Taylor series approach, which for selected examples requires a large calculation effort due to the necessary expansions. Audoly et al. (2001) note that the extension of Vajda et al. (1989) to the non-linear problems *"can easily fail when the dimension of the non-linear algebraic system is large"* and the method seems ill-suited for an automated procedure (Audoly et al., 2001).

Differential algebra In a framework generally referred to as differential algebra, a number of methods have been introduced. The general concept is to reduce the set of differential equations to a set of algebraic equations and manipulate these. Ritt (1950) introduces multiple concepts for manipulation of differential equations into an algebraic domain. The manipulation of differential equations into algebraic procedures are since used by Ljung and Glad (1994) to establish an algorithm for the identifiability problem. Ljung and Glad (1994) are among several authors (Audoly et al. (2001)) using the advances in symbolic manipulation software, specifically MAPLE or DAISY, to establish automated procedures for the symbolic manipulations.

The algebraic equations are polynomial constructs that can be analyzed. An infinite number of polynomials can be employed to describe a differential equation system, however the one with the lowest rank is called the characteristic set and preferred for the description of the system. The identifiability of the differential equation system can be discussed, when the set of equations has been ranked. The polynomial will appear as (Ljung and Glad, 1994)

$$\begin{aligned} &A_1(u,y),\ldots,A_p(u,y),B_1(u,y,\theta_1),B_2(u,y,\theta_1,\theta_2),\ldots,\\ &B_d(u,y,\theta_1,\theta_2,\ldots,\theta_d),C_1(u,y,\theta,x),\ldots,C_n(u,y,\theta,x) \end{aligned} \tag{7.12}$$

For identifiability purposes the occurrence of the part B is investigated. According to Ljung and

Glad (1994), the identifiability can be assessed as:

if B has $B_i = \dot{\theta}_i$ for any i the system is unidentifiable

if all B have B_i of order 0 and degree 1 in θ_i the system is globally identifiable

if all B have B_i of order 0 in θ_i and some B_j are above degree 1 in θ_j

the system is locally identifiable

Ljung and Glad (1994) note that physical insights can be used to reduce the possible parameter set, since some roots in the polynomial solutions may be impossible (for example negative roots for physical phenomena that cannot be negative). Ljung and Glad (1994) argue that this should be included in the theoretical analysis as all information should be available at the theoretical level.

7.4.6 Practical identifiability

For practical applications, methods used for the structural analysis can be applied, however, practical problems are also included. Unlike the theoretical approach, in the practical approach perfect data (no noise or measurement error) is no longer assumed, nor is there an assumption of the models description capability. As a result, parameters that are structurally identifiable may not be practically identifiable (Petersen et al., 2003). Miao et al. (2011) recommends that practical identifiability analysis is carried out after structural identifiability analysis. For practical identifiability two methods are encountered often: Monte Carlo simulations (Metropolis and Ulam, 1949) and sensitivity analysis (Saltelli et al., 2004).

Monte Carlo method

The Monte Carlo method was introduced by Metropolis and Ulam (1949) and the application has since grown across the scientific community to include a wide range of applications. The Monte Carlo method can be used to study uncertainties on models and their input. According to McKay et al. (1999) sources of uncertainty may be classified as

- simulation variability
  (stochastic uncertainty, which may come from the model itself)
- input uncertainty
  (for example from lack of knowledge about the model inputs)
- structural uncertainty
  (models are approximations to systems rather than an exact copy)

In order to apply Monte Carlo analysis for practical identifiability analysis, a structural identifiability analysis can be performed and afterwards Monte Carlo simulations can be used to

investigate whether structurally identifiable parameters can be estimated reliably (Miao et al., 2011). Monte Carlo simulation has been employed for crystallization operations (Samad et al., 2013) for investigations on the input uncertainty. Miao et al. (2011) outlines another procedure: Rather than assuming an input uncertainty on the model parameter, the model is solved with specified parameters (from parameter estimation, literature or other sources) to generate the output variables similar to experimental time points. A large number, N, of data sets with a given measurement error level are generated and for each data set a parameter set, θ_i is generated, where $i = 1,2,3 \ldots N$. With this, the average relative estimation error may be calculated as

$$\frac{1}{N}\sum_{i=1}^{N}\frac{\left|\theta_{0,k}-\theta_{i,k}\right|}{\theta_{0,k}}$$

where index k refers to the k^{th} element of the parameter vector. The average relative estimation error is then used to investigate whether a parameter can be estimated. For increasing measurement error, the average relative estimation error will increase as well, but the rate of increase will vary with parameter and if the rate is high Miao et al. (2011) claim that the parameter is not practically or statistically identifiable. The limit of *unacceptable high* is not clearly defined, but relies on the investigator (Miao et al., 2011).

7.4.7 Sensitivity analysis

The term *sensitivity analysis* has been used broadly for a range of problems (Saltelli et al., 2004, p. 42). Bode (1955) defined the sensitivity as

$$S = \frac{1}{\frac{\partial\theta}{\partial logW}}$$

for an element W to a parameter θ (Bode, 1955, p. 52). Multiple definitions have been given since and a sensitivity coefficient s_{ij} is defined as :

$$s_{ij} = \frac{\partial y_i(\theta)}{\partial\theta_j}$$

Here y_i is the i^{th} component of the output vector y, θ is the parameter vector and θ_j the j^{th} component of the parameter vector. As indicated, sensitivity analysis deals with the analysis of these sensitivity measures, the changes in model output from changes in model input and model parameters. Sensitivity analysis can be used in several ways to study the identifiability of a system. The sensitivity analysis combines elements of the practical and structural model identification techniques. Miao et al. (2011) note that the sensitivity analysis does not take measurement error into consideration. Brun et al. (2002) include the measurement error in the sensitivity as a scaling factor:

$$s_{ij} = \frac{\Delta\theta_j}{sc_i}\frac{\partial y_i(\theta)}{\partial\theta_j} \tag{7.13}$$

where $\Delta\theta_j$ is *"an a priori measure of the reasonable range of* θ_j*"*, the parameter uncertainty, and sc_i is a scaling factor with the same physical dimension as the observation. This introduces

weighing possibilities in the sensitivity, which may affect the outcome when comparing sensitivities or estimating an overall sensitivity measure.

Saltelli et al. (2004, p. 87) note that normalized sensitivity measures can be applied to make the sensitivity results independent of the units of the model. A normalized, local sensitivity matrix can be constructed as

$$\tilde{\mathbf{S}} = \left[\frac{\theta_j}{y_i} \frac{\partial y_i(\theta)}{\partial \theta_j} \right] \tag{7.14}$$

which is similar to the measure of Brun et al. (2002), (eq. 7.13), however, in this case a different scaling is used. Saltelli et al. (2004, p. 87) use a perturbation of 1% and hence the measure indicates the relative change in y_i with a change in θ_j of 1%. The sensitivity analysis requires input parameters and examination of the model output at a given time. As such, the model provides the *point identifiability* and Quaiser and Mönnigmann (2009) add *at-a-point* to the local/global identifiable concept to emphasize this requirement. Ljung and Glad (1994) operate with a similar concept as the definition in equation (7.8) declares the global/local identifiability at the parameter set θ_*, which can be considered a point in parameter space. In the method of Brun et al. (2002), a non-dimensional sensitivity matrix is constructed with elements s_{ij} as defined in equation 7.13. From this matrix the sensitivity measure δ_j^{MSQ} is calculated as:

$$\delta_j^{MSQ} = \sqrt{\frac{1}{N} \sum_{i=1}^{N} s_{ij}^2}$$

This measure represents the overall mean sensitivity model output to a parameter (Brun et al., 2002), which is used by Sin et al. (2010) to evaluate identifiability. Petersen et al. (2001) drive the output sensitivity functions for all parameters and plot the sensitivity calculation for all time points as a time series. Based on these sensitivities, the possibility of obtaining information at different times towards identifying parameters, is discussed.

7.4.8 Identifiability of crystallization model

Petersen et al. (2001) employed software for the analytical solution of the equations. An alternative approach is to employ numerical methods for analysis of the sensitivity. In this case a numerical procedure for the calculation of $\frac{\partial y}{\partial \theta}$ around a point θ_*(differential sensitivity analysis), which is concurrent with a data point for the measured variable, is employed. The method is applied for all data points and the procedure is checked through calculation of the central, backwards and forward perturbation. This is based on the assumption that all of the expressions of difference quotients in Equation (7.15) are equal, i.e.:

$$\left.\begin{array}{l}\frac{y(\theta+\Delta\theta)-y(\theta-\Delta\theta)}{2\Delta\theta}\\ \frac{y(\theta+\Delta\theta)-y(\theta)}{\Delta\theta}\\ \frac{y(\theta)-y(\theta-\Delta\theta)}{\Delta\theta}\end{array}\right\} \rightarrow \frac{dy}{d\theta} \quad for \quad \Delta\theta \rightarrow 0 \tag{7.15}$$

Calculating the central, forward and backwards difference quotients, it is possible to check if these are all equal. If the three are equivalent around a point, it is assumed that the function is valid for the method and $\Delta\theta$ is small enough for the numerical procedure to be applied. The central difference quotient is calculated for a wider range than the backward and forward quotients, however for the small range, the division by 2 should eliminate this if the method is valid.

The approach is integrated with the parameter estimation and for each parameter the vectors of the central, backwards and forwards difference quotients are generated. These can now be plotted to investigate where the sensitivity to the individual parameter is greatest, i.e. where the function output shows the greatest change with change in the parameter. The sensitivity measures are made on basis of the 6 concentration profiles shown in Figure 7.14. The 6 profiles are grouped in two sets of three short profiles and three longer profiles, respectively. For the three shorter (experiment 1 to 3) runs no seeding was used, for the longer profiles (4 to 6) seeding was used. The seven parameters shown in Table 7.15 were estimated and the sensitivity calculated. The system is simulated for all $\theta_k \in \theta_{estimated}$, where $\theta_{estimated} \subseteq \theta$ is the subset of estimated parameters given in Table 7.15, $\theta_{estimated} = \{k_{b1}, k_g, k_{b2}, b_1, b_2, g, E_a\}$.The sensitivity is calculated using a perturbation of 1‰ of the parameter value, i.e. $\Delta\theta = 1 \cdot 10^{-3}\ \theta_k$. The simulations were run using the expressions of Equation 7.15 as shown in Equations 7.16-7.18:

$$D_{qc} = \frac{y(\theta + 1 \cdot 10^{-3} \cdot \hat{\theta}_k) - y(\theta - 1 \cdot 10^{-3} \cdot \hat{\theta}_k)}{2 \cdot 10^{-3} \cdot \hat{\theta}_k} \tag{7.16}$$

$$D_{qf} = \frac{y(\theta + 1 \cdot 10^{-3} \cdot \hat{\theta}_k) - y(\theta)}{1 \cdot 10^{-3} \cdot \hat{\theta}_k} \tag{7.17}$$

$$D_{qb} = \frac{y(\theta) - y(\theta_k - 1 \cdot 10^{-3} \cdot \hat{\theta}_k)}{1 \cdot 10^{-3} \cdot \hat{\theta}_k} \tag{7.18}$$

The vector $\hat{\theta}_k$ is a vector in parameter space with the only element θ_k corresponding to the k^{th} coordinate, and hence $\|\hat{\theta}_k\| = \theta_k$. The result of the new estimation is shown in Table 7.16 and the concentration profiles and data are plotted in Figure 7.15

The parameters are perturbed and the results are plotted for each parameter in the six experiments. Figure 7.16 shows the result for the parameter k_{b1}, whereas the rest of the parameters are found in Appendix: Pertubation of parameters

In the calculations D_{qc}, D_{qf} and D_{qc} are calculated and plotted. For all parameters the plots are shown in Appendix: Pertubation, a single example is shown as Figure 7.17. All plots are for a

Table 7.16: *Parameters used for data generation and parameters estimated in a later estimation. Compare to table 7.15. All parameters, except for E_a are outside the range of the data generating parameters*

Parameter	Data generation	New estimate
k_{b1}	$2.024 \cdot 10^7$	$1.08 \cdot 10^5 \pm 2.95 \cdot 10^4$
b_1	4	$2.55 \pm 7.2 \cdot 10^{-2}$
k_{b2}	$2.656 \cdot 10^7$	$2.59 \cdot 10^8 \pm 5.95 \cdot 10^7$
b_2	2.232	$3.32 \pm 8.87 \cdot 10^{-2}$
k_g	$8.45 \cdot 10^3$	$1.82 \cdot 10^4 \pm 9.11 \cdot 10^2$
g	1.602	$1.76 \pm 1.02 \cdot 10^{-2}$
E_a	4.056e4	$4.04 \cdot 10^4 \pm 1.22 \cdot 10^2$

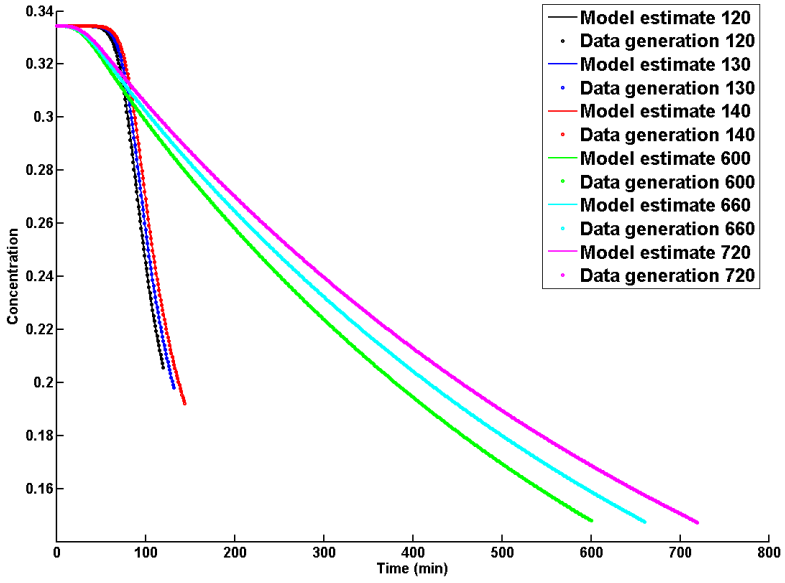

Figure 7.15: *The concentration profile, similar to figure 7.14, but generated by a model with a new parameter set. The visually good fit obtained with a new parameter set indicates an identifiability problem*

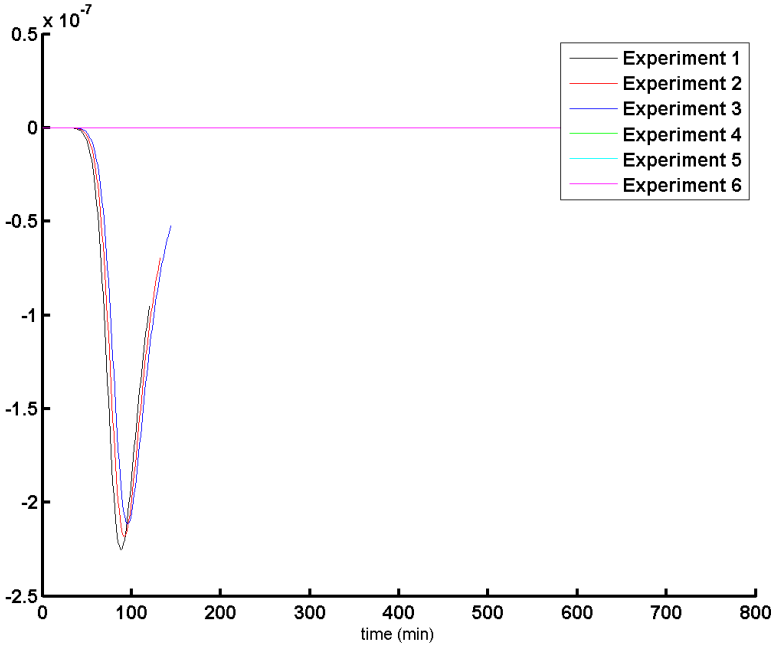

Figure 7.16: *The parameter k_{b1} is perturbed using a pertubation of* 1‰ *of the base parameter value. If the parameter responds, it can be related to an experiment indicating that information about the parameter can be found in the experiment in the region of the response. The nucleation parameters need the high supersaturation found in shorter experiments to show response, and the deviation from 0 here, indicates that information about the nucleation parameter may be found in the short experiments.*

perturbation of 1‰. For all plots at this perturbation, central, backwards and forwards difference quotients are close; viz. only one curve is visible in Figure 7.17 for each experiment

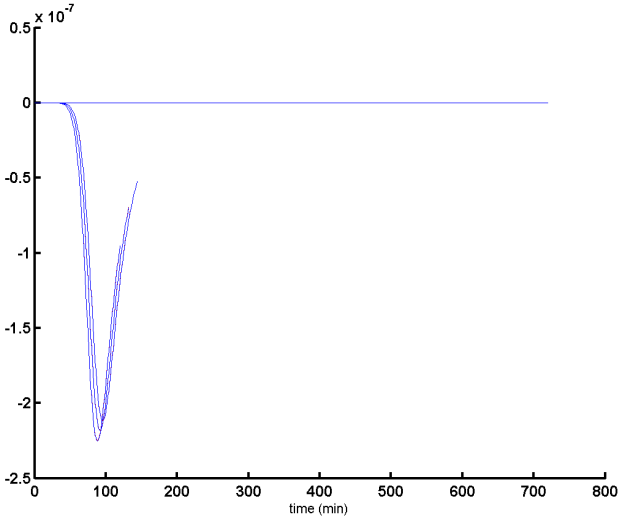

Figure 7.17: *Central, backwards and forwards perturbation of k_{b1} for a perturbation of 1‰. The central, backwards and forwards difference quotients are close; viz. only one curve is visible for each experiment*

Saltelli et al. (2004, p.83) note that a perturbation of 1% is "a good practical choice, but finding the best (or acceptable) value is a trial-and-error process". A small perturbation ensures that local linearity can be assumed, however, if the parameter change is small, the change between the perturbed and non-perturbed solution may be too small and a rounding error relatively high compared to this. To investigate the effect of increased perturbation, the perturbation is increased to 1% and figures similar to Figure 7.17analyzed. The parameter E_a has a clear difference between the central, backwards and forwards difference quotients as shown in Figure 7.18. A perturbation of 1% is found to be unacceptable for this experiment.

It is found that a pertubation of 1‰ is a reasonable range for this problem. Analyzing the subfigures in figure appendix C.-1,the respective parameters can be related to the different experiments. If a parameter responds to a pertubation, it indicates that information about the parameter can be found in the region of the response. Initially, the unscaled responses (Equation (7.16)) are plotted for the six experiments for each parameter (given in appendix C.-1). The difference quotients have dimension based on the dimension of the parameter they are related to and the values can *not* be compared between these plots. Rather the plots indicate in which experiments and where in the experiments information about a specific parameter may be obtained. The information is summarized in Table 7.17. It appears that experiment $1, 2, 3$ contain information on all parameters, which is to be expected as all phenomena are present. Nucleation parameters should be retrieved from experiment $1, 2, 3$, whereas the growth parameters can be retrieved from $4, 5, 6$.

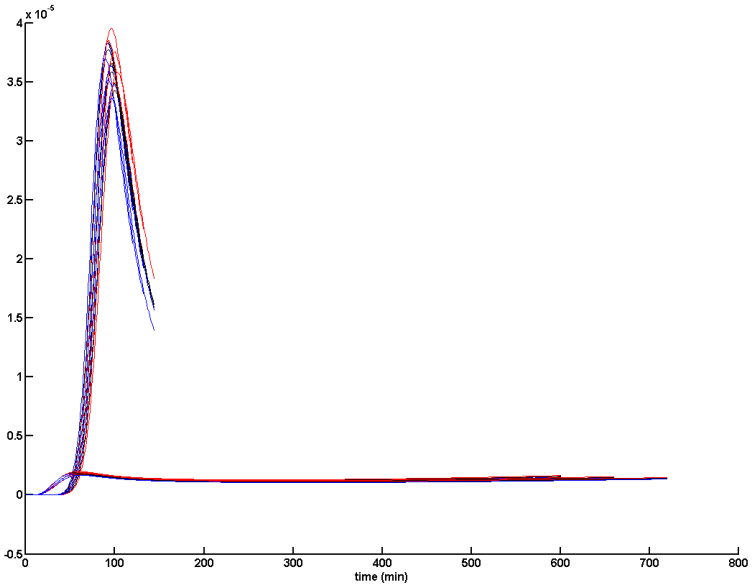

Figure 7.18: *The central, backwards and forwards difference quotients for the parameter E_a for a perturbation of* 1‰. *The central, backwards and forwards difference quotients are different and a perturbation of* 1‰ *is too high a value for this experiment*

Table 7.17: *Indication of which experiments that contain information for the parameters as summarized from the figures. Experiment* $1,2,3$ *contain information on all parameters, which is to be expected as all phenomena are present, whereas the nucleation parameters should be retrieved from experiment* $1,2,3$.

Parameter	Experiment
k_{b1}	$1,2,3$
b_1	$1,2,3$
k_{b2}	$1,2,3$
b_2	$1,2,3$
k_g	$1,2,3,4,5,6$
g	$1,2,3,4,5,6$
E_a	$1,2,3,4,5,6$

The information contained in the experiments is further analyzed using the scaled sensitivities (equation 7.14). With the scaling, it becomes possible to compare the different elements in the sensitivity matrix and for a given experiment, indications of which parameter estimates that can be obtained from the data, can be discussed. In Figures 7.19 and 7.20 it is shown which parameters are obtainable from the two types of experiments. The corresponding parameter sets for all figures are seen in Appendix: Parameter information in experiments

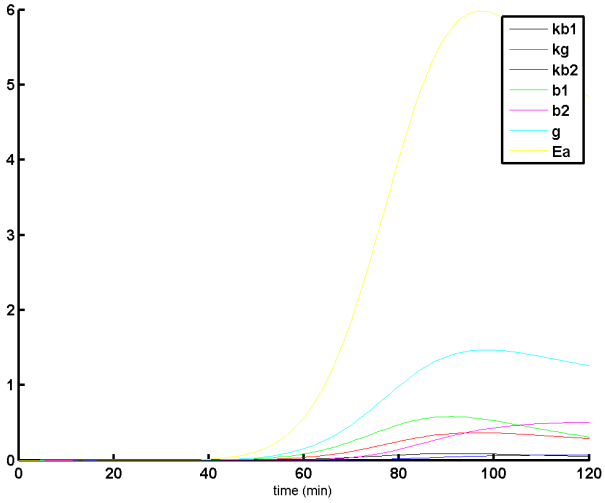

Figure 7.19: *The information contained in the experiments is further analyzed using the scaled sensitivities (equation 7.14). With the scaling, it becomes possible to compare the different elements in the sensitivity matrix and for a given experiment, indications of which parameter estimates that can be obtained from the data, can be analyzed. The figure indicates which parameters can be obtained from experiment 1. All parameters show similar responses, however the parameter E_a (yellow) has the highest value in the information window. This is the parameter with the smallest relative confidence intervals in the parameter estimation*

From the plots, the activation energy of the growth shows the greatest response followed by the exponent for the growth. These parameters are found to have relatively small confidence intervals, indicating that they can be estimated well from the data. Particularly the activation energy is the only parameter with the original value falling into the confidence interval of the estimate.

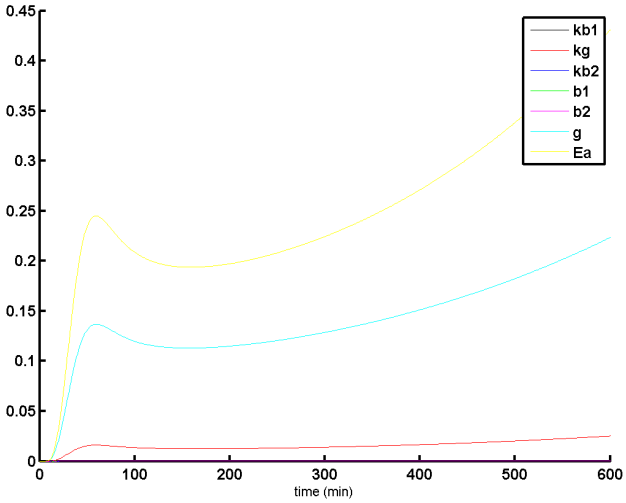

Figure 7.20: *The information contained in the experiments is further analyzed using the scaled sensitivities (equation 7.14). With the scaling, it becomes possible to compare the different elements in the sensitivity matrix and for a given experiment, indications of which parameter estimates that can be obtained from the data, can be analyzed. The figure indicates which parameters can be obtained from experiment 4. This experiment mainly contains information on the growth parameters with the parameter E_a (yellow) with the highest value in the information window. The parameter g has a very similar response in the information window.*

Noisy data

An aspect of the practical identifiability problem is noise in the data. If the data are very noisy, the parameters cannot be estimated as reliably. To investigate this problem, a noisy situation is simulated. The previously used data sets are added white noise with a range of 1 % of the smallest measurement (min(y)) corresponding to one standard deviation.

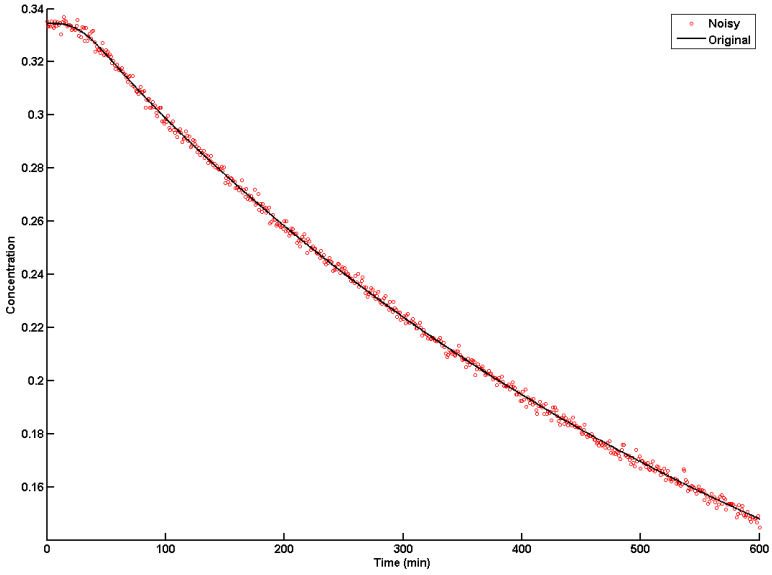

Figure 7.21: *An example of the generated noisy data for the experiment running 600 minutes. Original data for experiment 4 (black, solid line) is shown with the new data (red circles). The previously used data sets are added white noise with a range of 1 % of the smallest measurement (min(y)) corresponding to one standard deviation.*

To investigate whether the methods are applicable to this problem and information may be collected, a parameter identification procedure is run. The outcome of the parameter estimation is shown in Table 7.18 and the model and data are plotted in Figure 7.22

Inspecting the plot of the models and data, a reasonable fit appears. However, when the parameters are inspected, most have not been successfully identified as their 95% confidence intervals are too large compared to the parameter value (Table 7.18). A procedure similar to that of the ideal data is followed and the sensitivities investigated with the same method. The results of the pertubation are shown for two parameters, k_{b1} in Figure 7.23 and Figure 7.24. The results for all parameters are shown in Appendix: Pertubation of Noisy Parameters

The results of the pertubation are very similar to that of the ideal data set. The scales are different, however, the response curves have the same shape. This indicates that the method can

Table 7.18: *Parameters used for data generation and parameters estimated for the data with added noise. Compare to table 7.15. The parameters relating to the nucleation are highly dubious as their 95% are very large compared to the parameter value*

Parameter	Data generation	Noisy estimate
k_{b1}	$2.024 \cdot 10^7$	$1.77 \cdot 10^9 \pm 4.44 \cdot 10^9$
b_1	4	5.00 ± 0.704
k_{b2}	$2.656 \cdot 10^7$	$3.6 \cdot 10^8 \pm 2.30 \cdot 10^9$
b_2	2.232	2.84 ± 2.71
k_g	$8.45 \cdot 10^3$	$4.22 \cdot 10^4 \pm 2.84 \cdot 10^4$
g	1.602	1.39 ± 0.105
E_a	4.056e4	$4.75 \cdot 10^4 \pm 1.1 \cdot 10^3$

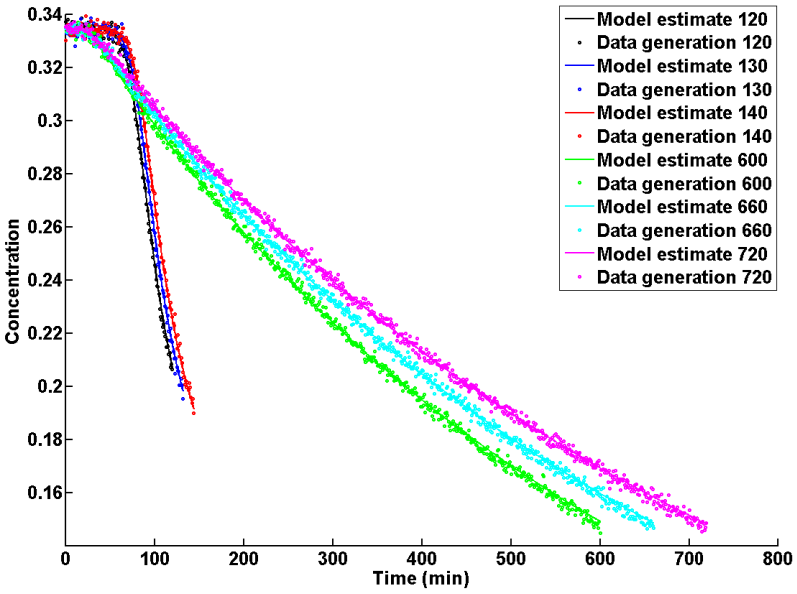

Figure 7.22: *Noisy data and the model with estimated parameters as shown in table 7.18. The model fits the data well from visual inspection.*

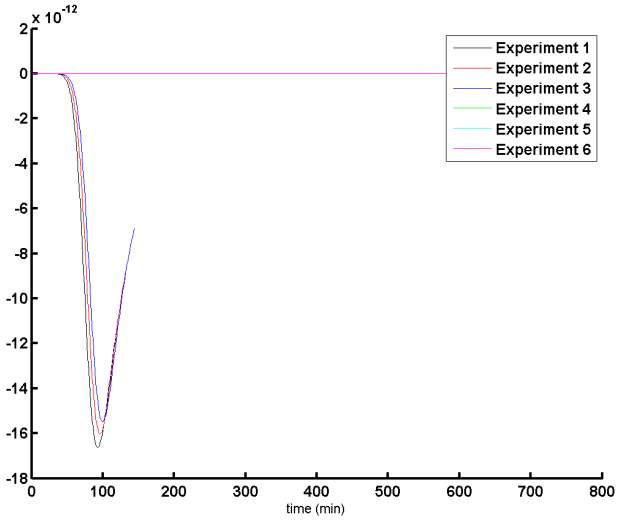

Figure 7.23: *The parameter k_{b1} is pertubed for the experiments with added white noise. If the parameter responds, it can be related to an experiment indicating that information about the parameter can be found in the experiment in the region of the response. Information on this parameter is found in shorter experiments, where high supersaturation is reached*

.

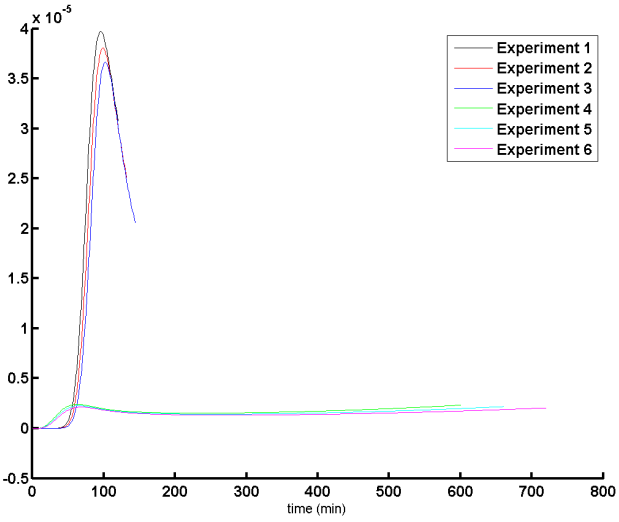

Figure 7.24: *The parameter E_a is pertubed for the experiments with added white noise. If the parameter responds, it can be related to an experiment indicating that information about the parameter can be found in the experiment in the region of the response. Information on this parameter is found in all six experiments*

.

be used to analyze the model structure in relation to the experiments. As with the ideal data, the scaled sensitivities are plotted for the six experiments. The results are shown for two experiments. Figure 7.25 shows the information available from experiment 1 and figure 7.26 shows which parameters are obtainable from experiment 6. The results for all experiments are shown in Appendix: Parameter information in noisy experiments.

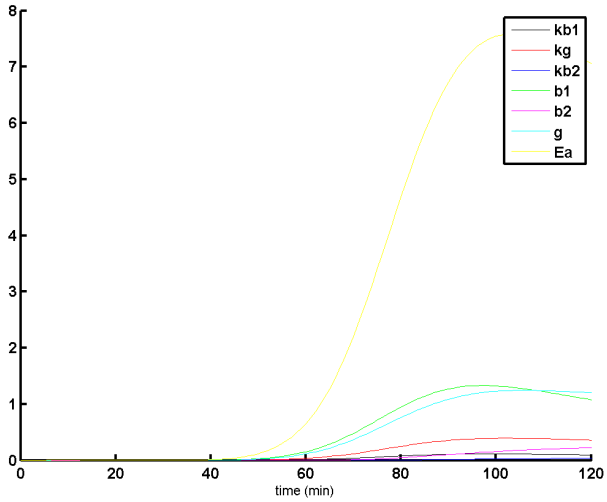

Figure 7.25: *Parameter information obtainable from experiment 1, where white noise has been added. The experiment is analyzed using the scaled sensitivities (equation 7.14). With the scaling, it becomes possible to compare the different elements in the sensitivity matrix. The available information is dominated by the parameter E_a (yellow)*

The results are similar to those for the data without noise (exemplified by Figure 7.19 and Figure 7.20), however, g and b_1 are ranked differently. E_a is still the highest normalized sensitivity now followed by b_1 for the three short experiments. For the longer runs (600-720 min) the ranking appears to be the same.

Correlation The correlation between the parameters is similarly calculated. The correlation is given in Table 7.19

The parameters are highly correlated, particular parameters relating to the same kinetic phenomenon appear to be interdependent. The activation energy has the lowest correlation with any of the other parameters, which is noted as it is estimated with the relatively smallest confidence interval.

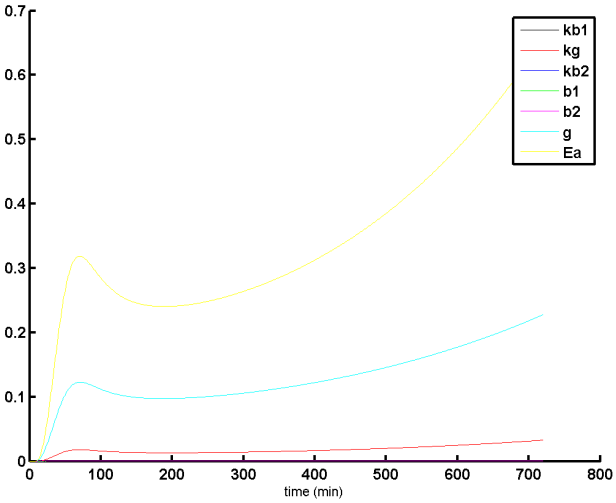

Figure 7.26: *Parameter information obtainable from experiment 6, where white noise has been added. The experiment is analyzed using the scaled sensitivities (equation 7.14). With the scaling, it becomes possible to compare the different elements in the sensitivity matrix. The available information is dominated by the growth parameters, notably E_a (yellow)*

	k_{b1}	k_g	k_{b2}	b_1	b_2	g	E_a
k_{b1}	1.0000	-0.6404	-0.3391	0.9606	-0.3286	-0.8558	0.0753
k_g	-0.6404	1.0000	0.0580	-0.4952	0.0410	0.7580	0.5958
k_{b2}	-0.3391	0.0580	1.0000	-0.5329	0.9992	-0.1004	0.2116
b_1	0.9606	-0.4952	-0.5329	1.0000	-0.5210	-0.6792	0.0794
b_2	-0.3286	0.0410	0.9992	-0.5210	1.0000	-0.1055	0.1917
g	-0.8558	0.7580	-0.1004	-0.6792	-0.1055	1.0000	-0.0717
E_a	0.0753	0.5958	0.2116	0.0794	0.1917	-0.0717	1.0000

Table 7.19: *Correlation between parameters*

Discussion

From the results of the identifiability analysis it is noted that for the different kinetic phenomena, information about a given parameter is located at the same times in the experiment, as the response is located at the same time. This makes reliable parameter estimation difficult. The difficulties are reflected in the large correlation between parameters as seen in Table 7.19 and the broad confidence intervals, particularly seen for the nucleation parameters. Estimating the parameters for crystallization simultaneously appears to be challenging. Possibly one way of overcoming this difficulty is to split experiments as different phenomena appear at different times. From the normalized sensitivity coefficient Figures 7.25 - 7.26, it is indicated that the growth parameters are possible to estimate from longer experiments, as k_g, g and E_a are above the other parameters in the normalized sensitivities. Fixing these would possibly allow parameters to be estimated from new ranges, which are heavily influence by the growth when simultaneous estimation is carried out. Investigating the range of the longest experiment (experiment 6), assuming the growth fixed, it is found that information is available for the secondary nucleation parameters as shown in Figure 7.27. Further more, the data available should be reviewed, to see if more information can be obtained to fix parameters. More data types could provide new possibilities for fixing parameters and estimating remaining parameters reliably. This merits investigation.

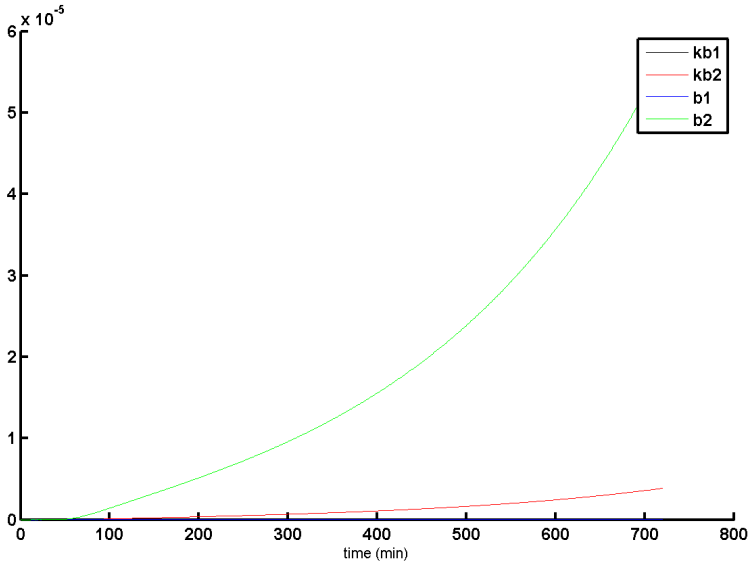

Figure 7.27: *Information in the 720 min experiment assuming growth parameters are estimated previously*

Conclusion

From the discussion, reliable parameter estimation based on concentration data cannot be achieved from the available measurements and simultaneous estimation for the crystallization operations. Further investigation is suggested in terms of experimental design and addition of new data types. Using the concentration profiles, the information about parameters are found at the same time, when cooling crystallization experiments are performed. The model responds similar to changes in different parameters, making it possible to compensate the response of one parameter with another. This is illustrated in the high correlation between parameters relating to different kinetic phenomena.

Part IV

Discussion and conclusion

CHAPTER 8

Discussion

This chapter is divided into sections discussing the relevance and the application of the different chapters.

8.1 Framework

Crystallization has been used as a means for separation for millenia, but has long been regarded as more of an art than science (Mullin, 2001). Within the last decades, the modelling of crystallization operations has gained increased interest (Myerson, 2002; Qu et al., 2014). The need for a framework for crystallization operations had been identified by Gernaey and Gani (2010) and a generic modelling framework for crystallization was proposed by Samad et al. (2011). A generic framework facilitates a systematic approach to modelling, by which a wide range of crystallization operations and chemical systems may be modelled without too much time spent, as the system specific information is provided and the model generated with models retrieved/extracted from a model library (Meisler et al., 2014).

8.1.1 Kinetic library

The kinetic model library has been created based on results from the literature, but accommodates experimental results as well. The systematic storage of models allows analysis and comparison of similar model structures and models for specific kinetic phenomena. The structure does not consider the time when an article describing a specific kinetic model has been published. As such, more recent results do not take precedence over older results in case authors have reported different results. As crystallization kinetics have been studied for several decades, trends in changing equipment, modelling practices, available technology (available data) and similar elements, may have an effect on the applied model types. However, no trend has been apparent for models stored in the library.

8.1.2 Process model

An expansion of the framework with a more generalized model for the crystallizer was established. This model accommodates different possible configurations of a vessel running in batch, semi-batch or continuous mode. The possibilities for description through the method of moments or the method of classes remain. As discussed in chapter 5, care must be taken when using inflow with a moments model, as the model incorporates distributions. When a stream is added, underlying assumptions about the distribution in the crystallizer or stream may have influence. If the solution employs a discretized method, the influx of particles should be matched to the grid used in the crystallizer. Several authors have discussed how different distributions may have similar moments and the reconstruction of the distribution from its moments is not trivial (Hulburt and Katz, 1964; McGraw, 1997; John et al., 2007; Aamir et al., 2009; Mortier et al., 2014).

8.2 Kinetic models

Models for the phenomena growth, nucleation, agglomeration and breakage have been collected. The phenomena growth and nucleation have been found to be best represented in the literature, as multiple authors have made the assumption that agglomeration and breakage would not be present in the crystallization operation. From the literature, correlations for the phenomena have been found to be widely applied. This is considered to be related to the multiple effects occurring in crystallization, through which the crystals may form or interact. The multiple effects occurring have led to a multitude of theories and models being formulated and no general agreement on which modelling approach is best appears clear. The description of supersaturation may be based on thermodynamics or different empirical correlations, all of which impacts the further modelling.

8.2.1 Growth mechanisms

Garside (1985) notes that several growth mechanisms have been proposed, these include Birth and Spread, Burton, Cabrera, Frank (BCF) (Burton et al., 1951) theory and Polynucleation. These mechanisms may be difficult to discern in an actual crystallizer, however, correlations which include all the mechanisms exist, and these have been extensively used in the literature. Mullin (2001) notes that these have been considered the only practically applicable models by several authors, and they are found widely applied. The growth correlations are found in different variations, and several authors include different phenomena in the description of the growth rates; this may be generalized into a general model, from which the relevant correlation to match a specific data set can be generated. The generalized growth model includes temperature, apparent size dependency and transport phenomena. In this thesis, the models have been stored in the kinetic library, where they have been classified according to the included terms. As discussed in section 8.3, the interaction of phenomena and parameters may result in the potential of describing an experimental set of data with more than one model parameterization and included phenomena. This is a general model structure selection problem, which is a problem faced in many research fields. This modelling approach accounts for this possibility through the model library and the possibility of extracting and comparing the different kinetic models within the framework to analyze for the importance of different parameters. It is possible to generate the necessary growth models used in the literature through this approach and several case studies from the literature have been analyzed to demonstrate the general use of the model library. Thus, the versatility of a generic framework is demonstrated.

8.2.2 Nucleation

Similarly to the growth models, nucleation models have been collected, characterized and stored in the kinetic model library. Within nucleation, several mechanisms exist. Foremost, the nucleation may be primary (stem from the solution) or secondary (stem from present crystals). In the literature, there is no general agreement on the phenomena to include and the models for it. Primary nucleation may be modelled from first principles models or from correlations. Secondary nucleation is modelled through correlations as the phenomenon is related to the practical conditions in the crystallizer. The phenomena may be represented together, either as separate or combined equations. Similar to crystallization, formulating a generalized model has been done for nucleation as well. This model is proposed as a generalized correlation including temperature, transport phenomena and the amount of crystals present. This model can be used to represent primary nucleation, secondary nucleation or both. When generating the nucleation model, a correlation to the generation of the growth model may be considered. In the model approach, this is considered in the framework depending on the modelling purpose. The correlations rely on different supersaturation descriptions, and this should be considered when the models are combined, where the model parameters for phenomena will interact.

8.2.3 Agglomeration and breakage

The models for agglomeration and breakage of crystals have been collected and stored in the library. Agglomeration and breakage are not commonly included in the models for crystallizers. Quintana-Hernández et al. (2004) included an overall term and other authors have investigated the phenomena (Zauner and Jones, 2000). Korovessi and Linninger (2006) found several first principles models to describe agglomeration and breakage, however, advanced growth mechanisms with multiple parameters, nucleation and dissolution are frequently assumed to account for changes in size of the particles and whereas agglomeration and breakage is assumed not to be present initially. Evaluation of model assumptions within crystallization modelling through sensitivity analysis has not been encountered often, and it is possible that these phenomena are present but the extent of their presence not really known.

8.2.4 Dissolution

Dissolution kinetic models have been added to the framework, allowing crystallization operations with dissolution to be simulated. This allows more versatile operations and operational scenarios, including cyclic operations. The dissolution is focused on the theories of Noyes and Whitney (1897) and Nernst-Brünner theory (Dokoumetzidis and Macheras, 2006), implemented as a negative growth rate.

8.3 Model parameters

The possibility of extracting information about specific parameters for the kinetic phenomena models was investigated. It was found that when information was available, it was related to the supersaturation. A full model including the kinetic phenomena growth, primary nucleation and secondary nucleation was analyzed using sensitivity analysis. This showed, that as the information was available with increased supersaturation, the information about a given parameter was located at the same time window in a crystallization experiment data set, resulting in parameter identifiability problems. Different parameter sets could be used to represent the available data, and particularly for the nucleation parameters broad confidence intervals were seen. Investigations into the possibilities of experimental design as a means to overcome this was undertaken. It is possible to design experiments to promote specific phenomena and particularly the growth and nucleation interaction can be separated. Growth of crystals is favoured at low supersaturations with crystals present and nucleation is favoured at high supersaturations. However, at low supersaturations, the growth models can not be reliably identified. This is illustrated by plotting the growth models from (Worlitschek and Mazzotti, 2004) and (Mitchell and Frawley, 2010) in figure 7.4, demonstrating the close overlap. This has an impact on the kinetic model library. It should be noted that the parameters stored here can be used to represent the constitutive relations

needed in the modelling of the crystallizer. However even though the models may have been constructed to have parameters with physical meaning, no such meaning should be assigned to the identified model parameter in case of identifiability problems, since the identifiability problems imply that parameters cannot be estimated reliably. In the model library, the original source of the parameters and/or data is stored along the model. This ensures, that the model assumptions are available to the model user.

8.4 Simulation case studies

The case studies have been selected to show the versatility of the modelling framework. The chosen chemical systems represent a limited testing of the capabilities of the framework but provides insight in the practical operation of the framework and interaction with the generic framework for a crystallization operation. Combining the operations is the practical use. Case studies show how the model framework can be used to identify a model and subsequently use the model in simulations of operational scenarios. This combination of data and models is considered useful within a systems approach to chemical engineering (Cameron and Gani, 2011) and may be useful for development of crystallization processes.

CHAPTER 9

Conclusion and further work

A generic and model-based framework for batch cooling crystallization operations has been extended in terms of model library, model analysis as well as simulation of continuous and fedbatch operations. New modules for the framework have been developed, including a module for reactions, allowing the study of reactive crystallization within the framework. A crystallization kinetic model library together with an ontology for knowledge representation has been developed, in which kinetic models and relations from the literature are stored along with the references and data

9.1 Conclusion

The results of the project are summarized below.

9.1.1 Generic modelling framework

The modelling framework has been expanded to incorporate dissolution and reactions and the continuous capability documented as a further increase in the applicability. The framework process model includes multiple configurations for batch, semibatch and continuous as well as different possibilities for supersaturation generation. Several case studies have been carried out

to demonstrate these possibilities within the framework and highlight the possibility of simulation of different operational scenarios within the framework, including inorganic and organic compounds.

9.1.2 Kinetic models and model library

Kinetic models for the crystallization kinetic phenomena encountered in crystallizations have been collected and their various assumptions discussed. A crystallization kinetic model library has been constructed and models added as a step towards a systematic approach to crystallization operation modelling. In the library, models incorporating various kinetic phenomena are stored along with the data and assumptions. The model library is integrated with the generic framework, which allows retrieval, use or reuse of the models and analysis and storage. It is possible to use the single phenomenon models as stand-alone models for analysis of a specific phenomenon and the use has been demonstrated. This is relevant when a model is to be verified: Single phenomenon models can be analyzed rapidly and through an expanded database and phenomenon knowledge the model output can be evaluated. The storing of the models in the library allows new models for know systems to be compared to existing results.

9.1.3 Model analysis

The crystallization kinetics within the full model (including mass, energy and population balance) have been evaluated using sensitivity analysis with data from simulated as well as physical experiments. It was found that reliable identification is not possible from the data, that is the parameter set which is estimated can be sued for the description of the data, but it may not be unique. The model parameters, which are assigned physical meaning, should not be considered to have such a meaning. it is possible to limit the correlation between the parameters associated with the different kinetic phenomena through planned experiments, however, the correlation between the parameters in a single phenomenon model increases simultaneously.

9.2 Future work

The developed framework should be expanded to cover more systems, expanding the knowledge base and case studies in order to investigate the versatility of the framework. Increased use and further development of the tools for model analysis is recommended. The possibilities of assigning uncertainties to the different aspects of crystallization operations may be helpful in determining the directions for new developments of measurement techniques and data types. Model reduction and structure should be considered and application to industrial problems with complex mixtures of chemicals and interactions made. In the model library context, it may be

valuable continuously to look for trends in models and observe model trends with time.

Appendices

APPENDIX A

Appendix: Pertubation

The central, backwards and forwards perturbation of the kinetic model parameters in the simulations are given for each kinetic parameter

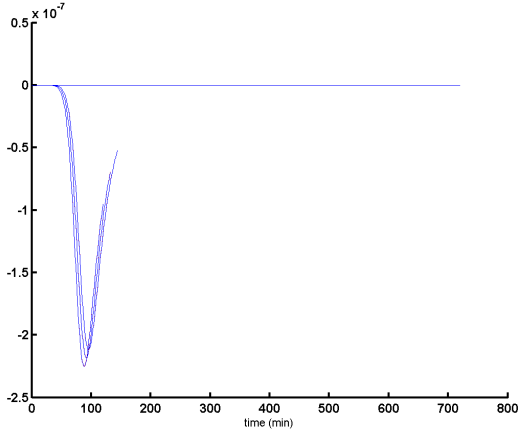

(a) *Central, backwards and forwards perturbation of* k_{b1}

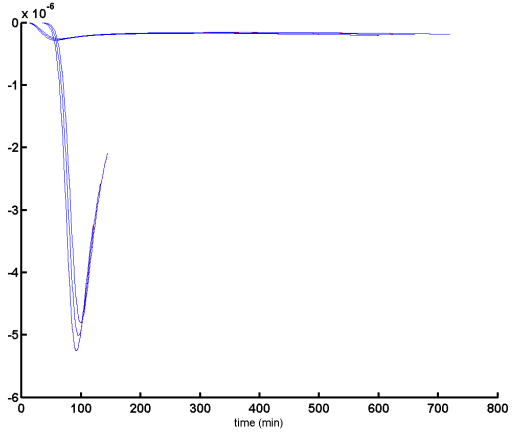

(b) *Central, backwards and forwards perturbation of* k_g

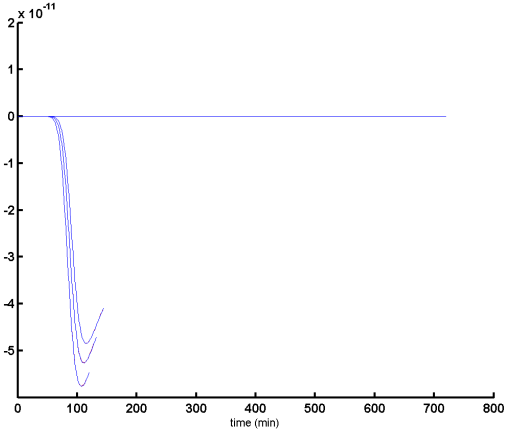

(c) *Central, backwards and forwards perturbation of* k_{b2}

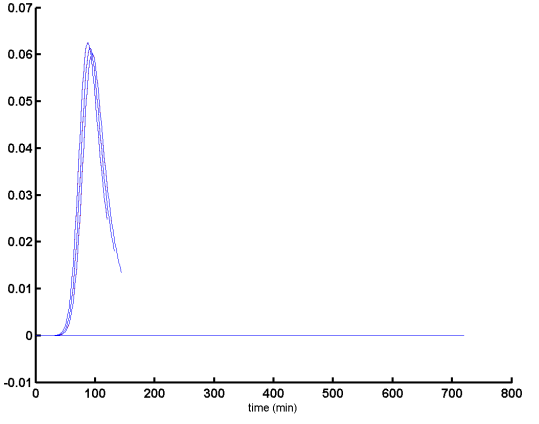

(d) *Central, backwards and forwards perturbation of* b_1

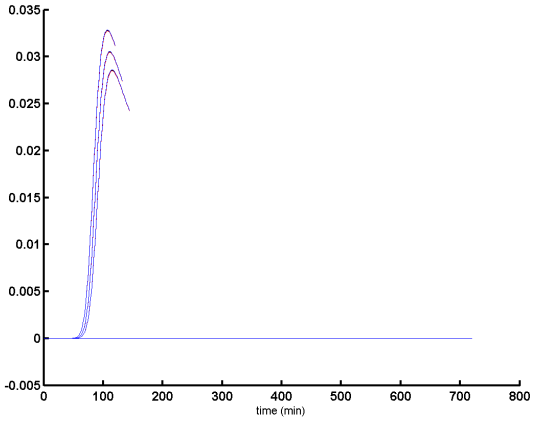

(e) *Central, backwards and forwards perturbation of* b_2

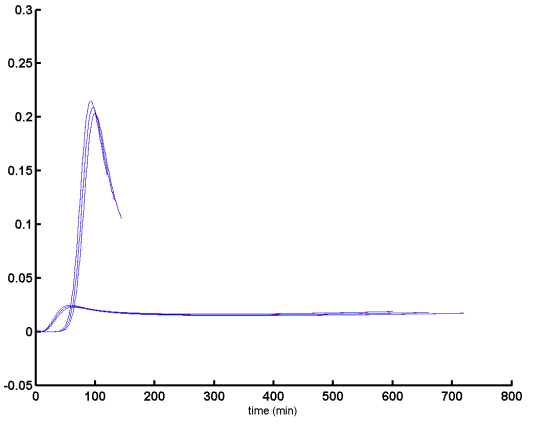

(f) *Central, backwards and forwards perturbation of* g

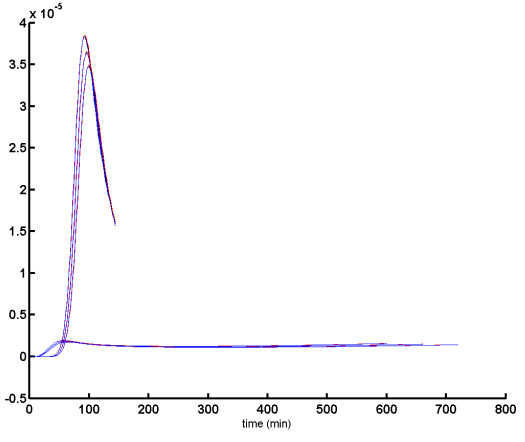

(g) *Central, backwards and forwards perturbation of* E_a

Figure A.-1: *Central, backwards and forwards perturbation of the parameters* $k_{b1}, k_g, k_{b2}, b_1, b_2, g, E_a$

APPENDIX B

Appendix: Experimental results

The experimental results from the crystallization of paracetamol from propan-2-ol, showing the concentration profile (dashed green), temperature profile (dashed red) and total FBRM count (solid blue) for six crystallization experiments

Parity plots for the models and experiments, showing the agreement between the model and experimental results, have been made:

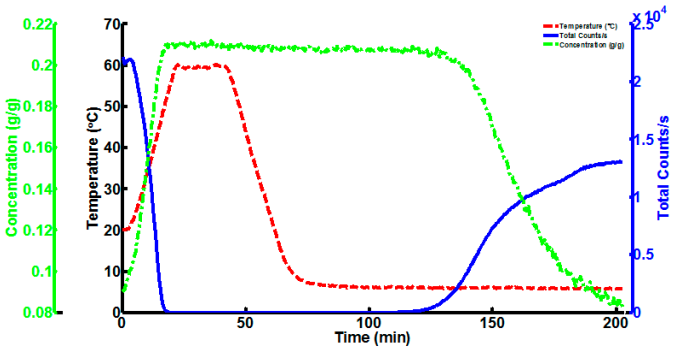

(a) *Concentration, temperature and total FBRM count for the experiment at 300 rpm and cooling of 2 °C*

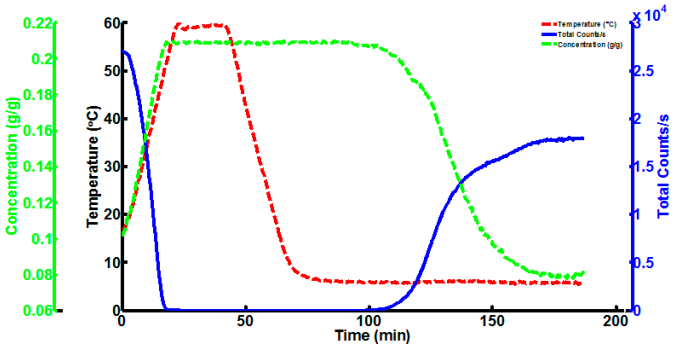

(b) *Concentration, temperature and total FBRM count for the experiment at 450 rpm and cooling of 2 °C*

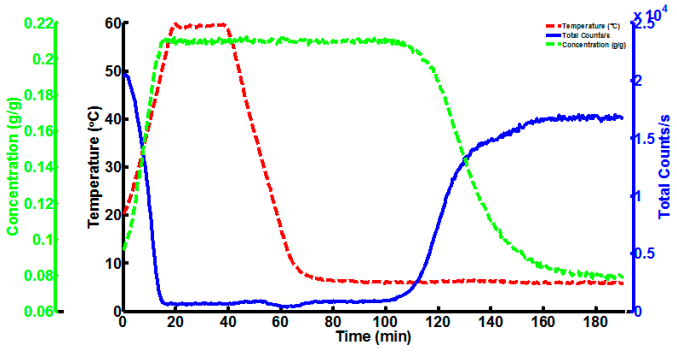

(c) *Concentration, temperature and total FBRM count for the experiment at 600 rpm and cooling of 2 °C*

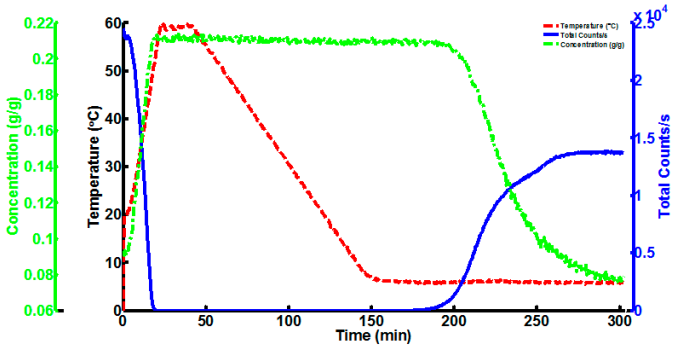

(d) *Concentration, temperature and total FBRM count for the experiment at 300 rpm and cooling of 0.5 °C*

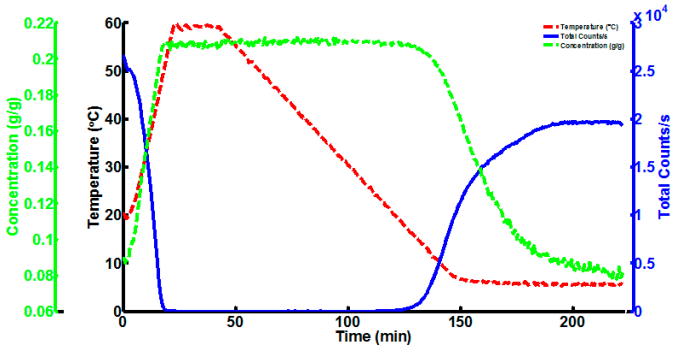

(e) *Concentration, temperature and total FBRM count for the experiment at 450 rpm and cooling of 0.5 °C*

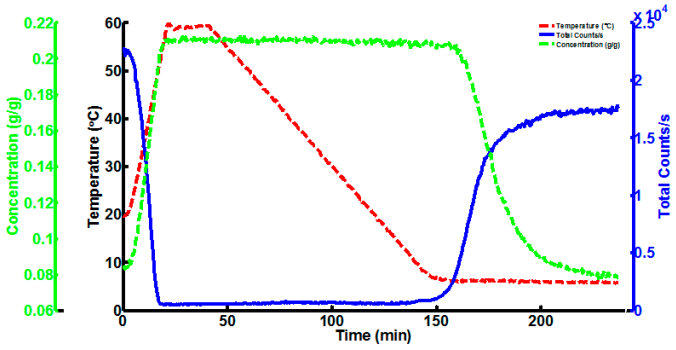

(f) *Concentration, temperature and total FBRM count for the experiment at 600 rpm and cooling of 0.5 °C*

Figure B.-1: *Concentration, temperature and total FBRM count for the experiments*

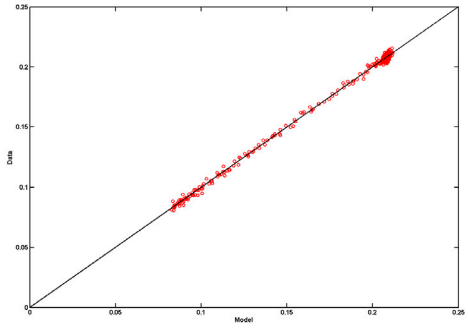

(a) *Parity plot for the experiment at 300 rpm and cooling of 2 °C*

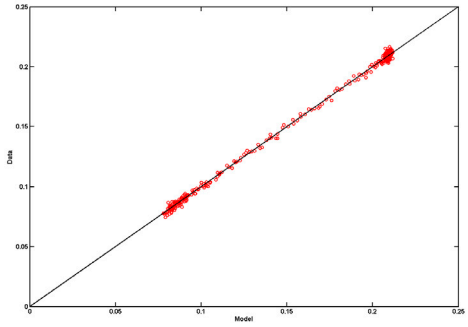

(b) *Parity plot for the experiment at 450 rpm and cooling of 2 °C*

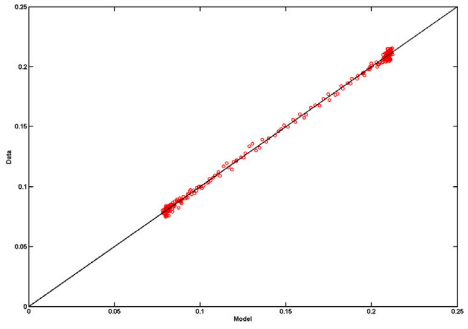

(c) *Parity plot for the experiment at 600 rpm and cooling of 2 °C*

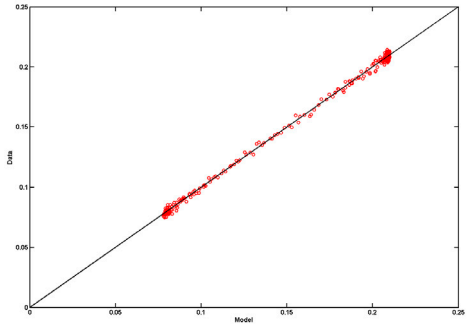

(a) *Parity plot for the experiment at 300 rpm and cooling of 0.5 °C*

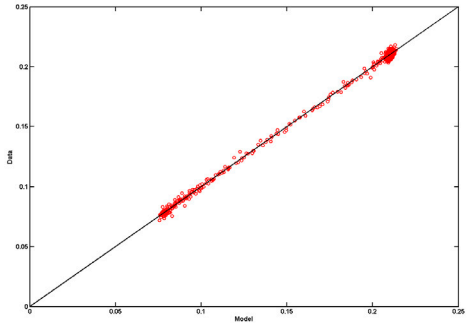

(b) *Parity plot for the experiment at 450 rpm and cooling of 0.5 °C*

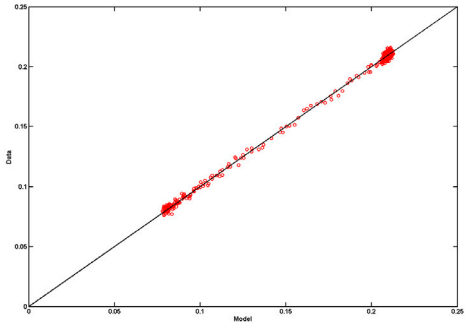

(c) *Parity plot for the experiment at 600 rpm and cooling of 0.5 °C*

APPENDIX C

Appendix: Pertubation of parameters

The pertubed parameters in the six different simulated experiments are shown. If the parameter responds, it can be related to an experiment indicating that information about the parameter can be found in the experiment in the region of the response. Information about growth parameters is available in all experiments, whereas nucleation parameters need the high supersaturation found in shorter experiments

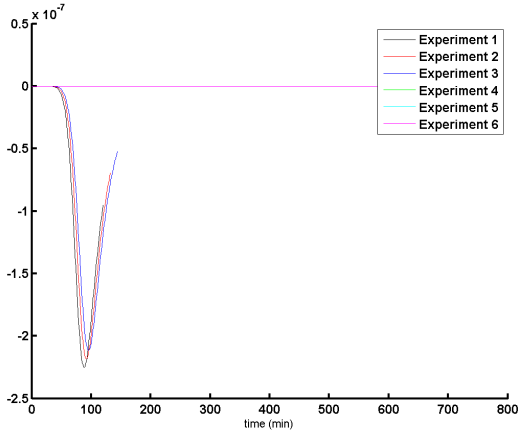

(a) *The parameter k_{b1} perturbed*

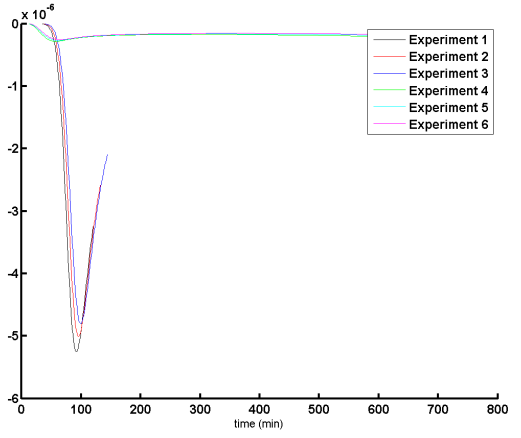

(b) *The parameter k_g perturbed*

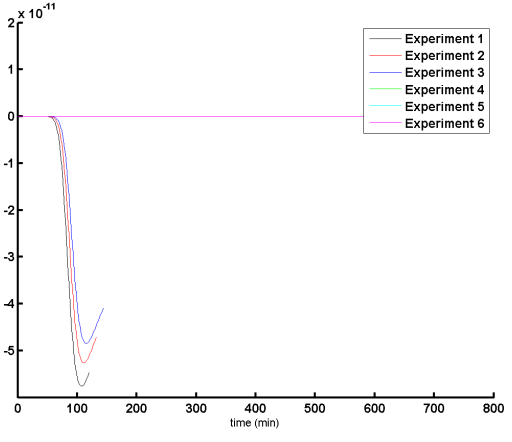

(c) *The parameter k_{b2} perturbed*

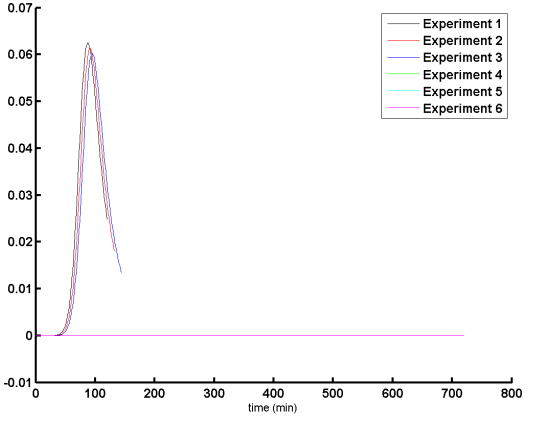

(d) *The parameter b_1 perturbed*

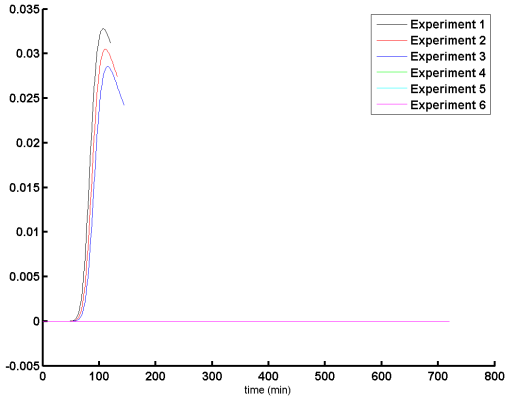

(e) *The parameter b_2 perturbed*

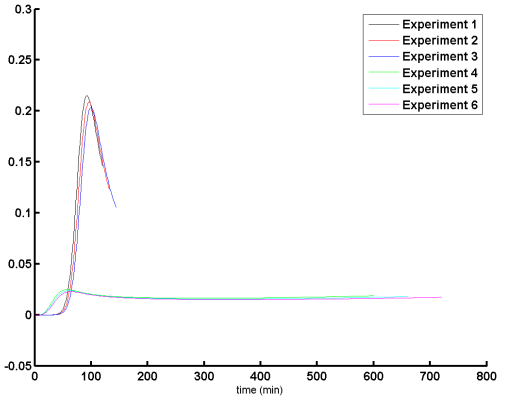

(f) *The parameter g perturbed*

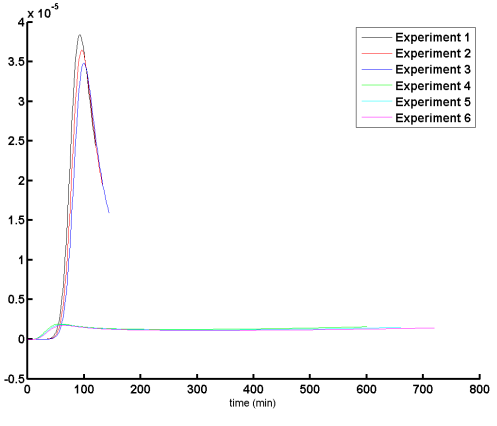

(g) *The parameter Ea perturbed*

Figure C.-1: *The parameters $k_{b1}, k_g, k_{b2}, b_1, b_2, g, E_a$ are perturbed, and the plot for each parameter is seen. If the parameter responds, it can be related to an experiment indicating that information about the parameter can be found in the experiment in the region of the response. Information about growth parameters is available in all experiments, whereas nucleation parameters need the high supersaturation found in shorter experiments*

APPENDIX D

Appendix: Parameter information in experiments

The information contained in the experiments is further analyzed using the scaled sensitivities (equation 7.14). With the scaling, it becomes possible to compare the different elements in the sensitivity matrix and for a given experiment, indications of which parameter estimates that can be obtained from the data, can be analyzed.

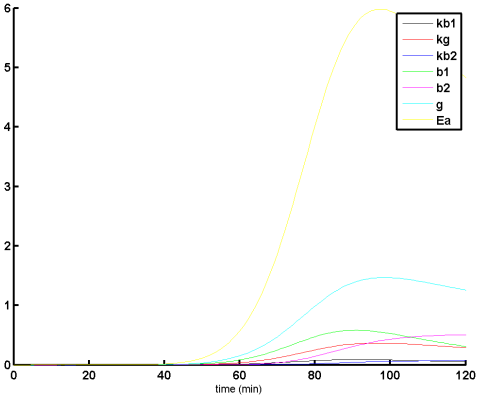

(a) *Parameter information obtainable from experiment 1*

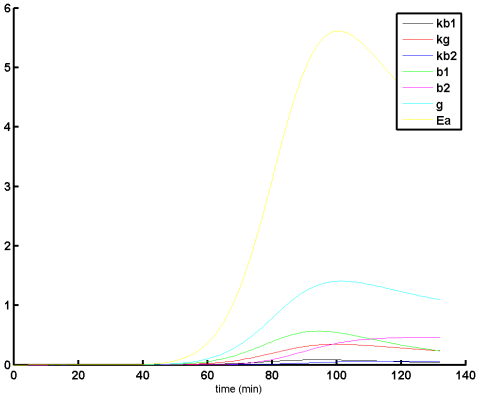

(b) *Parameter information obtainable from experiment 2*

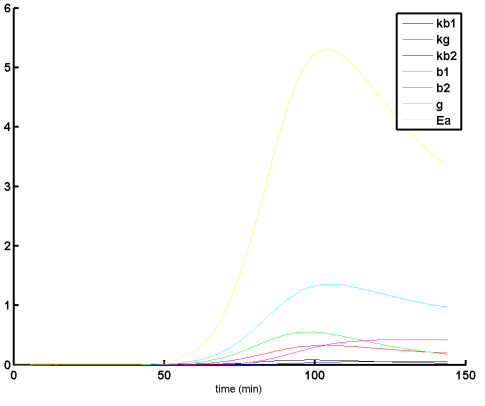

(c) *Parameter information obtainable from experiment 3*

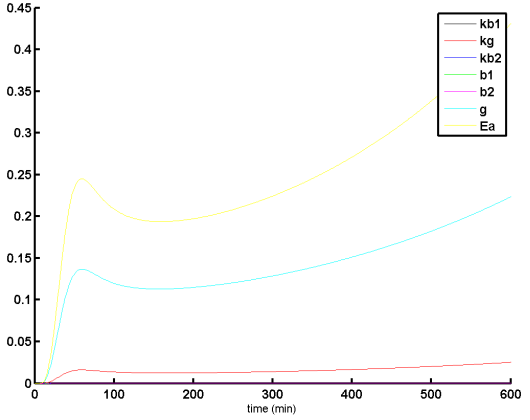

(d) *Parameter information obtainable from experiment 4*

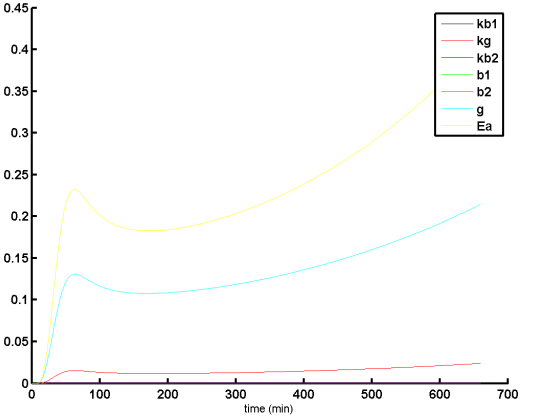

(e) *Parameter information obtainable from experiment 5*

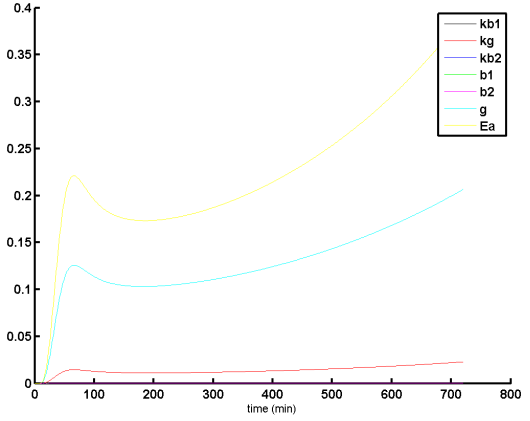

(f) *Parameter information obtainable from experiment 6*

Figure D.-1: *The information contained in the experiments is further analyzed using the scaled sensitivities (equation 7.14). With the scaling, it becomes possible to compare the different elements in the sensitivity matrix and for a given experiment, indications of which parameter estimates that can be obtained from the data, can be analyzed.*

APPENDIX E

Appendix: Pertubation of Noisy Parameters

The parameters $k_{b1}, k_g, k_{b2}, b_1, b_2, g, E_a$ are perturbed, and the plot for each parameter is seen. The experiemnts have been added white noise. If the parameter responds, it can be related to an experiment indicating that information about the parameter can be found in the experiment in the region of the response. Information about growth parameters is available in all experiments, whereas nucleation parameters need the high supersaturation found in shorter experiments

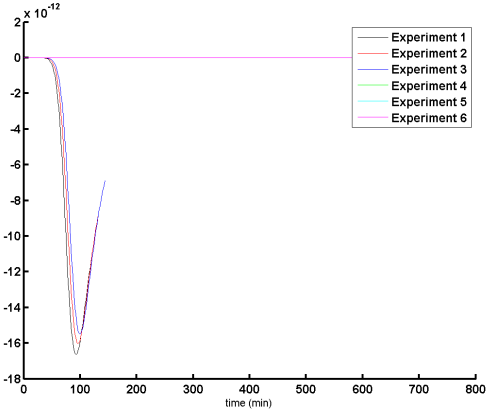

(a) *The parameter k_{b1} perturbed*

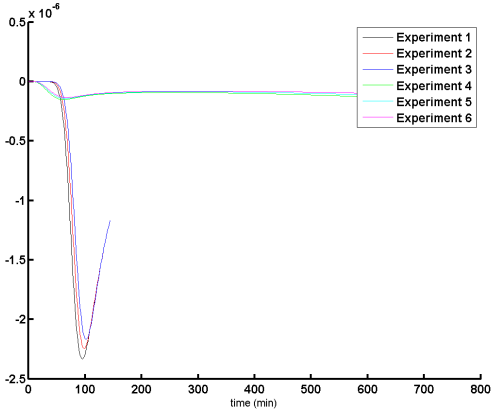

(b) *The parameter k perturbed*

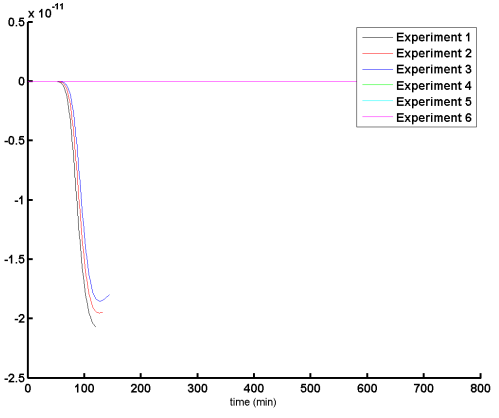

(c) *The parameter k_{b2} perturbed*

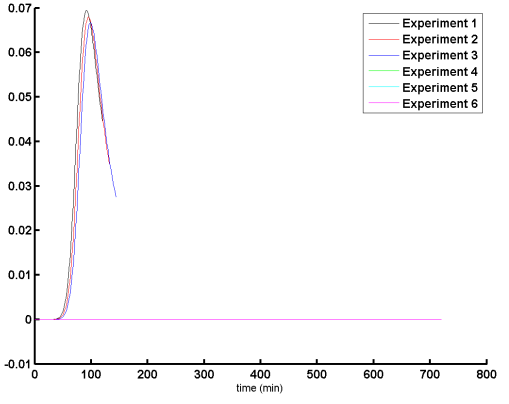

(d) *The parameter b_1 perturbed*

Figure E.-1: *The parameters $k_{b1}, k_g, k_{b2}, b_1, b_2, g, E_a$ are perturbed, and the plot for each parameter is seen. The experiemnts have been added white noise. If the parameter responds, it can be related to an experiment indicating that information about the parameter can be found in the experiment in the region of the response. Information about growth parameters is available in all experiments, whereas nucleation parameters need the high supersaturation found in shorter experiments*

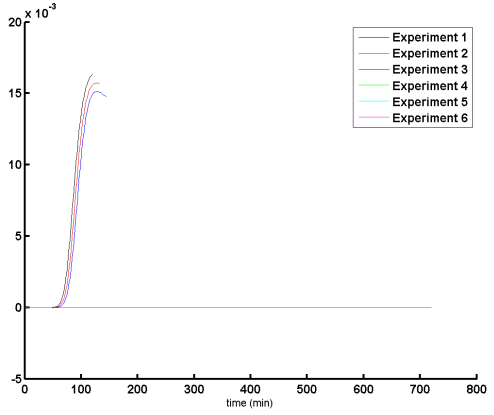

(e) *The parameter b_2 perturbed*

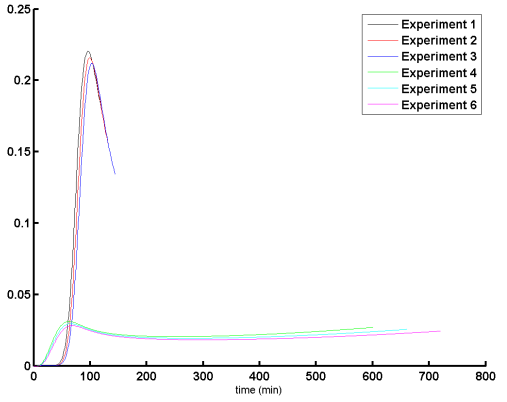

(f) *The parameter g perturbed*

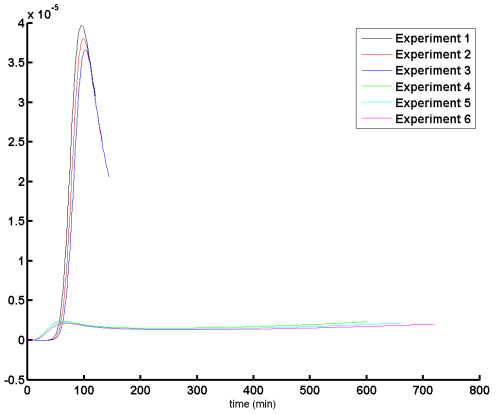

(g) *The parameter Ea perturbed*

APPENDIX F

Appendix: Parameter information in noisy experiments

The information contained in the noisy experiments is further analyzed using the scaled sensitivities (equation 7.14). With the scaling, it becomes possible to compare the different elements in the sensitivity matrix and for a given experiment, indications of which parameter estimates that can be obtained from the data, can be analyzed.

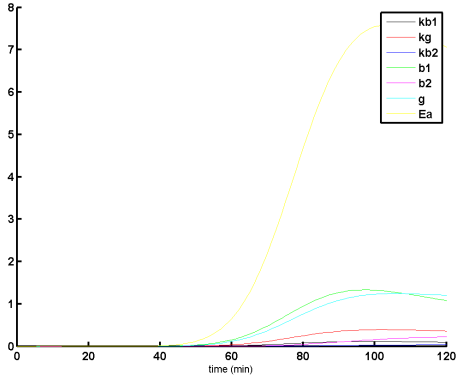

(a) *Parameter information obtainable from experiment 1*

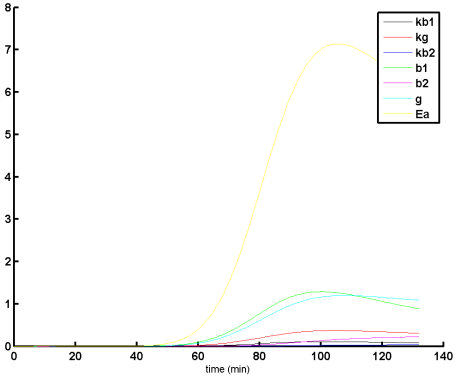

(b) *Parameter information obtainable from experiment 2*

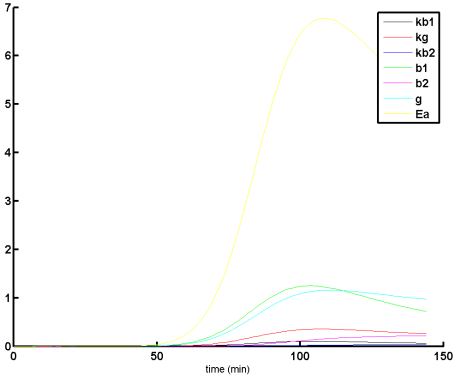

(c) *Parameter information obtainable from experiment 3*

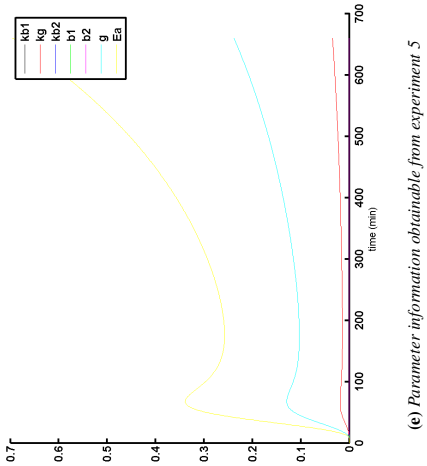

(e) *Parameter information obtainable from experiment 5*

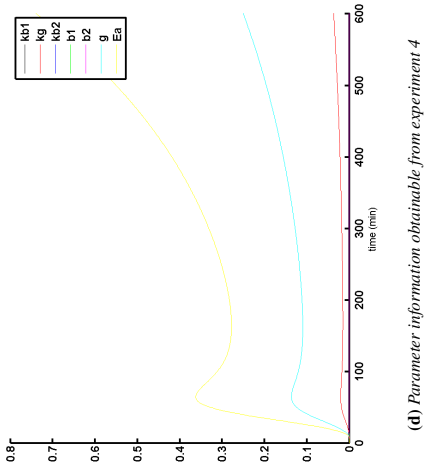

(d) *Parameter information obtainable from experiment 4*

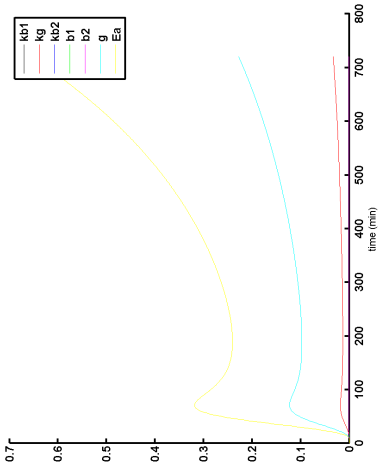

(f) *Parameter information obtainable from experiment 6*

Figure F.-1: *The information contained in the noisy experiments is further analyzed using the scaled sensitivities (equation 7.14). With the scaling, it becomes possible to compare the different elements in the sensitivity matrix and for a given experiment, indications of which parameter estimates that can be obtained from the data, can be analyzed.*

List of Figures

List of Tables

Bibliography

Aamir, E., Z. K. Nagy, C. D. Rielly, T. Kleinert, and B. Judat (2009). Combined quadrature method of moments and method of characteristics approach for efficient solution of population balance models for dynamic modeling and crystal size distribution control of crystallization processes. *Ind. Eng. Chem. Res. 48*, 8575–8584.

Abbas, A. and J. A. Romagnoli (2007). Multiscale modeling, simulation and validation of batch cooling crystallization. *Separation and Purification Technology 53*, 153–163.

Akrap, M., N. Kuzmanic, and J. P. Kardum (2012). Impeller geometry effect on crystallization kinetics of borax decahydrate in a batch cooling crystallizer. *Chemical Engineering Research and Design 90*, 793–802.

Alamdari, A., S. S. Nasab, and A. Jahanmiri (2010). Kinetic study of adductive crystallization of bisphenol-a. *Chemical Engineering Research and Design 88*, 1615–1623.

Alamdari, A., M. Rahimpour, N. Esfandiari, and E. Nourafkan (2008). Kinetics of magnesium hydroxide precipitation from sea bittern. *Chemical Engineering and Processing 47*, 215–221.

Aldaco, R., A. Garea, and A. Irabien (2007). Modeling of particle growth: Application to water treatment in a fluidized bed reactor. *Chemical Engineering Journal 134*, 66–71.

Ali, M. I. and P. A. Schneider (2008). An approach of estimating struvite growth kinetic incorporating thermodynamic and solution chemistry, kinetic and process description. *Chemical Engineering Science 63*, 3514–3525.

Alvarez, A. J. and A. S. Myerson (2010). Continuous plug flow crystallization of pharmaceutical compounds. *Crystal Growth & Design Vol. 10*(5), 2219–2228.

Angelov, I., J. Raisch, M. Elsner, and A. Seidel-Morgenstern (2008). Optimal operation of enantioseparation by batchwise preferential. *Chemical Engineering Science 63*, 1282–1292.

Audoly, S., G. Bellu, L. D'Angiò, M. P. Saccomani, and C. Cobelli (2001). Global identifiability of nonlinear models of biological systems. *IEEE Transactions on Biomedical Engineering 48*, 55–65.

Bao, Y., J. Zhang, Q. Yin, and J. Wang (2006). Determination of growth and breakage kinetics of l-threonine crystals. *Journal of Crystal Growth 289*, 317–323.

Bellman, R. and K. J. Åström (1970). On structural identifiability. *Mathematical Biosciences 7*, 329–339.

Bennema, P. (1967). Interpretation of the relation between the rate of crystal growth from solution and teh relative supersturation at low supersaturation. *Journal of Crystal Growth 1*, 287–292.

Bode, H. W. (1955). *Network Analysis and Feedback Amplifier Design* (10th print ed.). D. Van Nostrand Company.

Borissova, A. (2009). General systems modeling of multi-phase batch crystallization from solution. *Chemical Engineering and Processing: Process Intensification 48*, 268–278.

Bourne, J. R. and J. Davey (1976). The grrowth of hexamethylene tetramine crystals from ethanolic solutions. *Journal of Crystal Growth 34*, 230–238.

Brun, R., M. Kühni, H. Siegrist, W. Gujer, and P. Reichert (2002). Practical identifiability of asm2d parameters—systematic selection and tuning of parameter subsets. *Water Research 36*, 4113–4127.

Bund, R. and A. Pandit (2007). Rapid lactose recovery from buffalo whey by use of 'anti-solvent, ethanol. *Journal of Food Engineering 82*, 333–341.

Burton, W. K., N. Cabrera, and F. C. Frank (1951). The growth of crystals and the equilibrium structure of their surfaces. *Philosophical Transactions of the Royal Society of London. Series A, Mathematical and Physical Sciences 243*(866), 299–358.

Cameron, I. and R. Gani (2011). *Product and Process ModeModel - A Case Study Approach*. Elsevier.

Cesur, S. and C. Yaylaci (2012). Optimum kinetic parameters of mefenamic acid crystallization by pbm. *Journal of Crystallization Process and Technology 2*, 81–95.

Chernov, A. A. (1989). Formation of crystals in solutions. *Contemporary Physics Volume 30, Issue 4, 1989 30*, 251–276.

Chianese, A. and H. J. M. Kramer (Eds.) (2012). *Industrial Crystallization Process Monitoring and Control*. Wiley-VCH Verlag GmbH & Co. KGaA.

Costa, C. B., A. C. da Costa, and R. M. Filho (2005). Mathematical modeling and optimal control strategy development for an adipic acid crystallization process. *Chemical Engineering and Processing: Process Intensification 44*, 737–753.

Costa, C. B. B., M. R. W. Maciel, and R. M. Filho (2007). Considerations on the crystallization modeling: Population balance solution. *Computers and Chemical Engineering 31*, 206–218.

Cussler, E. L. (2009). *Diffusion: Mass Transfer in Fluid Systems; Cambridge Series in Chemical Engineering*. Cambridge University Press.

Czapla, F., N. Kail, A. Öncül, H. Lorenz, H. Briesen, and A. Seidel-Morgenstern (2010). Application of a recent fbrm-probe model to quantify preferential crystallization of dl-threonine. *Chemical Engineering Research and Design 88*, 1494–1504.

David, R., J. Villermaux, P. Marchal, and J.-P. Klein (1991). Crystallization and precipitation engineering -iv kinetic model of adipic acid crystallization. *Chemical Engineering Science 46*, 1129–1136.

Dokoumetzidis, A. and P. Macheras (2006). A century of dissolution research: From noyes and whitney to the biopharmaceutics classification system. *International Journal of Pharmaceutics 321 (2006) 1–11 321*, 1–11.

Faria, N., S. F. de Azevedo, F. A. Rocha, and M. N. Pons (2008). Modelling agglomeration degree in sucrose crystallisation. *Chemical Engineering and Processing 47*, 1666–1677.

Frawley, P. J., N. A. Mitchell, C. T. O'Ciardha, and K. W. Hutton (2012). The effects of supersaturation, temperature, agitation and seed surface area on the secondary nucleation of paracetamol in ethanol solutions. *Chemical Engineering Science 75*, 183–197.

Fredenslund, A., R. L. Jones, and J. M. Prausnitz (1975). Group-contribution estimation of activity coefficients in nonideal liquid mixtures. *AIChE Journal 21*, 1086–1099.

Garside, J. (1985). Industrial crystallization from solution. *Chemical Engineering Science 40*(1), 3–26.

Gernaey, K. and R. Gani (2010). A model-based systems approach to pharmaceutical product-process design and analysis. *Chemical Engineering Science 65*, 5757–5769.

Gherras, N. and G. Fevotte (2012). Comparison between approaches for the experimental determination of metastable zone width: A casestudy of the batch cooling crystallization of ammonium oxalate in water. *Journal of Crystal Growth 342*, 88–98.

Gimbun, J., Z. K. Nagy, and C. D. Rielly (2009). Simultaneous quadrature method of moments for the solution of population balance equations, using a differential algebraic equation framework. *Ind. Eng. Chem. Res. 48*, 7798–7812.

Grewal, M. and K. Glover (1976). Identifiability of linear and nonlinear dynamical systems. *IEEE Transactions on Automatic Control AC-21*, 883–887.

Hill, P. J. and K. M. Ng (1996). New discretization procedure for the agglomeration equation. *Process Systems Engineering 42.*, 727–741.

Hirata, G. A., A. Bernardo, and E. A. Miranda (2012). Determination of crystal growth rate for porcine insulin crystallization with co2 as a volatile acidifying agent. *Chemical Engineering and Processing 56*, 29–33.

Hofmann, S. and J. Raisch (2012). Solutions to inversionproblems in preferential crystallization of enantiomers—part i: Batch crystallization in a single vessel. *Chemical EngineeringScience80(2012)253–269 80*, 253–269.

Holmberg, A. (1982). On the practical identifiability of microbial growth models incorporating michaelis-menten type nonlinearities. *Mathematical Biosciences 62*, 23–43.

Hulburt, H. M. and S. Katz (1964). Some problems in particle technology: A statistical mechanical formulation. *Chemical Engineering Science 19*, 555–574.

Jacquez, J. A. and P. Greif (1985). Numerical parameter identifiability and estimability: Integrating identifiability, estimability, and optimal sampling design. *Mathematical Biosciences 77*, 201–227.

John, V., I. Angelov, A. Öncül, and D. Thévenin (2007). Techniques for the reconstruction of a distribution from a finite number of its moments. *Chemical Engineering Science 62*, 2890–2904.

Jones, A. G. (2002). *Crystallization Process Systems*. Butterworth-Heinemann.

Kadam, S. S., S. A. Kulkarni, R. C. Ribera, A. I. Stankiewicz, J. H. ter Horst, and H. J.M.Kramer (2012). A new view on the metastable zone width during cooling crystallization. *Chemical Engineering Science 72*, 10–19.

Korovessi, E. and A. A. Linninger (Eds.) (2006). *Batch Processes*, Chapter 6. Batch Crystallization, pp. 151–203. CRC Press.

Kossel, W. (1927). Zur theorie des kristallwachstums,. *Nachr. Ges. Wiss. Göttingen 2*, 135–145.

Li, X., Q. Yin, W. Chen, and J. Wang (2006). Solubility of hydroquinone in different solvents from 276.65 k to 345.10 k. *Journal of Chemical Engineering Data 51*, 127–129.

Ljung, L. and T. Glad (1994). On global identifiability for arbitrary model parametrizations. *Automatica 30*, 265–276.

Loudon, G. M. (2002). *Organic Chemistry*. Oxford University Press.

Ma, D. L., D. K. Tafti, and R. D. Braatz (2002). High-resolution simulation of multidimensional crystal growth. *Industrial & Engineering Chemistry Research 41*, 6217–6223.

Ma, Y., J. Zhu, K. Chen, Y. Wu, and A. Chen (2009). Study on growth kinetics of phosphoric acid hemihydrate using fbrm. *Journal of Crystal Growth 312*, 109–113.

Marchal, P., R. David, J. P. Klein, and J. Villermaux (1988.). Crystallization and preciptation engineering - i. an efficient method for solving population balance in crystallization with agglomeration. *Chemical Engineering Science 43*, 59–67.

Markande, A., A. Nezzal, J. Fitzpatrick, L. Aerts, and A. Redl (2012). Influence of impurities on the crystallization of dextrose monohydrate. *Journal of Crystal Growth 353*, 145–151.

Markande, A., A. Nezzal, J. J. Fitzpatrick, and L. Aerts (2009). Investigation of the crystallization kinetics of dextrose monohydrate using in situ particle size and supersaturation monitoring. *Particulate Science and Technology 27*, 373–388.

McCabe, W. L. and R. P. Stevens (1951). Rate of growth of crystals in aqueous solutions. *Chemical Engineering Progress 47*, 168–174.

McGraw, R. (1997). Description of aerosol dynamics by the quadrature method of moments. *Aerosol Science and Technology 27*, 255–265.

McKay, M. D., J. D. Morrison, and S. C. Upton (1999). Evaluating prediction uncertainty in simulation models. *Computer Physics Communications 117*, 44–51.

Meisler, K. T., N. von Solms, K. Gernaey, and R. Gani. (2013). Crystallization kinetics within a generic modelling framework. *Proceedings of 20th International Workshop on Industrial Crystallization (BIWIC2013)* -, p. 176–183.

Meisler, K. T., N. von Solms, K. V. Gernaey, and R. Gani (2014). Crystallization kinetics within a generic modeling framework. *Chemical Engineering & Technology 37*, 1383–1392.

Mersmann, A. (Ed.) (2001). *Crystallization Technology Handbook* (2nd ed. ed.). Marcel Dekker, Inc.

Metropolis, N. and S. Ulam (1949). The monte carlo method. *Journal of the American Statistical Association 44*, 335–341.

Mettler-Toledo (2013). Fbrm fact sheet. Technical report, Mettler-Toledo, LLC, 1900 Polaris Parkway, Columbus, OH 43240.

Miao, H., X. Xia, A. S. Perelson, and H. Wu (2011). On identifiability of nonlinear ode models and applications in viral dynamics. *Society for Industrial and Applied Mathematics (SIAM) Reviews 53*, 3–39.

Millan, A., O. Sohnel, and F. Grases (1997). The influence of crystal morphology on the kinetics of growth of calcium oxalate monohydrate. *Journal of Crystal Growth 179*, 231–239.

Mitchell, N. A. and P. J. Frawley (2010). Nucleation kinetics of paracetamol–ethanol solutions from metastable zone widths. *Journal ofCrystalGrowth 312*, 2740–2746.

Mohan, R. and A. S. Myerson (2002). Growth kinetics:a thermodynamic approach. *Chemical Engineering Science 57*, 4277 – 4285.

Mortier, S. T. F., T. D. Beer, K. V. Gernaey, and I. Nopens (2014). Comparison of techniques for reconstruction of a distribution frommoments in the context of a pharmaceutical drying process. *Computers and Chemical Engineering 65*, 1–8.

Mullin, J. W. (2001). *Crystallization* (4th ed.). Elsevier Butterworth-Heinemann.

Myerson, A. S. (Ed.) (2002). *Handbook of Industrial Crystallization* (2nd ed.). Butterworth-Heinemann.

Nagy, Z. K. and E. Aamir (2012). Systematic design of supersaturation controlled crystallization processes for shaping the crystal size distribution using an analytical estimator. *Chemical Engineering Science 84*, 656–670.

Nagy, Z. K., J. W. Chew, M. Fujiwara, and R. D. Braatz (2008). Comparative performance of concentration and temperature controlled batch crystallizations. *Journal of Process Control 18*, 399–407.

Nernst, W. (1904). Theorie der reaktionsgeschwindigkeit in heterogenen systemen. *Zeitschrift. Phys. Chem. 47*, 52–55.

Nowee, S. M., A. Abbas, and J. A. Romagnoli (2008). Antisolvent crystallization: Model identification, experimental validation and dynamic simulation. *Chemical Engineering Science 63*, 5457–5467.

Noyes, A. A. and W. R. Whitney (1897). The rate of solution of solid substances in their own solutions. *Journal of the American Chemical Society 19*, 930–934.

Nývlt, J., O. Söhnel, M. Matuchová, and M. Broul (1985). *The Kinetics of Industrial Crystallization*. Elsevier.

Ouiazzane, S., B. Messnaoui, S. Abderafi, J. Wouters, and T. Bounahmidi (2008). Estimation of sucrose crystallization kinetics from batch crystallizer data. *Journal of Crystal Growth 310*, 798–803.

Peres, A. M. and E. A. Macedo (1996). Thermodynamic properties of sugars in aqueous solutions: correlation and prediction using a modified uniquac model. *Fluid Phase Equilibria 123*, 71–95.

Petersen, B., K. Gernaey, M. Devisscher, D. Dochain, and P. A. Vanrolleghem (2003). A simplified method to assess structurally identifiable parameters in monod-based activated sludge models. *Water Research 37*, 2893–2904.

Petersen, B., K. Gernaey, and P. Vanrolleghem (2001). Practical identifiability of model parameters by combined respirometric-titrimetric measurements. *Water Science and Technology 43*, 347–355.

Puel, F., G. Fevotte, and J. P. Klein (2003). Simulation and analysis of industrial crystallization processes through multidimensional population balance equations. part 1: a resolution algorithm basedon the method of classes. *Chemical Engineering Science 58*, 3715–3727.

Qamar, S., A. Ashfaq, G. Warnecke, I. Angelov, M. P. Elsner, and A. Seidel-Morgenstern (2007). Adaptive high-resolution schemes for multidimensional population balances in crystallization processes. *Computers and Chemical Engineerin 31*, 1296–1311.

Qamar, S., M. P. Elsner, I. Hussain, and A. Seidel-Morgenstern (2012). Seeding strategies and residence time characteristics of continuous preferential crystallization. *Chemical Engineering Science 71*, 5–17.

Qu, H., J. Rantanen, and J. Ulrich (2014). Industrial crystallization. *Chemical Engineering & Technology 37*, 1279.

Quaiser, T. and M. Mönnigmann (2009). Systematic identifiability testing for unambiguous mechanistic modeling – application to jak-stat, map kinase, and nf-κb signaling pathway models. *BMC Systems Biology 3*.

Quintana-Hernández, P., E. Bolaños-Reynoso, B. Miranda-Castro, and L. Salcedo-Estrada (2004). Mathematical modeling and kinetic parameter estimation in batch crystallization. *AIChE Journal 50*(7), 1407–1417.

Ramkrishna, D. (2000). *Population Balances: Theory and Applications to Particulate Systems in Engineering.* USA: Academic Press.

Randolph, A. D. and M. A. Larson (1971). *Theory of Particulate Processes*. Academic Press.

Rawlings, J. B., S. M. Miller, and W. R. Witkowski (1993). Model identification and control of solution crystallization processes: A review. *Industrial & Engineering Chemical Research 32*, 1275–1296.

Ritt, J. F. (1950). *Differential Algebra*, Volume 33 of *Colloquium Publications*. American Mathematical Society, Providence, Rhode Island.

Ruf, A., J. Worlitschek, and M. Mazzotti (2000). Modeling and experimental analysis of psd measurements through fbrm. *Part. Part. Syst Charact. 17*, 167–179.

Saberi, A., A. S. Goharrizi, and S. Ghader (2009). Precipitation kinetics of sodium bicarbonate in an industrial bubble column crystallizer. *Crystal Research and Technology 44*, 159–166.

Saleemi, A. N. (2011). *Strategic Feedback Control of Pharmaceutical Crystallization Systems*. Ph. D. thesis, Loughborough University, dept. Chemical Engineering.

Saltelli, A., S. Tarantola, F. Campolongo, and M. Ratto (2004). *Sensitivity Analysis in Practice: A Guide to Assessing Scientific Models*. John Wiley & Sons, Ltd.

Samad, N. A. F. A., G. Sin, K. V. Gernaey, and R. Gani (2013). Introducing uncertainty analysis of nucleation and crystal growth models in process analytical technology (pat) system design of crystallization processes. *European Journal of Pharmaceutics and Biopharmaceutics 85*, 911–929.

Samad, N. A. F. B. A. (2012). *Control of Process Operations and Monitoring of Product Qualities through Generic Model-based Framework in Crystallization Processes*. Kgs.Lyngby : Technical University of Denmark, Department of Chemical Engineering.

Samad, N. A. F. B. A., K. T. Meisler, K. Gernaey, N. von Solms, and R. Gani. (2012). Systematic identification of crystallization kinetics within a generic modelling framework. *Computer Aided Chemical Engineering 31*, 945–949.

Samad, N. A. F. B. A., K. T. Meisler, G. Sin, K. Gernaey, and R. Gani (2012). A generic framework for systematic design of process monitoring and control system for crystallization processes. *Proceedings of the 22nd European Symposium on Computer Aided Process Engineering -*, –.

Samad, N. A. F. B. A., G. Sin, K. Gernaey, and R. Gani. (2013). Introducing uncertainty analysis of nucleation and crystal growth models in process analytical technology (pat) system design of crystallization processes. *European Journal of Pharmaceutics and Biopharmaceutics 85*, 911–929.

Samad, N. A. F. B. A., R. Singh, G. Sin, K. V. Gernaey, and R. Gani (2011). A generic multi-dimensional model-based system for batch cooling crystallization processes. *Computers & Chemical Engineering 35*, 828–843.

Seborg, D. E., T. F. Edgar, and D. A. Mellichamp (2004). *Process Dynamics and Control*. John Wiley and Sons.

Sin, G., A. S. Meyer, and K. V. Gernaey (2010). Assessing reliability of cellulose hydrolysis models to support biofuel process design—identifiability and uncertainty analysis. *Computers & Chemical Engineering 34*, 1385–1392.

Steyer, C., M. Mangold, and K. Sundmacher (2010). Modeling of particle size distribution for semibatch precipitation of barium sulfate using different activity coefficient models. *Industrial & Engineering Chemistry Research 49*, 2456–2468.

Ståhl, M., B. L. Åslund, and Åke C. Rasmuson (2001). Reaction crystallization kinetics of benzoic acid. *AIChE Journal 47*, 1544–1560.

Vajda, S., K. R. Godfrey, and H. Rabitz (1989). Similarity transformation approach to identifiability analysis of nonlinear compartmental models. *Mathematical Biosciences 93*, 217–248.

Valeton, J. P. P. (1923). Wachstum und auflösung der kristalle. *Z. Kristallogr. 59*, 335.

Worlitschek, J. and M. Mazzotti (2004). Model-based optimization of particle size distribution in batch-cooling crystallization of paracetamol. *Crystal Growth and Design 4*, 891–903.

Zauner, R. and A. G. Jones (2000). Determination of nucleation, growth, agglomeration and disruption kinetics from experimental precipitation data: the calcium oxalate system. *Chemical Engineering Science 55*, 4219–4232.

List of Symbols

A	Area. 7
C_{eq}	concentration. 6
D	Cooling rate. 124
E_a	Activation Energy. 25
E	Cooling rate. 134
J	Nucleation flux. 50
L	Characteristic length. 8
M_T	Magma density. 53
U	Heat transfer number. 7
V_c	Volume of crystals. 7
ΔC	absolute supersaturation. 6
ΔH_{cryst}	Enthalpy of crystallization. 7
β	kernel. 79
ε	Stirring rate. 78, 197
γ_{size}	size dependency constant. 26
γ	Activity coefficient. 6
μ_i	ith moment. 97
μ	chemical potential. 6
ω	Stirring rate. 25
ϕ	Phenomena. 97
ρ_c	crystal density. 7
σ	relative supersaturation. 6
τ	Transport Phenomena. 25
θ	Parameter. 31
a	Activity. 6

b	Nucleation order. 51
$c_{p,magma}$	Heat capacity of magma. 7
j	Magma density order. 53
k_b	Nucleation rate constant. 51
k_b	Nucleation rate constant. 51
m_{magma}	Mass of magma. 7
$m_{solvent}$	Mass of solvent. 7
n	Population. 8
p	Apparent size exponent. 27
q	Stirrer power. 25
u	Particle volume. 74
v	Particle volume. 74
x	Mole fraction. 6
B	Birth. 8
C	concentration. 6
g	Growth rate exponent. 23
R	Universal gas constant. 6
S	supersaturation ratio. 6
T	Temperature. 6
t	Time. 7
V	Volume. 70

CAPEC-PROCESS
Computer Aided Process Engineering/
Process Engineering and Technology center

Department of Chemical and Biochemical Engineering
Technical University of Denmark
Søltofts Plads, Building 229
DK-2800 Kgs. Lyngby
Denmark

Phone: +45 4525 2800
Fax: +45 4525 2906
Web: www.capec-process.kt.dtu.dk

ISBN : 978-87-93054-62-2